Development of a High Temperature Titanium Alloy for Gas Turbine Applications

Geraint Rhys Watkins

Department of Engineering Materials

The University of Sheffield

MPhil Thesis

March 2015

Summary

In order to maintain the rate at which the aerospace industry has grown in recent years, new aircraft are being designed with high emphasis on increased payloads. With this increase in payload, improvements in engine thrust output and efficiency are required. It is well known that one method of improving efficiency is to operate engines at high temperatures resulting in engine manufacturers increasingly choosing nickel based super alloys in favour of titanium alloys.

In order to successfully displace nickel with titanium in high temperature gas turbine conditions, a new titanium alloy is required to operate at temperatures exceeding the capabilities of existing alloy systems. While temperature is of utmost importance to this application, a number of other properties are to be considered during design. Materials must exhibit good creep and fatigue resistance as well as high strength and excellent corrosion resistance. Similarly, reasonable room temperature ductility must be employed to facilitate component manufacture.

The results prove the benefits of the addition of silicon to titanium alloys, however the loss in room temperature ductility brought by the addition of silicon to α-titanium has led to concentration on the use of β stabilisers to alloys of the Ti-Si system. An industry driven suggestion basing alloy design on analogies from nickel based super alloys, appears to have potential to provide improved ductility to such alloying system.

Through a combination of precipitation hardening and the formation of a protective oxide scale, titanium alloys containing chromium, niobium and silicon have proven to exhibit comparable and better oxidation resistance to Timetal 834 as well as improved tensile strength. Although ductility has still been outlined as a potential issue for such alloys, it would be beneficial to investigate the effect of the material processing route, and therefore the starting microstructure of such alloys.

TABLE OF CONTENTS

Acknowledgements

During both the completion of this work and the compilation of this thesis, I have benefited from the assistance and guidance of a number of colleagues and wish to acknowledge the support of everyone involved.

My first thanks goes to my primary supervisor, Brad Wynne, whose guidance has both assisted this academic achievement as well as enhanced my personal development. I would also like to thank my secondary supervisor Martin Jackson for the advice and interest during the course of this work.

I also owe acknowledgement to the EPSRC and Timet UK for the financial and technical support. Matthew Thomas has aided the completion of this work enormously.

Finally, I would like to thank my friends and family for the support, encouragement and persistence in pushing me to achieve all of my accomplishments to date.

1 Introduction

1.1Titanium in the Aerospace Industry

Titanium is a transition metal, and is given the symbol Ti (Atomic Number: 22) and is known as a low density metal which is strong and corrosion resistant *[1]*. Its alloys can have high strength to weight ratios at high temperatures, making them a desirable material within the aerospace industry and have been operating in gas turbine engines since 1952 *[2]*. Since then, the attractiveness of a range of alloys, some of which have the potential to exhibit tensile strengths exceeding 1500 MPa and the ability to operate at service temperatures of up to 650°C, has pushed the development of such alloys, in order to improve fuel efficiency in the industry *[3; 4]*. In modern jet turbine engines, titanium and its alloys typically make up approximately 30% of the material used, primarily in the 'forward region' of the engine including the medium to high pressure compressor stages i.e. where the temperature does not exceed approximately 600°C. Towards the rear of the engine, where higher temperatures are experienced, designers are forced into the use of nickel based super alloys, which are able to cope with the higher operating temperatures. While temperature is of utmost importance to this application, a number of other properties have to be considered during design. Materials must exhibit good creep and fatigue resistance as well as high strength and excellent corrosion resistance *[3]*. Similarly, reasonable room temperature ductility must be employed to facilitate component manufacture.

1.2 Existing Alloys

IMI 315, an α/β titanium alloy consisting of Ti - 2Al - 2Mn, used in Rolls Royce Avon engines in 1952, produced power for aircraft such as the Comet and Canberra *[3]*. Further developments revealed that small additions of silicon to titanium could drastically improve the creep resistance of such alloys, which led to the development of IMI 550, another α/β alloy consisting of Ti - 4Al - 2Sn - 4Mo - 0.5Si. It is thought that the silicide precipitation that comes with silicon addition contributes to the improved creep performance.

As titanium alloys developed, it was soon established that alloys capable of exceeding previous temperature limitations were obtainable using near α alloys and β-phase processing, producing a fully transformed β microstructure (IMI685 and IMI829). At present, the material most commonly used in medium and high pressure compressor stages of gas turbine engines is Timetal 834, consisting of Ti - 5.8Al - 4Sn - 3.5Zr - 0.7Nb - 0.5Mo - 0.35Si - 0.06C. Timetal 834 is a near α alloy, developed in the 1980s by IMI Titanium in the UK, with sufficient creep capability up to 600°C. However, as aircraft are constantly being designed with increased payloads, an increase in output from these engines is required. This desire for increased thrust means increasing temperature and decreasing space within engines therefore forcing engine designers to fall back on the use of the higher temperature capable nickel-based super alloys as a replacement for titanium. In order to successfully displace nickel with titanium in these conditions, a new titanium alloy is required to operate at temperatures exceeding capabilities of existing alloy systems, perhaps up to 750°C. This alloy would need to satisfy a number of key requirements:

- Resistance to oxidation / alpha case growth in service;
- Room temperature ductility;
- Strength/Creep resistance at service temperature.

This is clearly a difficult task but an industry driven suggestion basing alloy design on analogies from nickel based super alloys, or 'nimonics', appears to have potential. Thus, this work, with the support of TIMET UK, explores this idea and investigates the design of new titanium alloys with operating temperatures greater than that of the existing titanium alloys used in jet turbine engines.

1.3 Project Aim

To develop and investigate a suitable alloy matrix for a titanium alloying system for use in high temperature civil aircraft engines.

1.4 Project Objectives

- Using industrial standard thermodynamic simulation software at the University of Sheffield, the work will investigate a number of potential alloy matrices and elemental additions, obtained from literature ideas. The simulated thermodynamic effects will be used to determine suitability of alloys.

- Alloy systems determined to be potentially beneficial will be produced using the facilities of Timet in Witton, UK. Using metallographic and image analysis techniques the microstructures of the test alloys will be analysed such that micro structural features can be identified and related to elemental additions.

- Test materials will be subjected to heat treatments using both a thermo-gravimetric analysis (TGA) system as well as furnace oxidation investigations. Tensile testing carried out at room temperature will be investigated. The data obtained will be used in conjunction with electron and optical metallographic and image analysis techniques to again measure the effects of elemental additions on material microstructure after exposure to these conditions.

1.5 Thesis Outline

- **Chapter 2:** Literature Review. Relevant theoretical background behind the work will be included here. The aim of this chapter is to gain an understanding and appreciation of the field of work, as well as relevant methodologies;

- **Chapter 3:** Experimental Procedures. The methodology used during experimental work will be described in detail. Beta approach determination will be described as this was completed to validate the thermodynamic simulations. The chapter will then proceed to describe material preparation techniques for optical and electron microscopy, as well as for oxidation and mechanical testing;

- **Chapter 4:** Thermodynamic Simulations. This chapter includes a description of, and results obtained from thermodynamic simulations outputted from industry standard software such as ThermoCalc and JMatPro. This chapter is an important part of the thesis as results obtained were used in the development of sample materials for investigation;

- **Chapter 5:** Metallographic analysis of as-received material is presented in this chapter along with some characterisation of the microstructure;

- **Chapter 6:** Oxidation analysis. This chapter presents the results obtained from both furnace oxidation testing as well as thermo-gravimetric analysis of sample materials;

- **Chapter 7:** Mechanical Properties analysis. Results from room temperature tensile testing as well as other mechanical properties will be presented;

- **Chapter 8:** Summary of principle observations and discussion;

- **Chapter 9:** Drawing of conclusions and key findings;

- **Chapter 10:** Key areas for further investigation.

2 Literature Review

2.1 Introduction

In order to comprehend the effect of elemental addition to titanium, the fundamentals of titanium and its microstructures must be fully understood. Therefore, this literature review will include relevant background in order to gain an understanding into this field of work. This chapter will initially focus on the basic fundamental theory surrounding titanium and its alloys, paying particular attention to current high temperature aerospace alloy, Timetal 834, an alloy, which will act as the benchmark for replacement materials in terms of properties. The background will then move onto the mechanical properties expected of an alloy used in the application for which it is intended.

2.2 Titanium Crystallography

Titanium melts at a temperature of 1668^{o}C, an indication that titanium will exhibit good creep strengths over a large range of temperatures. At 882.5^{o}C an allotropic transformation occurs. At this temperature the structure transforms from a HCP (hexagonal close-packed) structure, known as the alpha (α) phase, to a BCC (body centre cubic) structure, known as the beta (β) phase, which is stable up to 1668^{o}C (the melting point).

Hexagonal Close-Packed Crystal Structure

The HCP unit cell is a common crystal structure for metals. Other structures include face centre cubic, FCC, and BCC. The cell contains upper and lower faces, which contain 6 atoms, which form hexagons surrounding an individual atom in the centre of the plane. Between these two planes, another plane, which consists of three atoms, exists. Therefore, there are theoretically 6 atoms in one unit cell. These consist of 1/6th of each corner atom from the upper and lower faces (12 in total), ½ of both centre face atoms and all mid plane atoms. A schematic diagram of this unit cell is shown in figure 2.2.1 below:

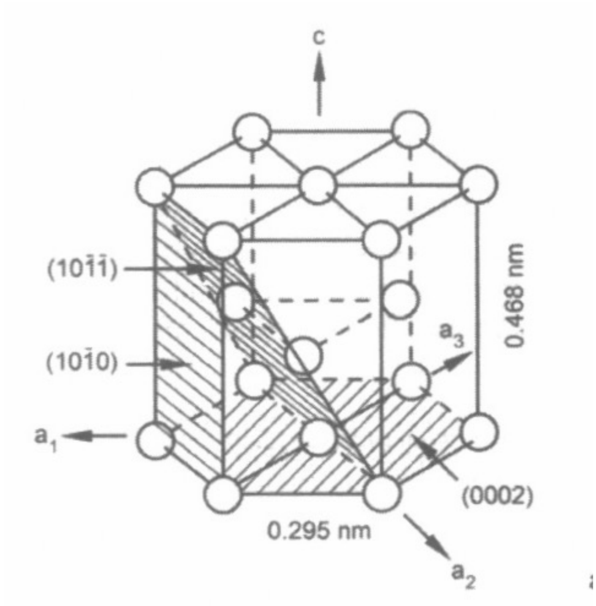

Figure 2.2.1 HCP unit cell [1].

The lattice parameters needed to define the unit cell can be seen in this diagram. The distance from the centre of the cell to the corner of the hexagon plane is known as **a**, while the distance between the hexagon planes is known as **c** *[5]*.

For pure α-titanium the values typically given for a and c are 0.295nm and 0.468nm respectively. This gives a c/a value of 1.587 and a packing density of 56.70 atoms/nm3. There are three planes which are shown to be most closely packed, the (0002) plane (basal plane), one of the {1010} planes (prismatic plane), and one of the {1011} planes (pyramidal plane) *[1]*.

Body Centre Cubic Crystal Structure

The BCC unit cell consists of a cube with atoms situated on every corner, and an individual atom at the centre. Therefore, there are theoretically 2 atoms in a BCC unit cell. These consist of 1/8th of each of the 8 atoms at the cube corners, and the whole centre atom. A schematic diagram of this unit cell is shown in figure 2.2.2 below:

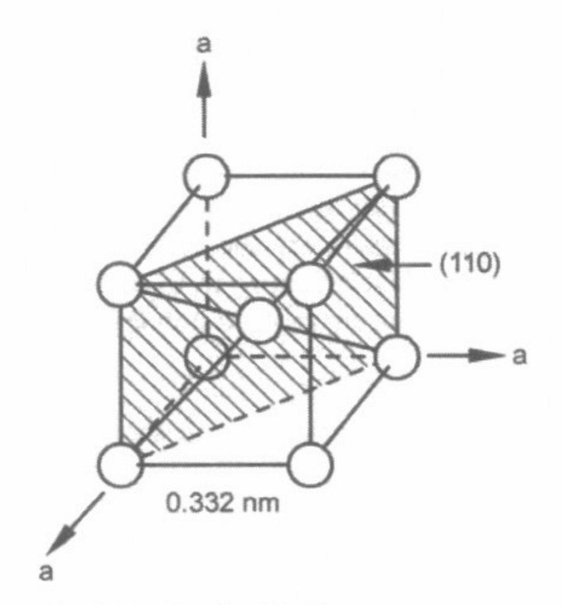

Figure 2.2.2 BCC unit cell [1].

One lattice parameter defines the BCC unit cell. The unit cell side length is known as a. For β-titanium the value given for a is 0.332 nm, giving a packing density of 54.65 atoms/nm^3. Therefore, during the transformation from α to β, a 3.75% increase in volume of the unit cell occurs. The planes that are the most closely packed are the {110} planes and the close packed directions are the <111> directions.

2.3 Classes of Titanium Alloys

The titanium rich sections of pseudo–binary phase diagrams enables titanium alloys to be categorized into three groups, defined by the major phases present at room temperature. Elements that dissolve in the α-phase, known as alpha stabilisers, expand the α-phase and therefore raise the α/β transus (diagram (a) below). Elements that dissolve in the β-phase, known as beta stabilisers, depress the α/β transus. These types of elements can be categorized within two groups. Those that result in the formation of a β-eutectoid (diagram (c)), and others, which form binary systems of the β-isomorphous type (diagram (b)). The main elements that promote these types are given in figure 2.3.1 below.

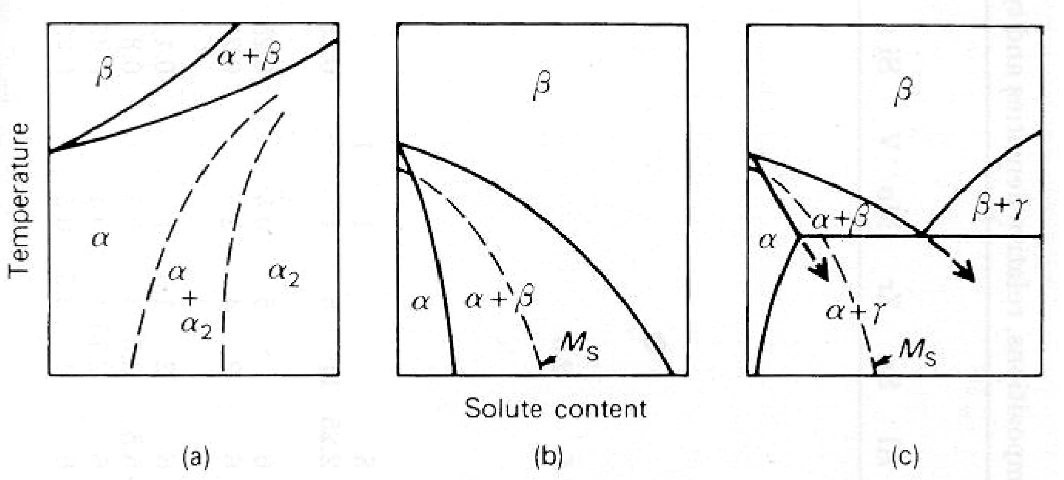

Figure 2.3.1 Basic types of phase diagrams for titanium alloys. The dotted phase boundaries in (a) refer specifically to the Ti-Al system. Alloying elements favouring the different types of phase diagram are (a) alpha stabilisers Al, O, C, Ga, N; (b) beta stabilisers Mo, W, V, Ta; (c) Cu, Mn, Cr, Fe, Ni, Co, H [3].

α - Titanium Alloys

Alloying elements that readily dissolve in the α-phase are aluminium (Al), oxygen (O), nitrogen (N) and carbon (C). α – alloys are further classified into fully-α and near-α alloys *[6]*.

Fully-α Alloys

This class of alloy is generally made up of several grades of commercially pure (CP) titanium. These are single phase alloys with relatively low strengths but reasonable creep properties at higher temperatures due to their high thermal stability.

Near-α Alloys

Near-α alloys consist primarily of α, but they retain a small amount of β (up to 2%). This class of alloy exhibits higher room temperature strength than fully-α alloys, and also show the greatest creep resistance of all titanium alloys at temperatures exceeding 400°C. For this reason, near-α titanium alloys are often used in aircraft applications, where high temperature performance is required.

α/β Titanium Alloys

This class of alloy contains approximately 4-6% beta stabilising elements and therefore extend the α+β phase field to room temperature. This in turn causes substantial amounts of the β phase to be retained on cooling of the alloy. α/β alloys offer relatively high strength and improved formability over α alloys, however creep resistance is reduced.

β - Titanium Alloys

These alloys contain enough β-stabilising elements to retain a fully β microstructure on quenching. Examples of such elements are molybdenum (Mo), tungsten (W), vanadium (V) etc. Beta alloys are further categorised into stable β, metastable β and β-rich α/β alloys *[6]*. These classes of alloy exhibit good formability, toughness and room temperature ductility.

Therefore it is evident that by appropriate alloying of titanium a large range of properties are available for titanium alloys. The schematic in figure 2.3.2 below indicates alloying effects on properties in titanium as a function of its microstructure *[7]*.

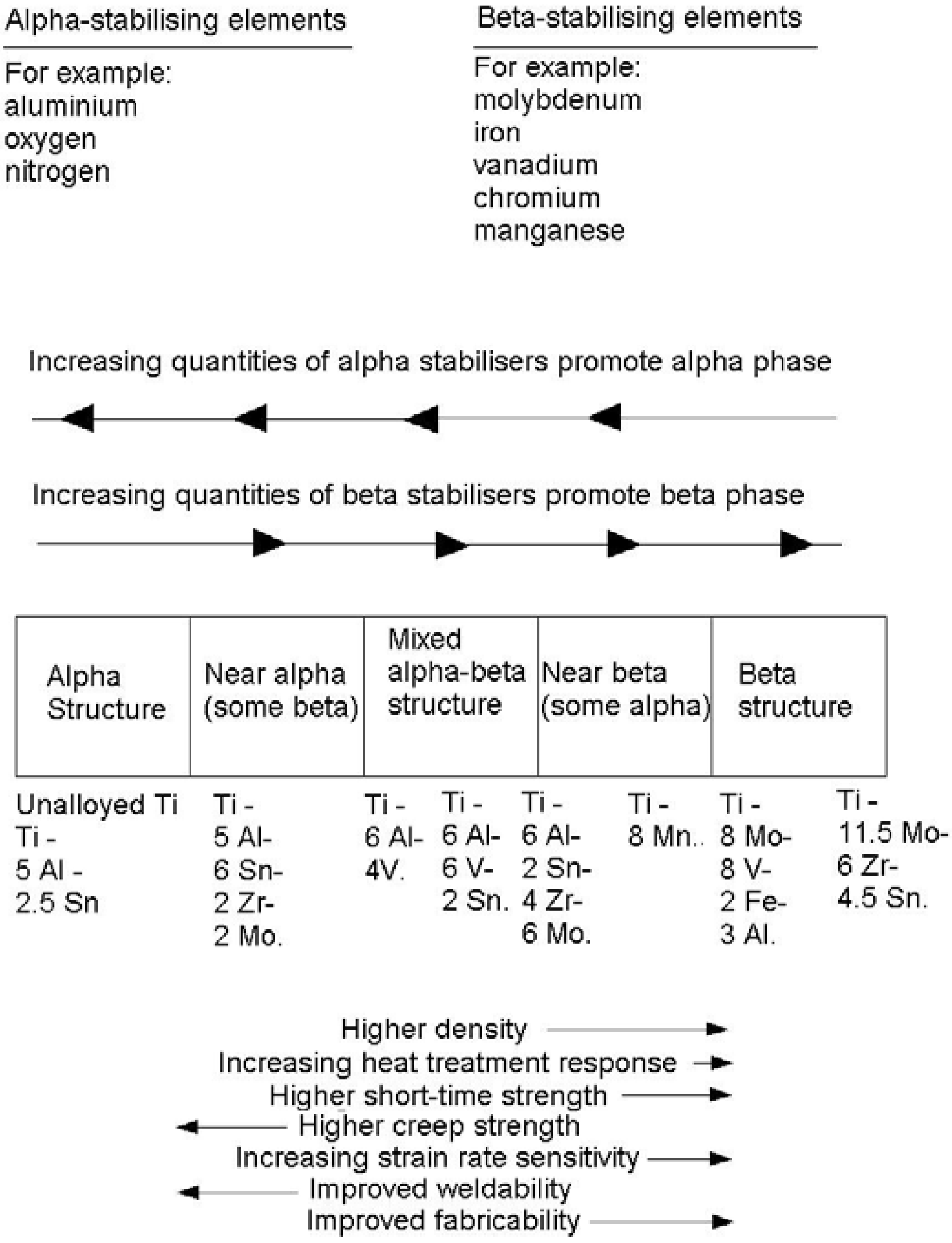

Figure 2.3.2 Effects of alloying elements on titanium [3]

2.4 High Temperature Titanium Alloys

The aerospace industry has been one of the largest drivers for titanium alloy development since the 1950s. With a density of 4.5 grams per cubic centimetre, the potential to exhibit tensile strengths exceeding 1500 MPa at room temperature and the ability to operate at service temperatures of up to 650°C, such alloys have huge potential to meet the ever developing needs of an industry where high strength to weight ratios at high temperatures are required to allow for improved fuel efficiency *[3; 4]*.

IMI 315, an α/β titanium alloy consisting of Ti - 2Al - 2Mn, used in Rolls Royce Avon engines in 1952, produced power for aircraft such as the Comet and Canberra *[3]*. Further developments revealed that small additions of silicon to titanium could drastically improve the creep resistance of such alloys, which led to the development of IMI 550, another α/β alloy consisting of Ti - 4Al - 2Sn - 4Mo - 0.5Si. It is thought that the silicide precipitation that comes with silicon addition contributes to the improved creep performance.

As titanium alloys developed, it was soon established that alloys capable of exceeding previous temperature limitations were obtainable using near α alloys and β -phase processing, producing a fully transformed β microstructure (IMI685 and IMI829). At present, the material most commonly used in medium and high pressure compressor stages of gas turbine engines is Timetal 834, consisting of Ti - 5.8Al - 4Sn - 3.5Zr - 0.7Nb - 0.5Mo - 0.35Si - 0.06C [2]. The addition of carbon was found to change the shape of the beta approach curve to allow for α and β processing as well as heat treatment. Timetal 834 is a near α alloy, developed in the 1980s by IMI Titanium in the UK, with sufficient creep capability up to 600°C *[8]*.

2.5 Timetal 834

Timetal 834 is believed to be the most developed titanium alloy operating industrially today. It is a near-α class of high temperature titanium alloy, with the potential to operate at temperatures exceeding 600°C. Therefore, Timetal 834 is currently finding use in European military jet engines and within the compressor sections of variations of Rolls Royce Trent engines *[1]*.

Effect of Alloying Additions on Timetal 834

As previously understood, elemental additions to titanium alloys are classified as α or β stabilisers. The α stabilisers added to Timetal 834 increase the α to α+β transus temperature and in doing so also increase the size of the α phase field. Although the addition of oxygen and nitrogen to titanium alloys can be beneficial to strengthening at low temperatures, it is documented that for alloys containing a high percent of intermetallic phases (e.g. silicides), oxygen and nitrogen addition is detrimental to the ductility of such alloys *[9]*.

It is well documented that aluminium is added to titanium alloy to both reduce the density of such alloys, as well as to offer improvements to tensile and creep strengths [3, 7]. However, it is thought that adding aluminium to silicon containing titanium alloys is detrimental to the formation of much sought after silicides in terms of retarding precipitate nucleation and growth. Similarly, the formation of ordered Ti_3Al precipitates can detrimentally affect alloy ductility *[10]*.

Small amounts of β stabilisers, such as molybdenum and niobium are also present in Timetal 834. The addition of molybdenum to titanium is documented to promote an increase in both strength as well as hardenability at low temperatures *[11]*. Molybdenum can help to mitigate ordering by occupying lattices that are normally occupied by aluminium. This then increases the amount of aluminium that can be added, giving further creep strength without detrimentally effecting ductility *[1; 3; 12]*. Niobium can be added to titanium to improve the high temperature oxidation resistance of such alloys. Niobium also has the same ordering mitigation effect as molybdenum [3].

In general during the development of such alloys, it is important to consider the aluminium equivalent which is known to reduce ductility in titanium alloys. The effect of aluminum is calculated using the following equation;

$$\text{Al eq.} = \text{wt.\%Al} + 1/3\text{wt.\%Sn} + 1/6\ \text{wt.\%Zr} + 10\text{wt.\%O}$$

An aluminium equivalent of more than 9 wt.% tends to encourage the precipitation of Ti_3Al which is an alloy-embrittling intermetallic *[3]*.

Carbon addition contributes to solid solution hardening and therefore increases strength. Carbon also increases the β transformation temperature and therefore expanding the α+β phase field allowing more control on the volume fractions of α and β phase during heat treatment. The development of Timetal 834 involved heat treatment sub β transus to maintain a small amount of primary alpha (α_p) which retards β grain growth. Upon cooling, this results in a bimodal microstructure consisting of approximately 15% α_p dispersed within fine grained secondary alpha (α_s) *[8]* that helps to provide the excellent strength, fatigue and creep resistant properties enjoyed by Timetal 834. The small addition of carbon gives the alloy a relatively shallow β approach curve, leading to accurate control of the α_p volume fraction without the need for impractical temperature control during thermal processing. The beta transus approach curve of IMI 834 compared to that of its predecessor IMI 829 is shown in figure 2.5.1 below. The effective α/β temperature range is significantly larger than that of IMI 829, owing to the addition of carbon within IMI 834 *[18]*.

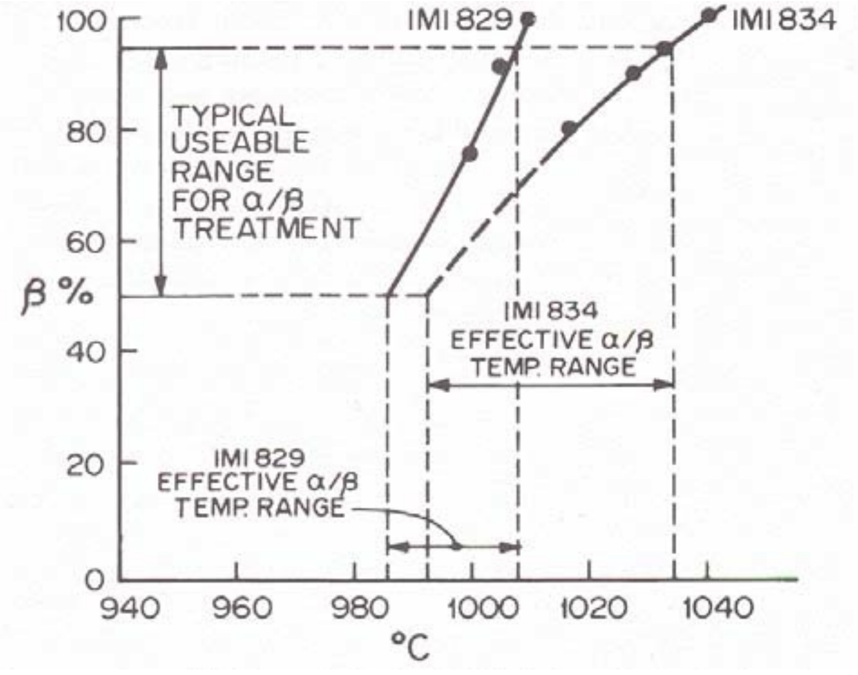

Figure 2.5.1 Beta approach curves for IMI 829 and Timetal 834 *[3]*.

Tin and zirconium are neutral elements possessing high solubility in the both the α and β phase fields. However, both increase hot strength *[8]* and retard the rates of transformation *[7]*. The addition of zirconium to silicon containing titanium alloys also promotes uniform nucleation of silicides or silicide bearing precipitates and offers improved stability to the alloy *[8; 12]*.

Silicon is also present in Timetal 834 as it has a major influence on the creep resistance forming the compound Ti_5Si_3 as well as giving considerable static strength [9; 11; 13].

2.6 Mechanical Properties

Creep Resistance

Timetal 834 is capable of operating for extended service at 550-625^{o}C *[3]*. Creep deformation in Timetal 834 at a temperature of approximately 600^{o}C is governed by dislocation motion within the α phase. The creep resistant properties of Timetal 834 are seen to improve with time at solution heat treatment temperatures (between 30 and 240 minutes) and when ageing treatment temperature is increased *[11]*, a fine dispersion of $(Ti,Zr)_5Si_3$ silicides have been observed within the transformed beta lamellae in creep specimens. These silicides are believed to precipitate out of the solid solution at dislocation sites during deformation, which helps to hinder further dislocation motion and therefore deformation. The amount of precipitation depends on the ageing cycle, where less time and lower ageing temperature results in increased precipitation of silicides during the treatment and therefore reduced silicon able to precipitate during deformation [11].

Ultimate Tensile Strength (UTS)

The room temperature tensile strength of titanium alloys covers a large range. The minimum recorded data being approximately 240 MPa in commercial grades (CP Ti) to 1400 MPa in an alloy Transage 129 (Ti-2Al-2Sn-11Zr-11V). According to manufacturer datasheets [13], the tensile strength of Timetal 834 is a minimum of 1030 MPa. However, it is possible to increase the UTS by altering heat treatment cycles. For example if Timetal 834 is solution heat-treated, oil quenched and aged, it is capable of tensile strengths of up to 1050 MPa [13].

2.7 Nimonic Alloys

As nickel is the ‘competitor material’ in this application, it is worth investigating the basics of such materials.

Materials from the nickel-chromium system are known as nickel-based super alloys, or Nimonic alloys. Due to their relatively high strength to weight ratio, when compared to that of steel, Nimonic alloys’ main application is within the gas turbine industry. However, the alloys are found in other applications, particularly those in which a material is required to withstand harsh working environments. This is due to the fact that nickel-based super alloys maintain high corrosion resistance, mechanical fatigue and shock, thermal fatigue and shock as well as creep resistance at high temperatures *[14]*. As previously discussed, nickel-based super alloys are replacing titanium due to nimonic alloys exhibiting the higher temperature capabilities required as the gas turbine industry develops.

Nimonic alloys consist of a face centre cubic solid solution nickel matrix with chromium, tungsten and rhenium added as solid solution strengthening elements *[14; 15; 16]*. Precipitation hardening is achieved in Nimonic alloys through the addition of aluminium or titanium. This results in the precipitation of an intermetallic compound, $Ni_3(Al, Ti)$ which is commonly referred to as the gamma prime phase (γ’) *[16]*. These precipitates exist coherently within the nickel-chromium matrix (γ). It is the good heat and creep resistant properties associated with γ’ precipitates which is thought to provide high temperature strength and long term stability of the alloy.

Carbon is introduced to nimonic alloys in order to improve strength at grain boundaries. This is achieved through the formation of $Cr_{23}C_6$ carbides *[5]*. These carbides, situated at grain boundaries, prevent grain boundary sliding and therefore offer significant improvements to rupture strength *[17]*. This phase, $Cr_{23}C_6$ can also be found coherently within grains, where the small precipitates act as obstacles to dislocations. Coherency with the matrix is achieved as the cube faces of the carbide relate to the orientation of the matrix instead of the dislocation line directions to which they owe their formation. This coherency with the matrix provides strong bonding forces which in turn prevents the formation of cracks, and so pinning dislocation lines and improving the strength of the interface *[15; 16]*.

It is hoped that analogies used in the development of nimonics can be utilised to develop a new, highly β stabilised, silicon containing titanium alloy capable of the higher temperatures required of the recent developments in the gas turbine industry. It is believed that creating silicides that are coherent with the matrix of the alloy, problems with alloy ductility can be avoided.

2.8 Addition of Silicon to Titanium

2.8.1 Effect of Silicon on the Properties of Titanium Alloys

According to Jiang et al, many of the improvements in properties of titanium-silicon alloys are thought to be related to its microstructure. For example, a titanium alloy with 8.5 wt% Si contains mainly α-Ti and some titanium silicides, namely Ti_3Si and Ti_5Si_3. The microstructure of alloy castings of this nature is of colony-like eutectic structure, which generally consists of a eutectic mixture of finely divided α-Ti and Ti_5Si_3 [18]. As silicon content is increased in the alloy, the features of this structure vary from slice chrysanthemum to short rod (Figure 2.8.1). The particles contained within this structure are usually equiaxed. The increased strength of Ti-Si alloys over pure titanium owes itself to this feature. As silicon content in titanium alloys increases, the strength of these alloys increases to a peak, and then starts to decrease. This is thought to be the result of Ti_5Si_3 particles, which in lower Si content are fine, causing both increases in strength and ductility. However, as silicon content increases, particles become more coarse resulting in decreases in strength, although enhanced creep resistance and fatigue crack growth accompany this [18; 19].

Although many researchers agree that silicon has a profound effect on strength of titanium alloys, there are a number of hypothesis as to what causes this effect. Saha and Xua [17; 19] both agree that silicides formed by the addition of silicon, is the contributor to increased strength, however, Paton and Mahoney (1976) believe that the greatest strength is achieved when silicon remains in solution [1; 17; 19].

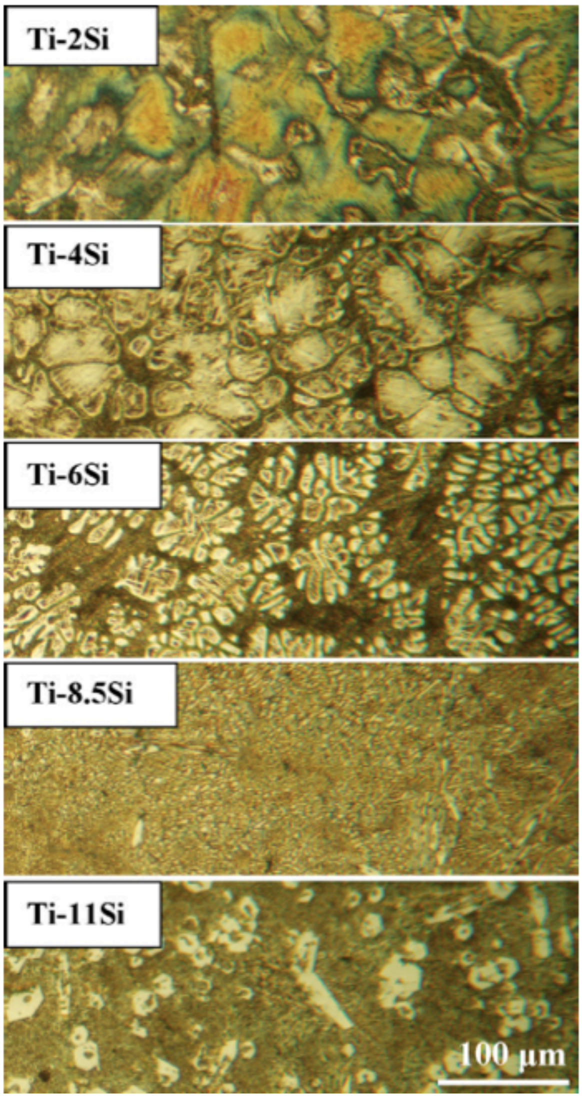

Figure 2.8.1: Optical Micrographs of the cross-section of Ti-Si rods [19]

This increase in strength however comes at a cost for room temperature ductility of the alloy. As the Si content is increased, elongation decreases along with reduction in area (Figure 2.8.2). However, investigations conducted by Saha et al. have concluded that the addition of bismuth in small quantities to Ti-Si alloys may overcome this degradation on ductility, without sacrificing strength. Small additions of bismuth to 6.5wt % Si alloy improve ductility due to the morphology of finer silicides within the eutectic region. These silicides reduce or eliminate interconnectivity as well as increase the volume fraction of dendrites *[19]*.

An alternative to this could be the use of a highly beta (β) stabilised matrix, which is known to be a more ductile matrix *[3]*

Si (wt %)	Ultimate tensile strength (MPa)	0.2% Yield strength (MPa)	Elongation (%)
0.0	315	207	30
0.6	535	423	21
1.0	686	608	18
2.0	780	726	1.0
3.0	589	-	<0.1
4.5	711	687	0.7
6.5	834	736	0.8
8.5	775	726	0.4

Figure 2.8.2: Table displaying effect of Si addition on tensile properties of Ti-Si alloys [19]

It has been reported that it is common for silicon to segregate, as a result of the freezing process of vacuum arc re-melting. This causes a higher than normal level of silicon content in some locations within casts. This issue results in a reduction in fracture toughness in parts of the material. With this information, it has been suggested that increased silicon addition may result in increases in yield strength and ultimate tensile stress accompanied by undesirable decreased in fracture toughness *[12]*.

These issues have been associated with high levels of silicon i.e. >0.20%. These increased concentrations cause a greater chance of silicides to form during short heat treatments. It was also noted that if silicon levels were increased to over 0.31%, the fracture mode of the material shifted from trans-granular ductile, to inter-granular brittle fracture *[12]*.

Creep Resistance

Creep resistance in titanium silicon alloys is widely recognised as being improved with silicon content. Increasing addition of silicon consistently increases creep resistance, with the microstructure with highest creep resistance being that with the greatest amount of silicon in solution (Figure 2.8.3). This is further showed in existing titanium alloys used in gas turbine engines, i.e. TIMETAL 834 which contains up to 0.35Si *[6, 20]*. Again, there are opposing opinions as to the reasons for these improvements, whether it be caused by the formation of silicides [1; 19], or silicon in solution *[20]*. The theory relating to the formation of silicides believes that Ti_5Si_3 silicides nucleate at grain boundaries during ageing. These precipitates are thought to retard dislocation movement at elevated temperatures, resulting in enhanced creep resistance.

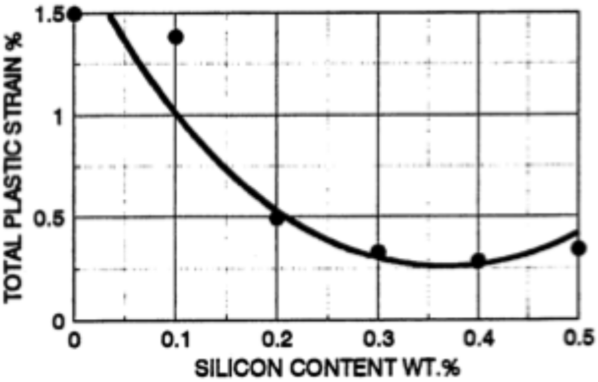

Figure 2.8.3: Effect of silicon on the creep performance of IMI 834 [6]

Oxidation Resistance of Ti Alloys with Silicon

It is believed that silicon can play a protective role in the oxidation of titanium alloys with added silicon. The roles played by silicon, according to Vojtech et al. are:

- Silicon reduces the penetration depth of oxygen into alloy substrate;
- Silicon, dissolved in a titanium oxide surface layer, reduces the diffusion rate of oxygen through this layer.
- Silicon modifies the stress relaxation processes in the oxide layer, leading to a more compact scale with lower porosity. *[21; 22]*.

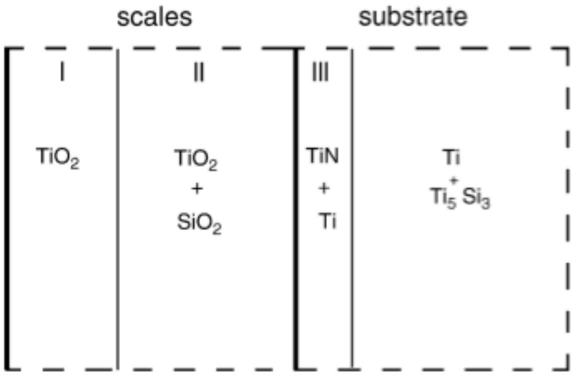

Figure 2.8.4: Schematic diagram indicating the internal structure of scales on the oxidized Ti–Si alloys. [21]

Vojtech et al. conducted investigations on how different concentrations of Si content in Ti alloys affect the resistance to oxidation. The outcomes of this concluded that the rate of oxidation in Ti alloys is significantly reduced due to the addition of silicon, however this reduction is not proportional to the silicon concentration within the alloy *[21; 22]*.

It was found that after oxidation at 850°C for 320 hours, the Ti-Si2 alloy developed scales on the surface of the material that were dense, compact and free of significant cracking. The scale contained two parts, a titanium oxide outer sub layer and an inner sub layer containing nitrogen (Figure 2.8.4 and 2.8.5). This thin TiN layer could be acting as a barrier to the penetration of oxygen into the metallic substrate, and thus protecting the alloy from further oxidation. This observation of the scale could be due to the presence of silicon oxide particles, which are finely dispersed within the scale, inhibiting the re-crystallisation of titanium oxide and therefore producing a more compact scale *[21; 22]*.

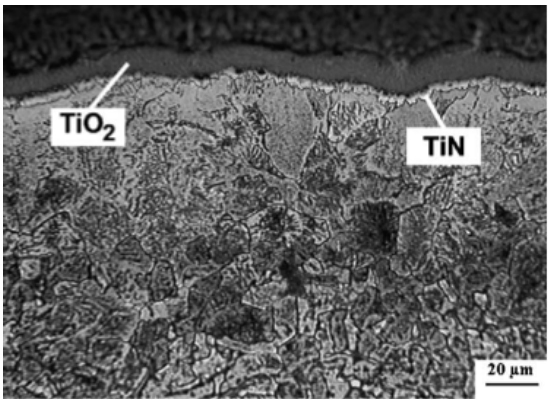

Figure 2.8.5: Optical micrograph of the area near the surface for TiSi2 alloy oxidised at 850◦C for 320 h [21]

Increasing the concentration of silicon (Ti-Si8) proved that after the same oxidation environment, the scales were less compact, and contained cracks running parallel to the scale metal (Figure 2.8.6). These cracks could be the result of a reaction between coarse silicides and oxygen, resulting in the formation of silica. The high specific volume of silica combined with its low thermal expansion coefficient may cause stresses in the scales, resulting in the observed cracks [21, 22].

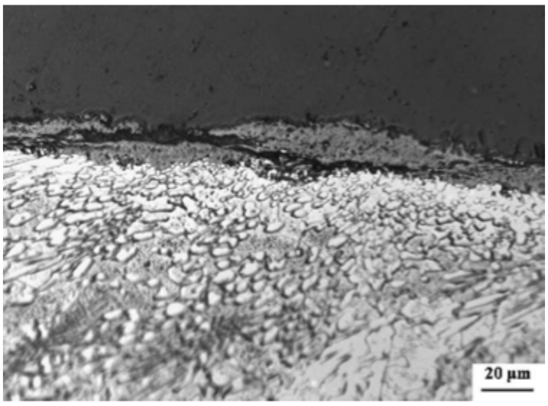

Figure 2.8.6: Optical micrograph of the area near the surface for TiSi8 alloy oxidised at 850◦C for 320 h [21]

The investigation conducted by Vojtech et al. concludes that it is the reaction between silicide particles and oxygen (during oxidation) in titanium silicon alloys that causes the release of silicon to the scales. This eventually leads to a slow increase in oxidation resistance with time *[21]*.

In order to produce a more useful and better representation of the oxidation environment in a jet engine, Vojtech et al have investigated the effect of silicon addition on cyclic oxidation. In this experiment, the same alloys were investigated as previously, and cyclic oxidation was measured at $850^{o}C$ and $1050^{o}C$. The cycle involved heating at high temperature for 12 hours followed by rapid cooling at a rate of $400^{o}C/min$, in airflow [22].

This experiment had very similar conclusions to the previous experiment, with reference to the lower temperature oxidation ($850^{o}C$). At this temperature cycle, it was found that the thickness of the scale for both alloys did not exceed 30μm, and was compact with little significant cracking (Figure 2.8.7 (a-c)).

At the higher temperature however, it was found that cracking occurred, even in the low silicon content alloy, probably caused by the rapid cooling experienced as part of the cycle. Despite these cracks, the scale was still fairly compact near to the metallic substrate. For the higher silicon content alloy, many more cracks were present in the scale, and the scale was observed to be much more porous (Figure 2.8.7 (d-f)).

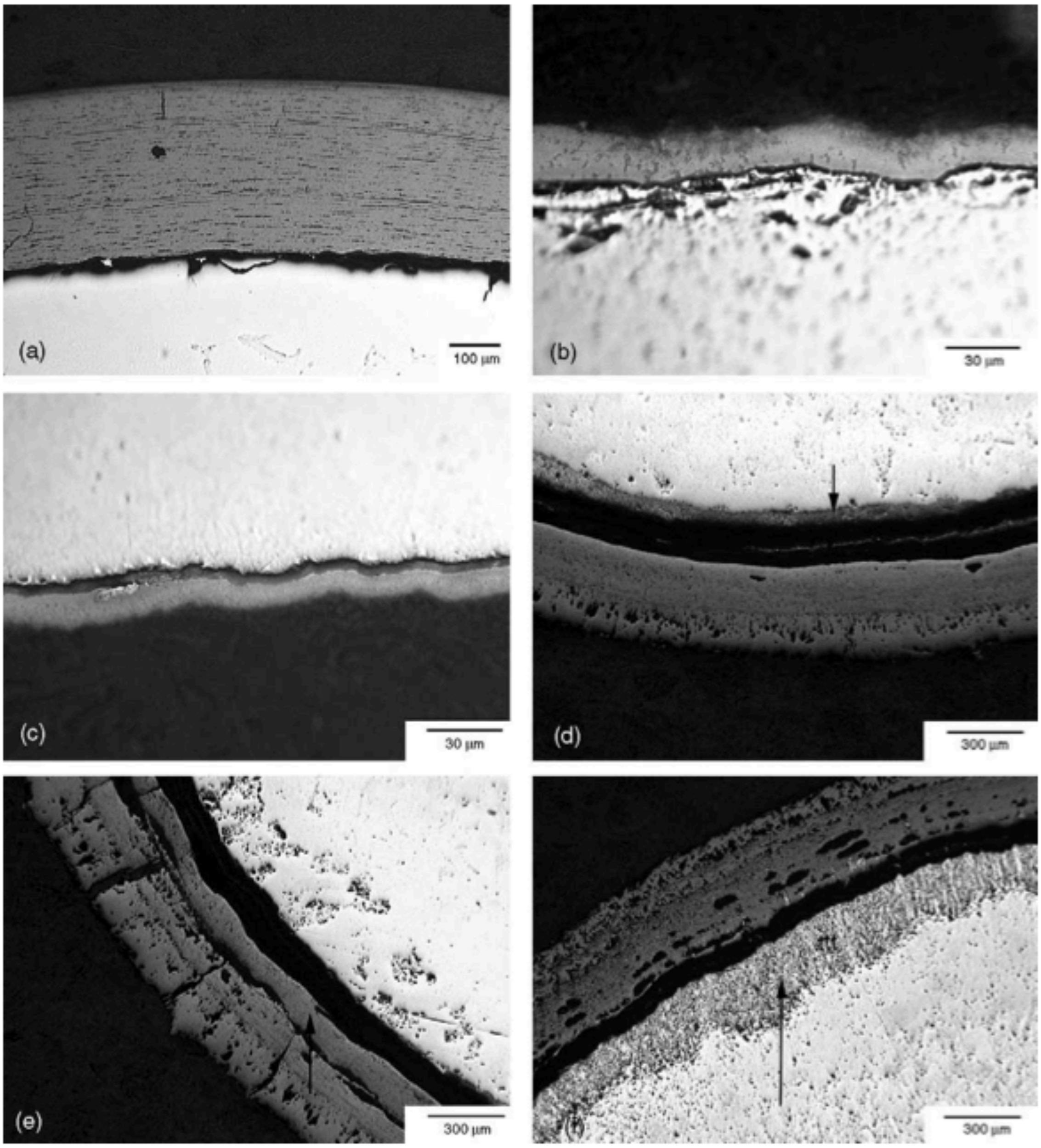

Figure 2.8.7: Optical micrograph of cross section of scales on pure Ti (a), the TiSi2 alloy (b, d, e) and the TiSi8 alloy (c and f) after cyclic oxidation at 850^{o}C (a–c) and 1050 ^{o}C (d–f) for 72 h. Arrows indicate nitride layers (d and f). [22]

The conclusive points to be made from this investigation include the fact that thermal cycling does in fact reduce the protective effect of the scales formed during oxidation, by introducing cracks to the scales upon rapid cooling. The cracks create micro channels for the passage of oxygen atoms deep into the scale. The reduction in protection becomes more evident as temperatures are increased

It can be considered that Ti-Si alloys can provide sufficient oxidation resistance for elevated temperature applications where cyclic oxidation occurs [22]. However, at higher temperatures (above 850°C) increasing the silicon concentration is not effective in improving the resistance to oxidation [21; 22].

2.8.2 The Titanium – Silicon System

The equilibrium phase diagram for titanium silicon alloys is shown in Chapter 4, Figure 4.2.3. From the diagram, it is clear that that the solubility of silicon in titanium is low, at a maximum of ~0.47wt%Si. Solubility decreases as temperature decreases in α-titanium. It is this, combined with the mass of beta stabilising elements added to the alloy, which significantly influences the alloy structure and its properties. The silicide phases of Ti_3Si and Ti_5Si_3 can also be seen *[23]*.

Because of the low solubility of silicon in titanium, properties are influenced both by silicon in solution, as well as silicides in these phases.

In beta titanium, 3wt%Si can be dissolved at the eutectic temperature, 1339°C. At 865°C, the eutectic transformation $\beta \rightarrow \alpha + Ti_3Si$ occurs *[23]*.

2.8.3 Structure and Properties of Ti_5Si_3 silicides

It has been established that the benefits of adding silicon to titanium alloys owe to the precipitation of silicides, in particular Ti_5Si_3 silicides formed at grain boundaries [20]. In order to be able to match these precipitates coherently with the matrix of a β titanium alloy, it is necessary to first determine the structure of such silicides.

Crystal structure of Ti_5Si_3

Investigations by Williams, 1992 on characterisation of Ti_5Si_3 silicides, conclude that such silicides exist as hexagonal D88 structures of the space group $P6_3/mcm$. The unit cell of Ti_5Si_3 contains two titanium sites, at 4d sites (⅓, ⅔, 0), and at 6g sites (XTi, 0, ¼) where XTi ≈ 0.25, and one silicon site at 6g sites, (XSi, 0, ¼) where XSi ≈ 0.61.

The Ti_5Si_3 structure consists of two chains of atoms. One linear chain of Ti 4d atoms, formed parallel to the c axis, and another chain of 'face shared trigonal antiprisms' formed by Ti6g atoms along the c axis. 'Silicon atoms form a chain of distorted face shared trigonal antiprisms, parallel to the c axis such that one Ti 4d is at the centre of each antiprism' *[9]*.

This leads to an ABAC stacking sequence along the c direction. The A plane consists of only Ti4d atoms. The B and C planes consist of Ti6g and Si atoms. These atoms form the shared faces of the antiprisms. The $D8_8$ structure of Ti_5Si_3 is shown schematically in Figure 2.8.9.

Interestingly, observations by Barin, 1993 showed that Ti_5Si_3 is one of the most stable silicides, due to its D88 structure, using the diagram below (Figure 2.8.8).

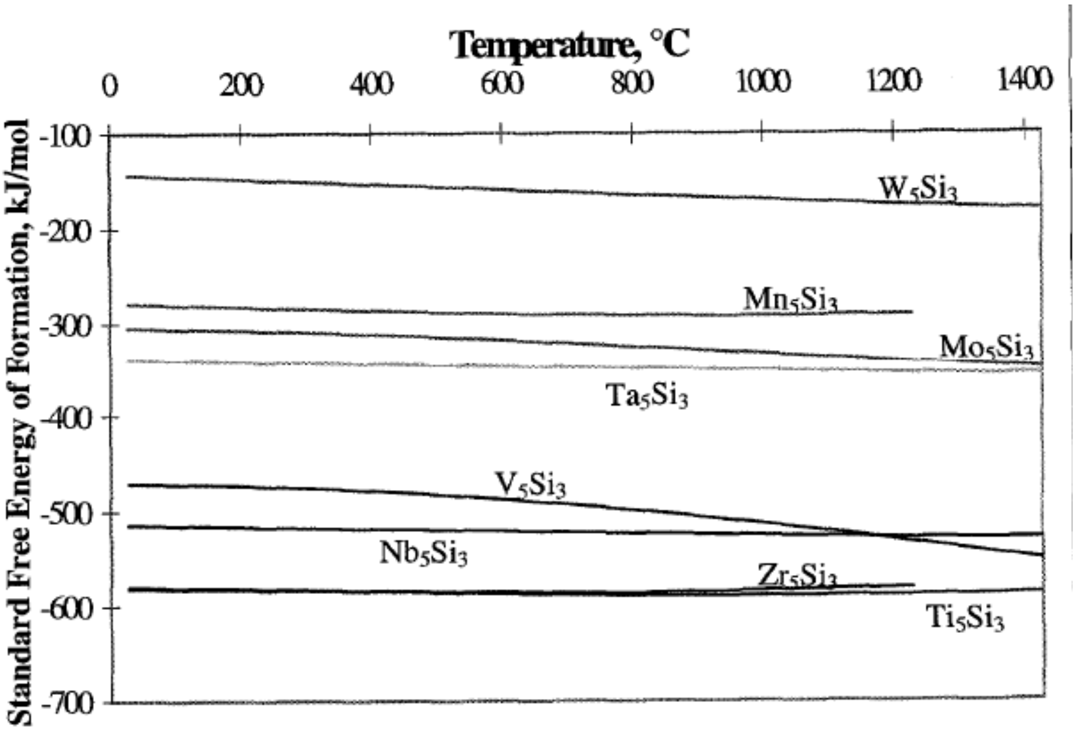

Figure 2.8.8: Stability of various silicides, shown by their standard free energies of formation. Ti_5Si_3 is generally one of the most stable structures [9].

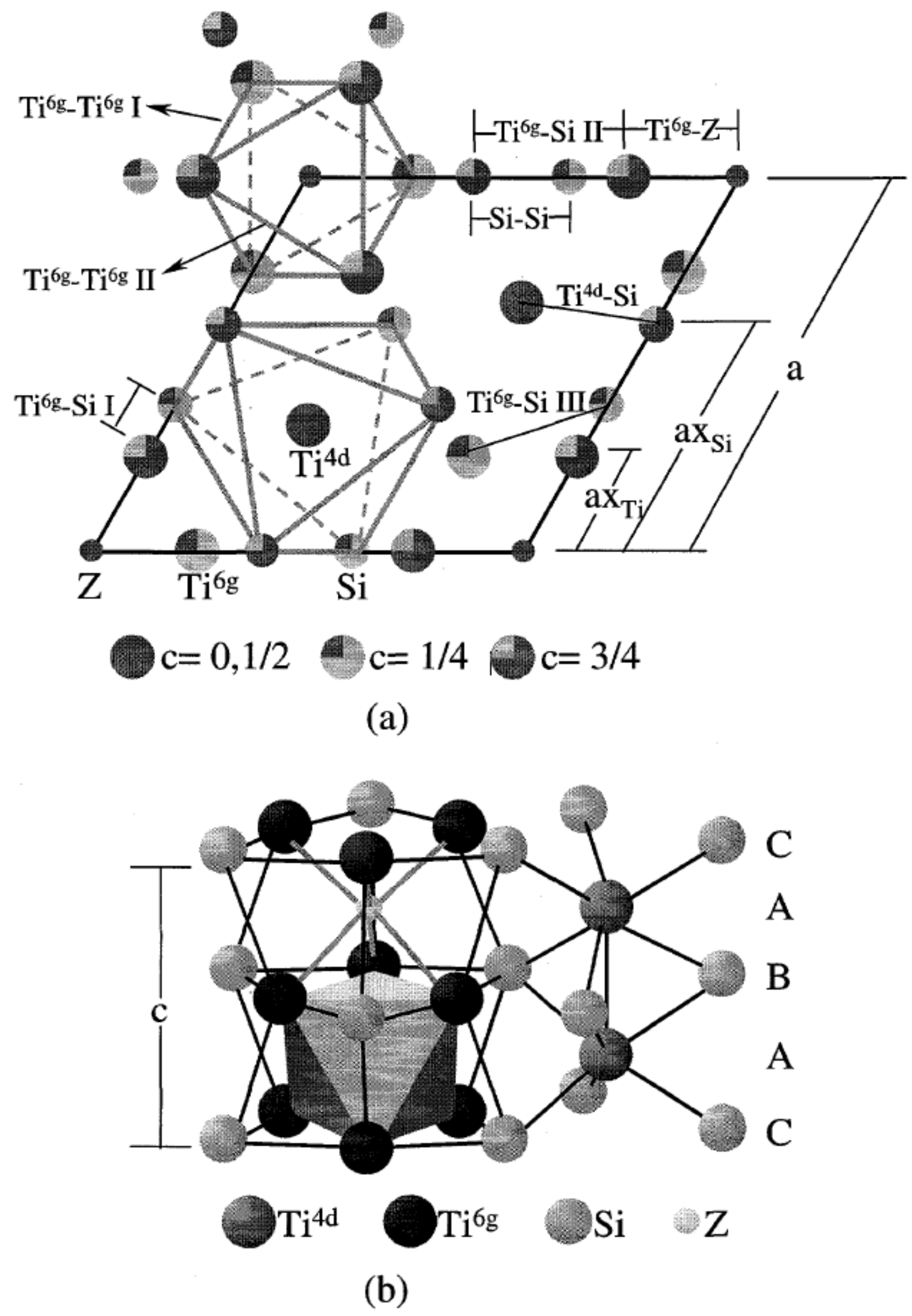

Figure 2.8.9: D8$_8$ crystal structure of Ti$_5$Si$_3$. [9]

2.9 Justification for Addition of Alloying Elements

As chromium is a beta stabilising element, its addition to titanium alloys helps to β stabilise the matrix, as well as provide some resistance to oxidation *[13]*. Silicon should also be added to improve oxidation resistance as well as other mechanical properties, as outlined within this chapter.

Zirconium serves to help suppress the martensite start temperature and also modify and/or stabilise any silicides that form in the alloy *[10]*.

In terms of the addition of these elements to titanium, the binary phase diagram for titanium and chromium is shown in Chapter 4 (figure 4.4.1). The diagram indicates that 16wt% chromium, being the β-eutectoid composition, could be a beneficial composition. Also, additions of chromium above about 20wt% are believed to dramatically improve the oxidation resistance of titanium, therefore an addition of 25wt% chromium could be appropriate. However, at this composition the chromium may segregate therefore another sample containing 40wt% chromium could be less prone to this, due to the liquidus being flat through a minimum at this point. However, at 40wt% chromium poor ductility may be an issue.

Similar to their additions in Timetal 834, molybdenum and niobium could also be beneficial in adding beta stability to the alloy. Molybdenum is documented to promote an increase in both strength as well as hardenability at low temperatures *[11]*, and niobium can be added to improve the high temperature oxidation resistance of such alloys.

2.10 $TiCr_2$ Precipitates

While the literature has explained the role of silicides in silicon containing alloys, information on chromium precipitates has not been investigated as part of this work. Based on the thermodynamic simulations conducted during this work, it can be expected to see the $TiCr_2$ phase in titanium-chromium alloys. The literature surrounding this phase, *[24; 25; 26]* has highlighted that:

- $TiCr_2$ has 2-3x higher oxidation resistance than pure Ti @1073K;
- For Ti-30Cr (at%) $TiCr_2$ exists as lath shape structure at grain boundaries with an orientation which allows some degree of coherency in BCC matrix;
- For Ti-40Cr (at%) Bimodal distribution of equiaxed $TiCr_2$ precipitates are expected;
- The lath structures can be deformed to much larger strains than equiaxed precipitates;
- Deformation of lath precipitates occurs due to twin formation, faults and shear bands.

2.11 Summary

This literature review has highlighted the fundamental issues to consider in the development of a new high temperature titanium alloy for use in an aerospace application. The key points for consideration are:

Previous investigations suggest that alloy strength increases with silicon content up to a maximum of ~6wt% Si. This increase in strength is thought to be the result of the microstructure observed in silicon containing titanium alloys. This microstructure contains titanium silicides Ti_5Si_3. It is the fine nature of these silicides which is believed to contribute to increased strength. However, as content exceeds ~6wt% Si, these silicides become more coarse, and so alloy strength tends to decrease.

It is widely recognised that creep resistance in titanium alloys is improved with the addition of silicon. This explains why silicon is commonly added to commercial titanium alloys for use in high temperatures. It is thought that the addition of silicon to titanium causes nucleation of Ti_5Si_3 silicides at grain boundaries during ageing. These precipitates are thought to retard dislocation movement at elevated temperatures, resulting in the enhanced creep resistance observed in titanium silicon alloy systems, compared to that of a nickel based super alloy.

As silicon content is increased, elongation tends to decrease in titanium alloys. Previous investigations show that there is a substantial drop in room temperature ductility when silicon content exceeds ~1wt% Si in α-titanium. Knowing that β-titanium alloys exhibit good room temperature ductility, this could be a solution worthy of further exploration.

In terms of benefits in oxidation resistance brought by the addition of silicon to titanium, it can be considered that silicon containing titanium alloys can provide sufficient oxidation resistance for elevated temperature applications where cyclic oxidation occurs. However, at higher temperatures (above 850^{o}C) increasing the silicon concentration is not effective in improving the resistance to oxidation.

The idea of increasing the silicon content in titanium alloys used in the applications outlined was based on nimonic analogies. From this analogy, it is obvious that coherency is of utmost importance in relation to precipitates within the alloy matrix.

As a final conclusion, it is believed that there is in fact the potential for a titanium silicon alloying system to become a next generation alloy for use in compressor stages of high output jet engines. It is hoped that the analogies used in the development of nimonic alloys can be utilised to develop a new, highly β stabilised silicon containing alloy, capable of the higher temperatures required of the recent developments in the gas turbine industry.

3 Experimental Procedure

3.1 Introduction

This work has adopted a number of different techniques in terms of laboratory, testing and analytical procedures. This chapter aims to describe these operating procedures, in detail, so that all results obtained are reliable and the tests used are repeatable.

3.2 Thermodynamic Simulation

Knowledge gained during compilation of the literature review was used as an aid in the use of specialised simulation software, 'Thermocalc'. This software calculates a wide range of material properties for alloys and is particularly aimed at multi-component alloys. Calculations can be made for:

- Stable and metastable phase equilibrium
- Solidification behaviour and properties
- Mechanical properties
- Thermo-physical and physical properties
- Phase transformations
- Chemical properties

The software has been used to simulate the phase transformations occurring over temperature, and then the data used to estimate volume fractions of each phase present in the materials for given temperatures. The software holds a number of databases, which hold thermodynamic property data for a range of elements that could be used to build an alloy of interest (or indeed an existing alloy for use as a comparison).

Thermocalc utilises three different modules. The database module where the user chooses the correct database, in this case database TTTI3 – the titanium database, and also inputs the elements of interest. The Poly-3 module where the user inputs the chosen data to be used to calculate the phase equilibria, and the Post module where diagrams are drawn based on the calculations obtained in Poly-3.

For the purposes of this project, Thermocalc has been used to draw 'step' diagrams. These diagrams are graphs showing the percentages of each phase present vs. Temperature for the collection of elements that have been input. An example 'step' diagram output for a common titanium alloy, Ti-6Al-4V is shown below as figure 3.2.1.

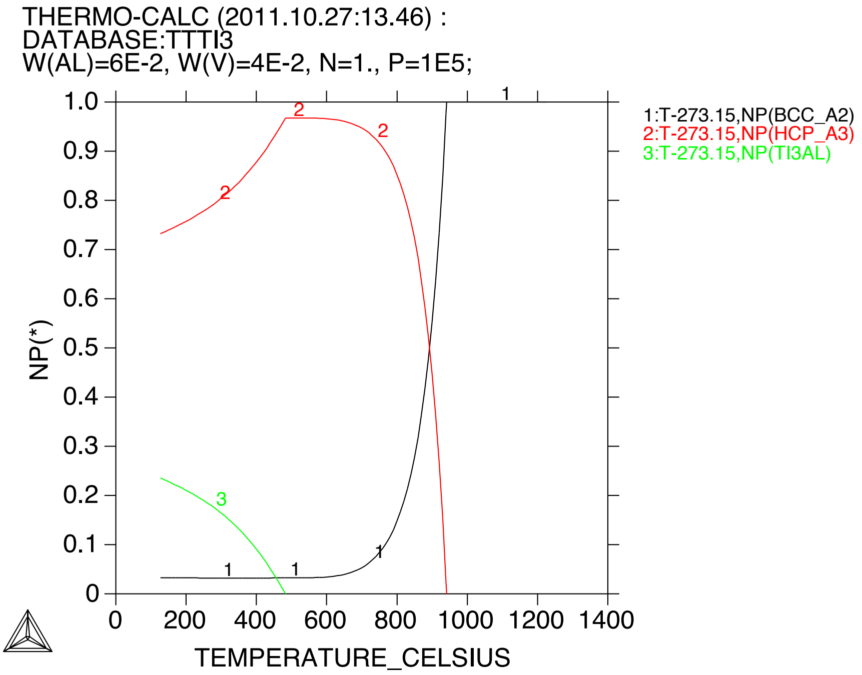

Figure 3.2.1 Step diagram showing Volume Fraction vs. Temperatures for Ti-6-4.

The example above shows that three phases are expected across the temperature range simulated. The ß phase indicated by the black (BCC) line, the α phase indicated by the red (HCP) line, and the titanium aluminide (Ti_3Al) phase indicated by the green line.

3.3 Pseudo Phase Diagram

A procedure similar to beta approach determination was used in order to validate the phase diagrams that were obtained using the thermodynamic software. The volume fraction of the matrix present was determined, rather than the volume fraction of beta grains only. The diagrams were obtained using furnace treatments at a range of temperatures, followed by optical microscopy and analysis. Samples were sectioned to 3mm cubes using a Struers Minitom cut off machine using a diamond cut off wheel. The samples were then placed into a preheated chamber furnace set at a range of different temperatures (Table 3.3.1). A thermocouple was fed through the furnace chimney and located so that the end was almost touching the samples so as to ensure that the temperature recorded was as close to the sample temperature as possible.

Table 3.3.1 Temperatures used to determine the pseudo phase diagrams.

Sample	Temperature (ºC)
1	500
2	550
3	600
4	650
5	700
6	750
7	800

When the temperature of the furnace had stabilized following the introduction of the sample, the sample was held at temperature for a period of 30 minutes. The sample was then removed from the furnace and immediately quenched in water to room temperature. The resultant microstructure differed between materials, but generally consisted of various precipitates in a beta matrix.

The samples were then sectioned in half (a depth beyond which oxygen pick up could have affected the microstructure observed), and prepared for examination using a Nikon optical microscope with attached camera. Polarized light was used to obtain contrast between different phases present in the microstructure. Figure 3.3.2 shows a typical microstructure viewed using this method at 100 times magnification. Good contrast can be observed between the matrix and precipitates in the microstructure.

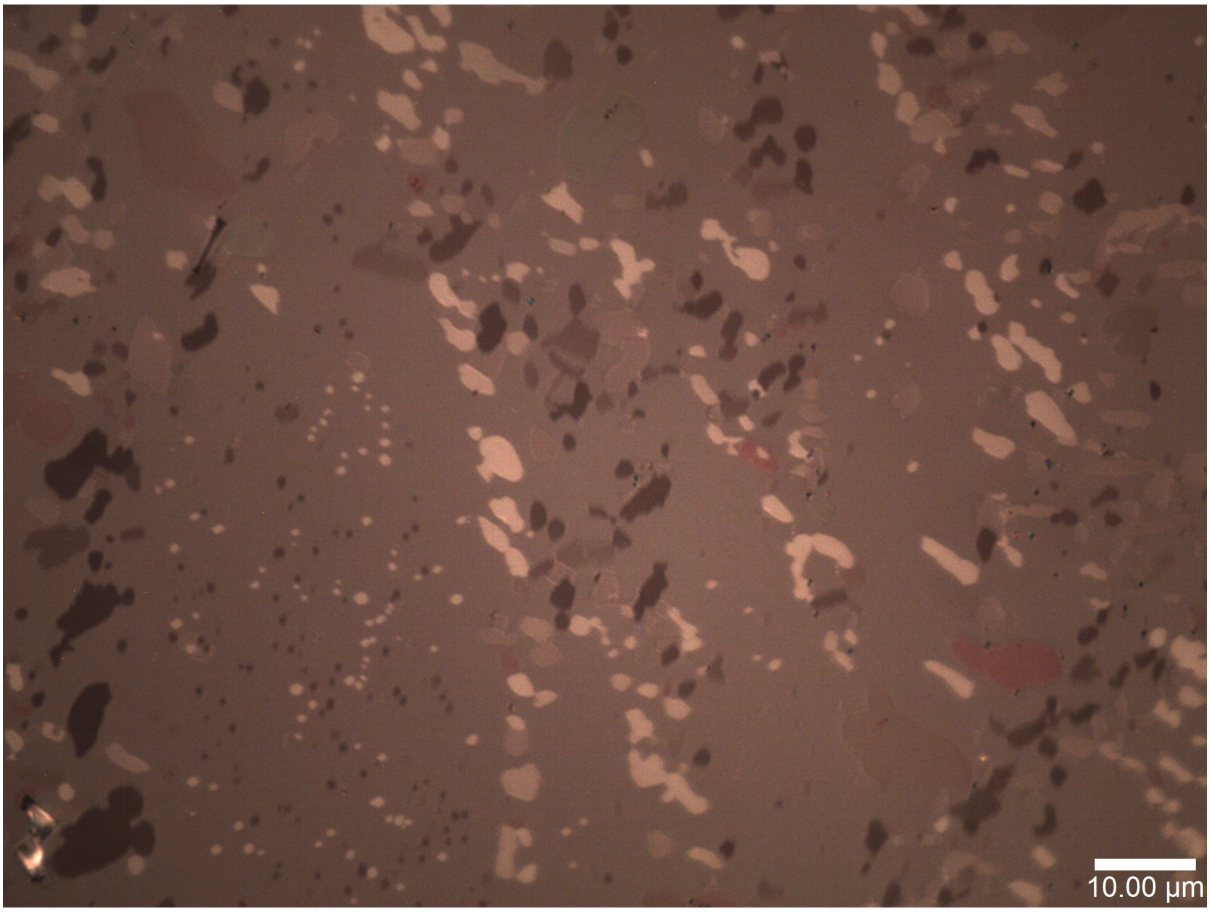

Figure 3.3.2 Typical micrograph showing contrast between phases.

Image analysis software called ImageJ was used to calculate the volume fraction of the matrix by measuring the variation in reflected light intensity. The software was able to measure the volume fraction based on a user defined intensity threshold to allow the quantification of the phases.

Occasionally, it was difficult to distinguish the contrast between phases effectively enough for the software to quantify the results reliably. In these instances, manual point counting analysis was adopted. This method involved placing a grid over a micrograph image and counting the points, which fall within the boundary of a precipitate. These counts were recorded as a percentage of the total number of points of the grid. The volume fraction of the matrix was then calculated from this percentage.

3.4 Sample Production Route

The production route adopted in the production of sample alloys at Timet UK, Witton is outlined below, and is considered necessary in order to fully understand the process history of samples.

The production of sample alloy ‘buttons’ begins with the mixing of the raw materials. Titanium sponge and elemental additions (e.g. Cr, Nb, Si, Zr, Mo), are mixed together in a series of hoppers. During the Vacuum Arc Remelt (VAR) process the mix is then placed in a copper crucible, and a spark initialised with a tungsten electrode to create a melt pool in the mixture. This process is continued until the mixture is fully melted. A further melt is then carried out to aid the removal of any impurities within the alloy. The second melt is carried out with the mixture inverted in order to distribute and break up any segregation within the material. This double melt VAR process produces a ‘coffin’ shaped button sample (85mm x 35mm x 20mm) of the desired alloy (Figure 3.4.1).

Figure 3.4.1. Coffin shaped button following VAR.

The coffin shaped button is then hot forged in order to produce a square cross section and to break down the cast microstructure produced using the VAR process. The button is soaked for 30 minutes at high temperature (well above the beta transus), before being removed from the furnace and worked using a manual forge press. This is repeated until a cross section of approximately $34mm^2$ is achieved (Figure 3.4.2)

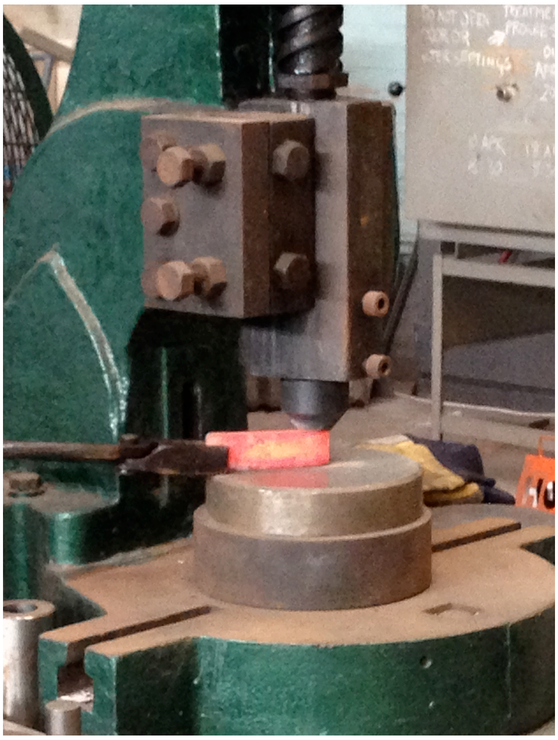

Figure 3.4.2. Button is forged to make a square cross section

Following forging, the buttons are reheated, again, well above the beta transus, before being passed through a set of rollers a number of times produce a square cross section of approximately 13mm^2 (Figure 3.4.3).

Figure 3.4.3. Final alloy button geometry.

The exact temperatures of the forging steps and number of roll passes made are determined by the simulated thermodynamic properties.

3.5 Sample Preparation and Analysis

During this work, samples were routinely investigated:

- As received material;
- Pseudo Phase Diagram determination;
- Oxidation resistance determination;
- Effect of mechanical testing on microstructure.

The basis of the techniques used in sample preparation remains the same whether it is for optical microscopy, Scanning Electron Microscopy or Energy Dispersive X-ray Spectroscopy.

3.5.1 Sample Sectioning

Sectioning of materials was achieved with the use of a low feed rate cutting disk in order to reduce the effect of burning caused by friction during the machining process. The samples were sectioned to a smaller area of interest using a hand operated rotational saw called an Abrasimet. Further, more accurate cuts were made using either an Isomet or Minitom machine with material-specific cut off wheels. These machines are able to provide a more precise, programmable cutting process.

3.5.2 Metallographic Preparation

Due to the multi phase nature of the samples prepared during this work, and the differences in mechanical grinding and polishing responses associated with them, the metallographic preparation was difficult. Titanium itself is also a relatively ductile material, especially in its beta phase. This also hindered the cutting, grinding and polishing for preparation for microscopic evaluation.

For microscopic evaluation, the expected outcome of the grind and polish process is to create a smooth, flat and clean surface for examination. Following sectioning, specimens were mounted in a 35mm Bakelite mount using a Beuhler hot mounting press. Specimens were then ground, using Struers silicon carbide grinding papers, and polished using a Struers Largo honeycomb pad with 9μm diamond suspension. Rotation speeds of the disks were set to 150rpm combined with 150N downward load applied to the specimens. Colloidal silica was used as a chemical/mechanical polish was used on a Struers Chem polishing disk as a final polising technique for an improved surface finish. The depth of polish during this final technique was controlled by the addition of 10% Hydrogen Peroxide to the colloidal silica. This helped to reduce the chances of observing a shadowing effect during stage tilting in electron microscopy.

If samples were to be examined using electron microscopy, the specimens were broken out of the Bakelite mount and stored submerged in methanol before use.

If samples were to be examined using optical microscopy, chemical etching was required to show up the microstructure. Because titanium is well known for its high corrosion resistance, traditional chloride-based etchants commonly used for steels are not effective. Therefore stronger fluoride-based acids such as hydrofluoric were used. Kroll's Reagent was found to be effective during this work, and was made up of:

- 3ml Hydrofluoric Acid
- 6ml Nitric Acid
- 91ml Water

The most effective etching technique was found to involve submerging the specimen into the etchant for a period of 10-30 seconds, depending on the alloy. Following this the specimen was soaked in a lime solution for 30 seconds then held under running water for 1 minute. The time submerged in the etchant depended on the microstructure of the specimen. The quality of the etched surface was found to decrease with time after etching, therefore specimens were examined as quickly as possible after etching.

3.5.3 Optical Microscopy

Specimen surfaces were examined under reflected light at a range of magnifications. Images were taken using a digital camera attached to a Nikon Microscope with associated software. Graticules, where required, were captured the same way. This microscopy technique was used throughout this work to capture microstructural changes between different alloy samples and different heat treatment conditions. Macroscopic inspection (low mag) was achieved this way before the decision was made to look at particularly interesting areas at higher magnification (microscopic). Optical microscopy was also used to obtain quantitative details such as precipitate size, phase volume fraction and distribution.

3.5.4 Scanning Electron Microscopy

The ‘Inspect F’ field emission gun SEM was used to produce secondary and backscattered electron images which provided fast elemental analysis for determining material properties, topography and elemental composition. The Inspect F SEM low vacuum and high-resolution system produced stable images, which were used for structure and composition characterization for the samples examined.

3.5.5 Energy Dispersive X-ray Spectroscopy (EDX)

The JEOL JSM 6400 SEM was used to provide quantitative EDX elemental analysis. This equipment featured an Oxford link turreted pentafet detector and ISIS 300 processing unit for EDS analysis. Inca software was used for EDX analysis, and was calibrated before each session using a cobalt standard.

3.6 Oxidation Analysis

3.6.1 Furnace Oxidation Analysis

In order to gain an understanding into the oxidation resistive properties of sample alloys, it has been necessary to complete some furnace heat treatments of samples. Cube shaped samples of dimension $3mm^3$ were cut from the bar, and the surfaces of these samples were polished using progressively finer grit paper to P4000. The samples were washed in methanol, dried and weighed using an analytical balance with a precision to 0.0005g. These samples were then placed into a preheated electric chamber furnace, as used in pseudo phase diagram compilation, at 650, 750, and 850ºC and held at temperature. After 150 hours, the samples were removed from the furnace, cooled in air to room temperature and then weighed again using the same analytical balance. The weight increase (as a percentage of the original weight) as a result of the heat treatment was calculated. Two samples were taken for each composition and temperature, to determine each experimental point. The microstructure and oxide layer were then examined using microscopy techniques described previously in this chapter.

3.6.2 Thermo-Gravimetric Analysis (TGA)

As a comparison to the furnace oxidation tests, samples of the same dimensions and surface polish were sent to TIMET, UK where thermo-gravimetric analysis was performed using a SDT Q600 machine. TGA involves placing the sample into a small chamber with a controlled atmosphere and temperature, and constantly measuring weight changes over a period of time. The benefit of TGA over furnace oxidation tests, is that TGA offers a high level of precision in weight, temperature and temperature change. In order to use this as a comparison to the furnace treatments, the samples were analysed at the same temperatures and held for the same time, in air. Samples were flash pickled and acetone cleaned before the TGA run. The surface area of the sample was measured for oxidation rate calculations per unit area.

3.7 Mechanical Testing

Specimen bars were machined into cylindrical dumbbell shaped test pieces and tensile testing was carried out on specimens using a Mayes CM100 testing machine, in accordance with BS EN 2002-1:2005 and BS EN ISO 6892-1. Before testing, original gauge length and diameter of the test pieces was measured and recorded. Rubicon software, attached to the machine, was used to set up and record the tests. An extensometer was used during the tensile testing of the specimens. Tensile tests were performed at a strain rate of 0.0030 mm/min. After proof was attained, the extensometer was removed and the test continued. Final gauge length and diameter of the test pieces was measured and used to calculate % elongation. Stress vs strain curves are recorded by the machine software.

3.8 Material Received

Following thermodynamic simulations, sample alloys were decided. Material from Timet UK, Witton was supplied in the form of a button produced using the process described in chapter 3. The material was received in two stages. Following the testing carried out after the first batch, thermodynamic simulation software was used again to develop more potentially suitable alloy chemistries. The first batch of material, with composition measured in wt %, was:

- Ti-16Cr-4Zr-0.35Si
- Ti-25Cr-4Zr-0.35Si
- Ti-40Cr-4Zr-0.35Si

The second batch of material, with composition measured in wt %, was:

- Ti-16Cr-4Zr-3.5Si
- Ti-12Nb-3Cr-4Zr-3.5Si
- Ti-8.8Cr-7.2Mo-4Zr-3.5Si
- Ti-16Cr-4Zr-3.5Si-0.2Y

Timetal 834 of the composition shown below was tested throughout these works alongside sample alloys to be used as a benchmark for material properties.

- Ti-5.8Al-4Sn-3.5Zr-0.7Nb-0.5Mo-0.35Si-0.06C

4 Thermodynamic Simulation and Analysis

4.1 Introduction

This chapter describes the thermodynamic simulations and associated discussion completed during this work. The chapter starts with an analysis of existing data, including industry standard data received from Timet UK, with the aim of using this data to validate the applicability of the simulation software. With the software validated, it was used to simulate expected thermodynamic properties for potential alloy systems including the titanium-silicon system. Once these were confirmed, they were combined with other elements to provide thermodynamic properties for an alloying system with a suitable matrix, which can provide the desired precipitates to achieve the properties required for this work.

The data achieved as a result of the work completed in this chapter was important to allow a request for material hardware, from Timet UK, to continue the work.

4.2 Industrial / Existing Data

Industrial data received from Timet UK were based on existing alloys that are currently in production, and were taken from Timet official data sheets for these alloys. Information on transus temperatures and physical properties was used to compare outputs from simulation software to validate the software. Figure 4.2.1 Shows part of a typical Timet data sheet for Timetal 834. The data sheet provides information on alloy content in Table 1 and also physical properties including transus temperature in Table 2.

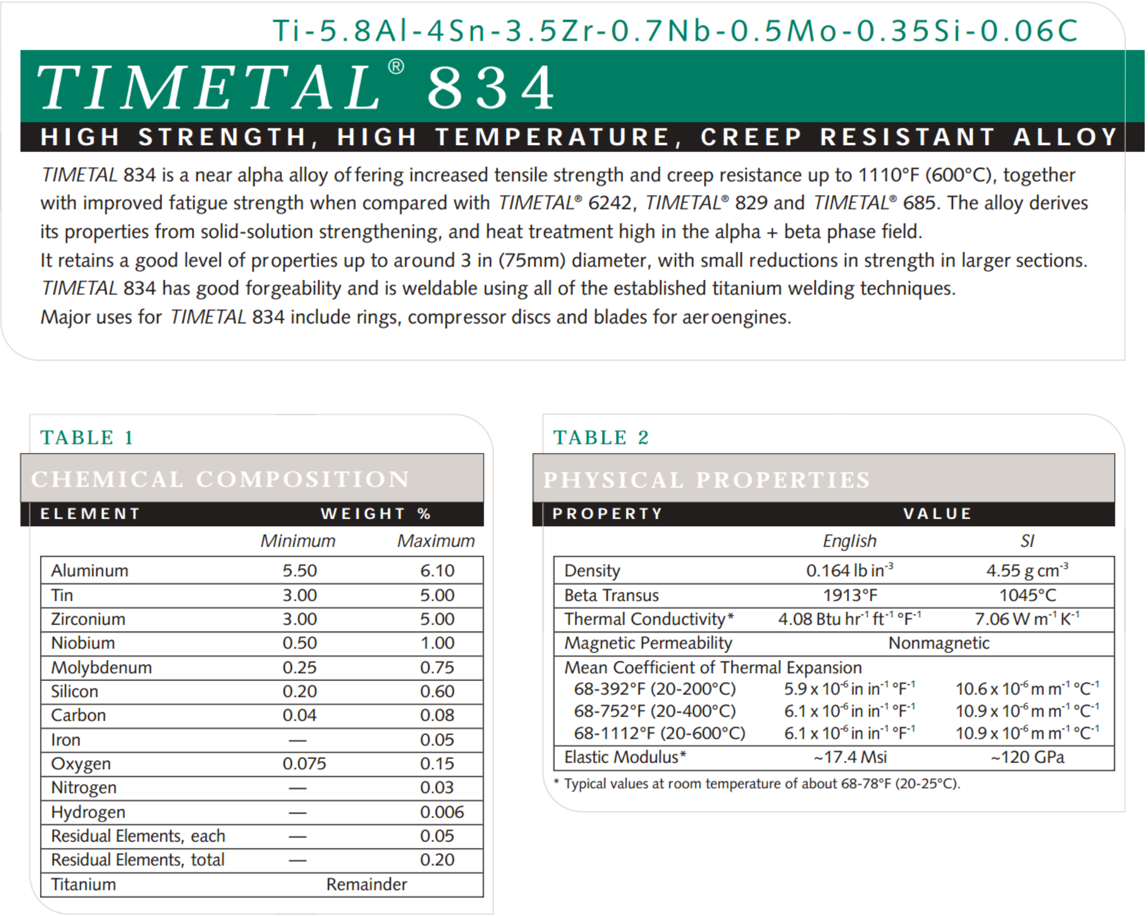

Ti-5.8Al-4Sn-3.5Zr-0.7Nb-0.5Mo-0.35Si-0.06C

TIMETAL® 834

HIGH STRENGTH, HIGH TEMPERATURE, CREEP RESISTANT ALLOY

TIMETAL 834 is a near alpha alloy offering increased tensile strength and creep resistance up to 1110°F (600°C), together with improved fatigue strength when compared with *TIMETAL®* 6242, *TIMETAL®* 829 and *TIMETAL®* 685. The alloy derives its properties from solid-solution strengthening, and heat treatment high in the alpha + beta phase field.

It retains a good level of properties up to around 3 in (75mm) diameter, with small reductions in strength in larger sections.

TIMETAL 834 has good forgeability and is weldable using all of the established titanium welding techniques.

Major uses for *TIMETAL* 834 include rings, compressor discs and blades for aeroengines.

TABLE 1

CHEMICAL COMPOSITION

ELEMENT	WEIGHT %	
	Minimum	*Maximum*
Aluminum	5.50	6.10
Tin	3.00	5.00
Zirconium	3.00	5.00
Niobium	0.50	1.00
Molybdenum	0.25	0.75
Silicon	0.20	0.60
Carbon	0.04	0.08
Iron	—	0.05
Oxygen	0.075	0.15
Nitrogen	—	0.03
Hydrogen	—	0.006
Residual Elements, each	—	0.05
Residual Elements, total	—	0.20
Titanium	Remainder	

TABLE 2

PHYSICAL PROPERTIES

PROPERTY	VALUE	
	English	*SI*
Density	0.164 lb in^{-3}	4.55 g cm^{-3}
Beta Transus	1913°F	1045°C
Thermal Conductivity*	4.08 Btu hr^{-1} ft^{-1} °F^{-1}	7.06 W m^{-1} K^{-1}
Magnetic Permeability	Nonmagnetic	
Mean Coefficient of Thermal Expansion		
68-392°F (20-200°C)	5.9 x 10^{-6} in in^{-1} °F^{-1}	10.6 x 10^{-6} m m^{-1} °C^{-1}
68-752°F (20-400°C)	6.1 x 10^{-6} in in^{-1} °F^{-1}	10.9 x 10^{-6} m m^{-1} °C^{-1}
68-1112°F (20-600°C)	6.1 x 10^{-6} in in^{-1} °F^{-1}	10.9 x 10^{-6} m m^{-1} °C^{-1}
Elastic Modulus*	~17.4 Msi	~120 GPa

* Typical values at room temperature of about 68-78°F (20-25°C).

Figure 4.2.1 *Section of Timetal 834 datasheet available from Timet UK, 2010*

The literature on titanium-silicon alloying systems is in agreement concerning the binary equilibrium phase diagram associated with these elements *[10; 19; 20; 27; 28]*. Figure 4.2.3 below shows a typical phase diagram for this system.

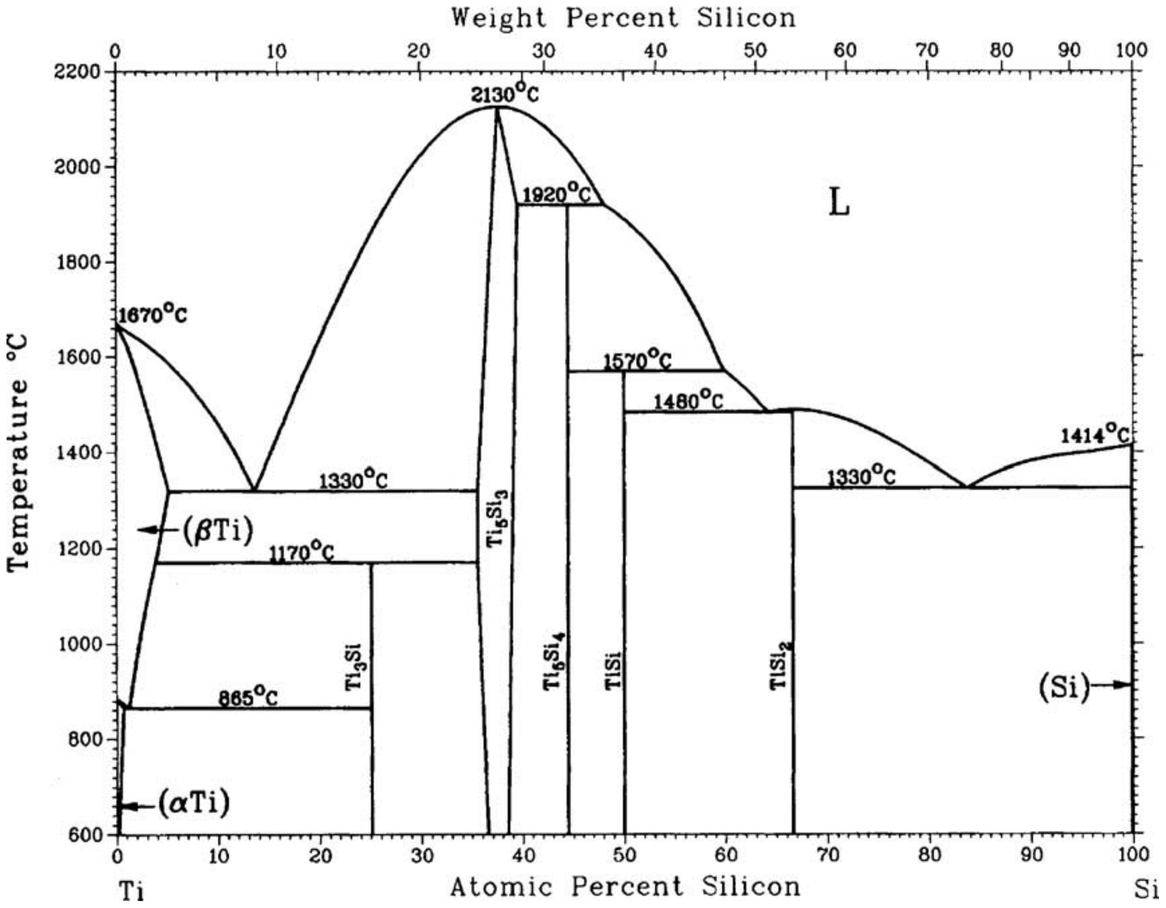

Figure 4.2.3 *Equilibrium phase diagram for a titanium-silicon alloying system. [29]*

From the diagram, it is clear that that the solubility of silicon in titanium is low, at a maximum of ~0.47wt% silicon. Solubility decreases as temperature decreases in α-titanium. The silicide phases of Ti_3Si and Ti_5Si_3 can also be seen. Because of the low solubility of silicon in titanium, properties are influenced both by silicon in solution, as well as silicides in these alloying systems. In beta titanium, 3wt% Si can be dissolved at the eutectic temperature, 1339°C. At 865°C, the eutectic transformation $\beta \rightarrow \alpha + Ti_3Si$ occurs.

4.3 Comparison of Available Software

There are a number of industry standard thermodynamic simulations software packages on the market today. Two of the most commonly used of these are ThermoCalc and JMatPro. In order to understand the differences, if any, between these software packages simulations were performed on a number of existing alloys including Timetal 6-4, Timetal 834, and Beta 21S. A step diagram was produced for each alloy, as this type of diagram was to be extensively used throughout this work. Each of the two software packages uses the same method for simulating thermodynamic properties, the CALPHAD method, and so a similar output was expected from both.

Figure 4.3.1 and figure 4.3.2 shows the diagram outputs from JMatPro and Thermocalc respectively, for Timetal 834. As expected, both software packages produced similar diagrams, where the beta transus temperature is at approximately 1050°C. This was observed in all of the diagrams produced for the existing alloys investigated, allowing the assumption that there is little difference between software packages.

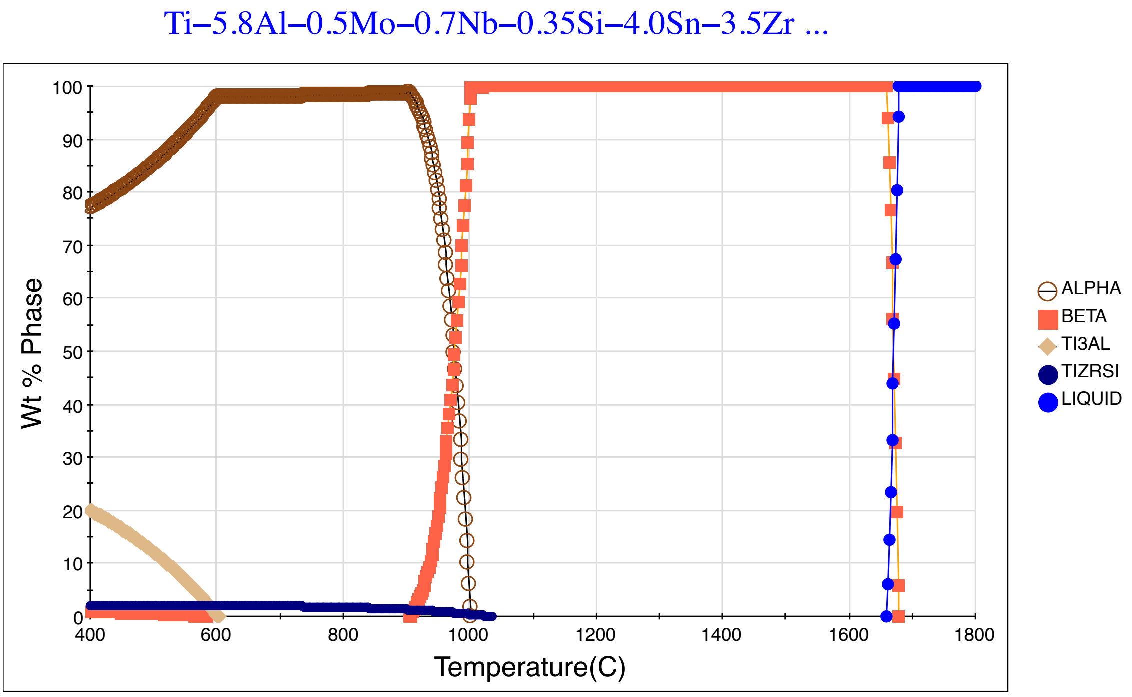

Figure 4.3.1 *JMatPro Step Diagram for Timetal 834*

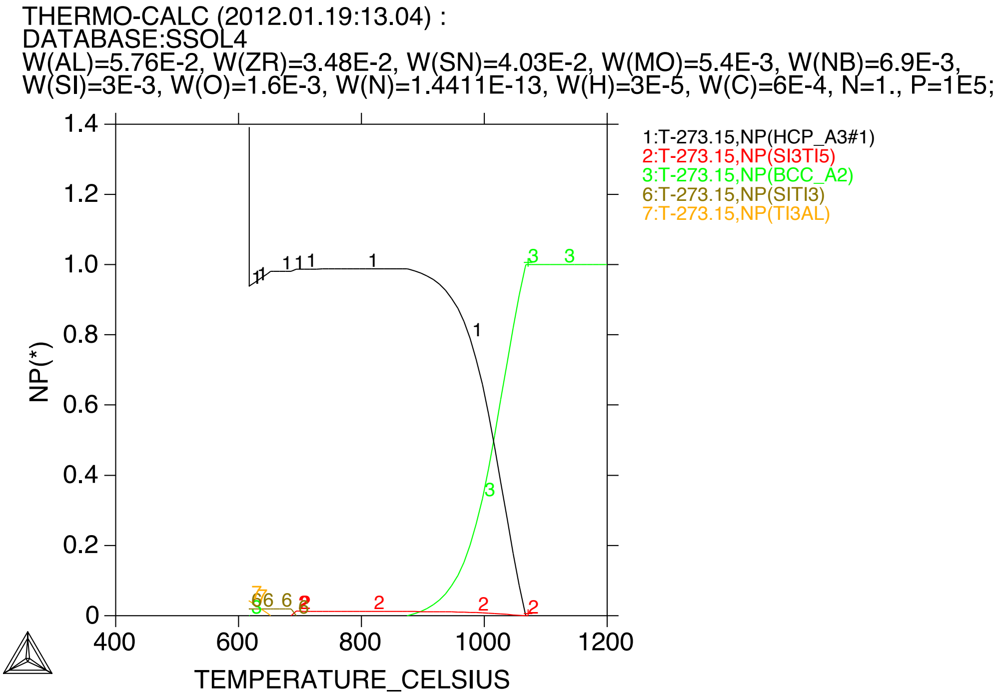

Figure 4.3.2 *ThermoCalc Step Diagram for Timetal 834*

The data obtained from these comparisons was used to add to Table 4.2.2, in order to provide a validation to the applicability of the thermodynamic simulation software. Table 4.3.3 shows the range of alloys and the beta transus temperature comparison between literature and simulation. Again, there is little significant difference between the expected, and simulated transus temperatures, allowing the assumption that the simulated thermodynamic properties of materials investigated as part of this work is a good representation of those properties.

Table 4.3.3 *Comparison of the beta transus temperatures between TIMET Data Sheets and thermodynamic simulation software.*

Timet Alloy	**Beta Transus Temperature (°C)**		
	TIMET Data Sheets	**JMatPro Simulation**	**ThermoCalc Simulation**
Timetal 834	1045	1050	1050
Timetal 829	1015	1000	1000
Timetal 6-4	996	980	980
Timetal 6-2-4-2	995	1000	1000
Timetal 6-2-4-6	935	900	900
Beta 21S	807	800	800
Timetal 10-2-3	800	800	800

Since the validation of the software against other software packages as well as existing alloy data had been achieved, the work began with simulations on binary alloying systems.

4.4 Initial Simulations and Analysis

Based on the literature, a number of alloying elements were thought to be a good starting point for the alloy matrix. It was decided that chromium should be included to β stabilise the matrix, as well as to provide some resistance to oxidation. Silicon should also be added to improve oxidation resistance as well as other mechanical properties, as outlined in the literature review conducted as part of this project. Similarly, zirconium helps to suppress martensite start temperature and also to modify and/or stabilise any silicides that form in the alloy. It was decided that this titanium, chromium, zirconium, silicon system would act as the base for alloy development.

In terms of the addition of these elements to titanium, it was decided that 16wt% chromium, being the β-eutectoid composition could be beneficial. Also, additions of chromium above about 20wt% are believed to dramatically improve the oxidation resistance of titanium, therefore a sample containing 25wt% chromium would be appropriate. However, at this composition the chromium may segregate therefore another sample containing 40wt% chromium would be less prone to this, due to the liquidus being flat through a minimum at this point. However, at 40wt% chromium poor ductility may be an issue. The binary phase diagram for titanium and chromium is shown in figure 4.4.1.

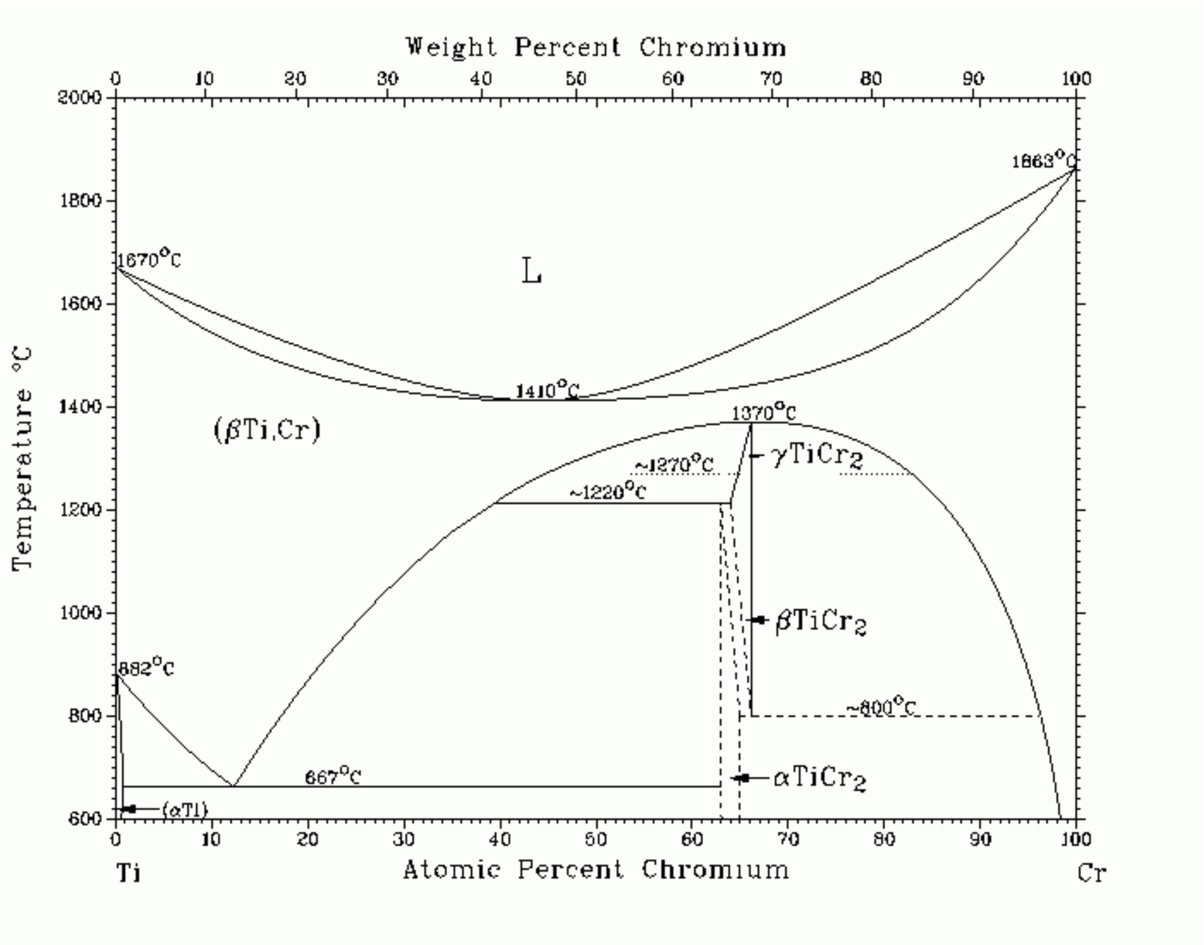

Figure 4.4.1 *Equilibrium phase diagram for a titanium chromium alloying system.* [30]

In terms of silicon addition, an addition of 0.35wt% silicon has been known to be beneficial (hence its inclusion in Timetal 834). Studying this was also useful to observe the effects of a small addition of silicon to the titanium chromium matrix.

In order to achieve the highest level of stability by the addition of zirconium without detrimentally affecting ductility 4wt% zirconium was included.

Therefore, the alloying systems simulated as part of the initial investigations were (in wt%):

Ti-16Cr-4Zr-0.35Si, as shown in figure 4.4.2.

Ti-25Cr-4Zr-0.3Si, as shown in figure 4.4.3.

Ti-25Cr-4Zr-0.35Si, as shown in figure 4.4.4.

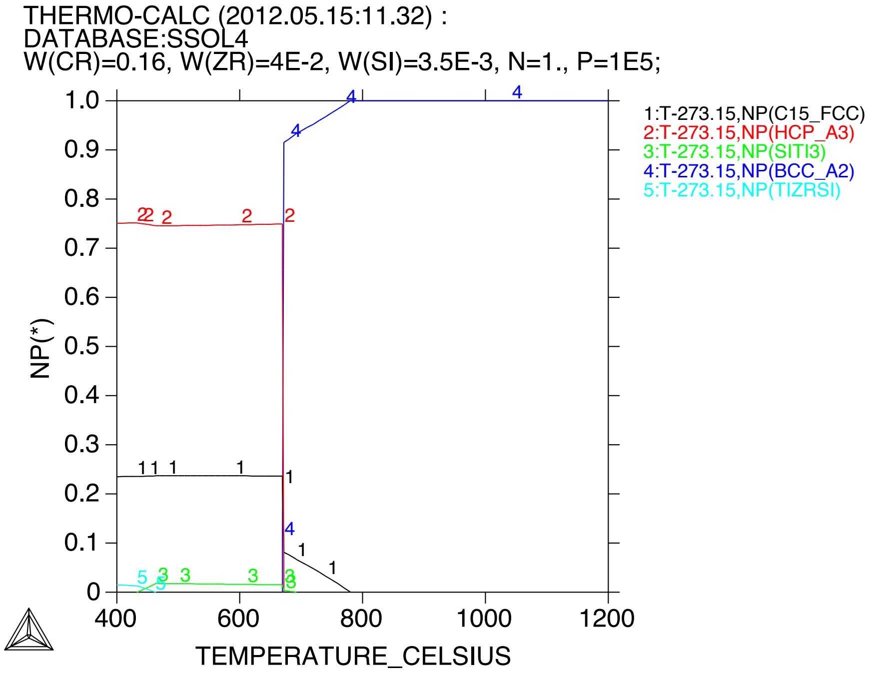

Figure 4.4.2 *ThermoCalc Step diagram for Ti-16Cr-4Zr-0.35Si alloy.*

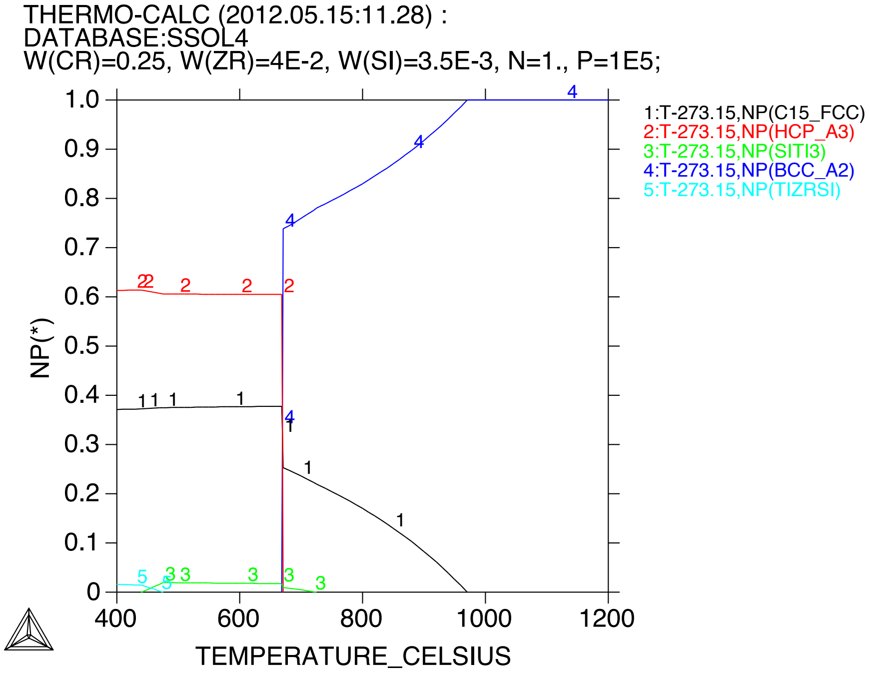

Figure 4.4.3 *ThermoCalc Step diagram for Ti-25Cr-4Zr-0.35Si alloy.*

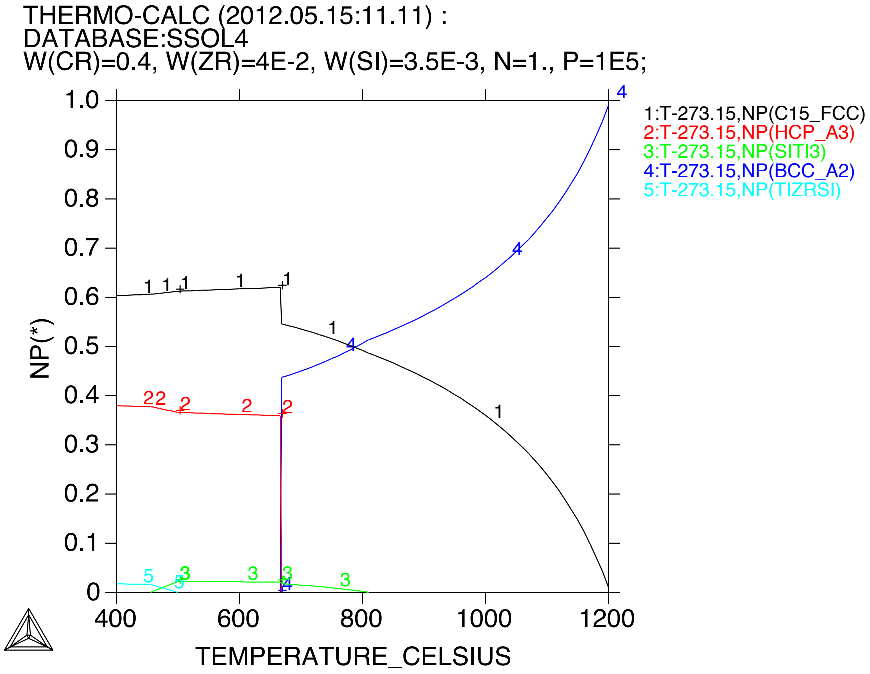

Figure 4.4.4 *ThermoCalc Step diagram for Ti-40Cr-4Zr-0.35Si alloy.*

In order to continue to increase the silicon composition into the investigated alloys, a composition of 3.5wt. % silicon has been calculated based on analogies with nimonic alloys. Looking at a nimonic alloy with a typical volume fraction of γ’, the atomic percentage of γ’ formers was calculated and converted to weight percentage to determine the level of silicon to be included in these alloys. Figure 4.4.5 below shows the ThermoCalc step diagram for an alloy containing Ti-16Cr-4Zr-3.5Si (wt%).

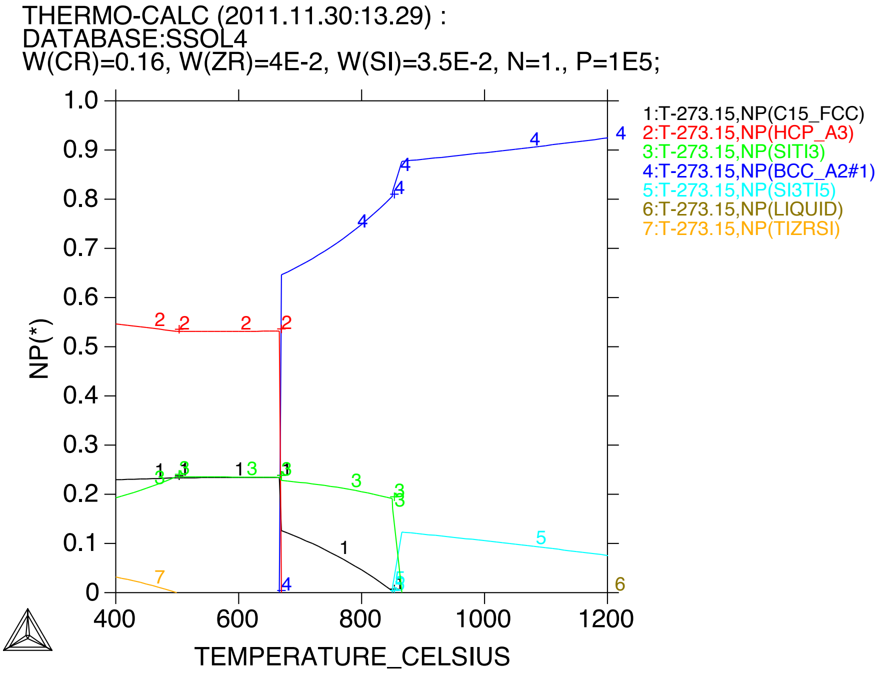

Figure 4.4.5 ThermoCalc Step diagram for Ti-16Cr-4Zr-3.5Si alloy.

In order to aid the analysis of the information provided by the diagrams, the data was exported to Microsoft Excel. Pie charts showing the phases present at room temperature and at the proposed operating temperature (~700ºC) are shown in figures 4.4.6, 4.4.7, 4.4.8 and 4.4.9 below.

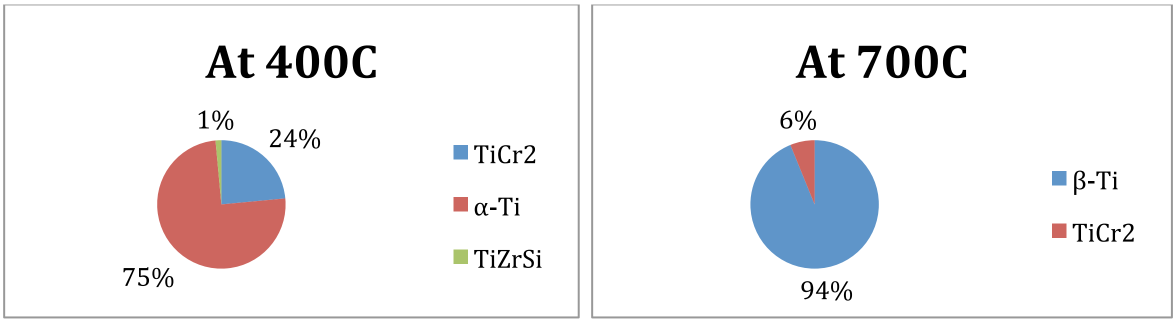

Figure 4.4.6 *Phases present at 400ºC (left) and 700ºC (right) for Ti-16Cr-4Zr-0.35Si alloy.*

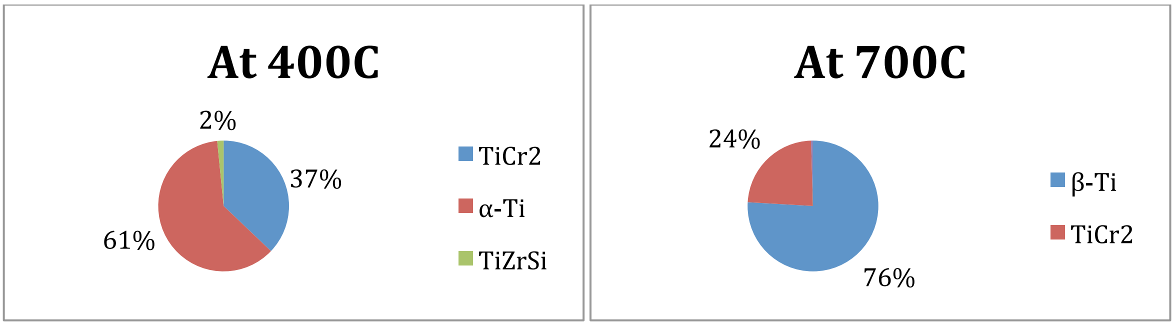

Figure 4.4.7 *Phases present at 400°C (left) and 700°C (right) for Ti-25Cr-4Zr-0.35Si alloy.*

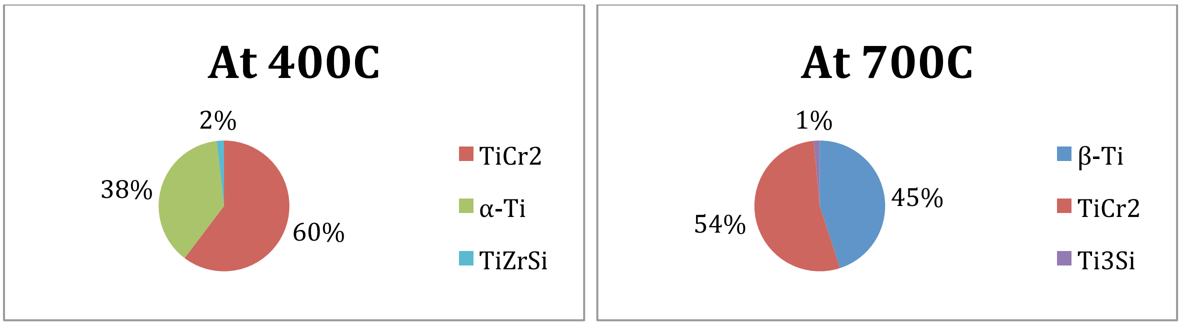

Figure 4.4.8 *Phases present at 400°C (left) and 700°C (right) for Ti-40Cr-4Zr-0.35Si alloy.*

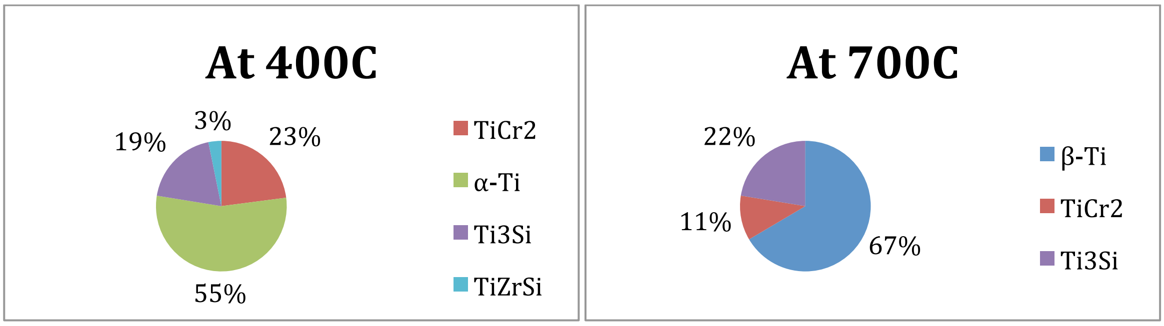

Figure 4.4.9 *Phases present at 400°C (left) and 700°C (right) for Ti-16Cr-4Zr-3.5Si alloy.*

The data obtained as a result of the simulations indicates that for the alloy containing Ti-16Cr-4Zr-0.35Si at 700˚C, the phases present are ß-Ti and $TiCr_2$ intermetallic phase, at a ratio of 94% and 6%. At room temperature (or 400˚C) the phases present are α-Ti and $TiCr_2$ intermetallic phase, at a ratio of 75% and 24%. The simulations also suggest the presence of a silicide phase (TiZrSi) with 1% present at room temperature.

Increasing the concentration of chromium added to the alloy an increase in $TiCr_2$ phase in place of ß-Ti is observed. A similar scenario is observed at room temperature with an increase in $TiCr_2$ in place of α-Ti.

It is important to note that with the alloys containing 0.35 wt. % silicon, no ß-Ti is retained at room temperature.

By increasing the silicon concentration to 3.5 wt. % as seen in the Ti 16Cr-4Zr-3.5Si alloy, we observe 67% ß-Ti, 22% Ti_3Si (silicide phase), and 11% $TiCr_2$ at 700˚C. Therefore we can observe that as expected, increasing the silicon concentration provides a greater ratio of a silicide phase in place of $TiCr_2$ intermetallic phase and ß-Ti. At room temperature the phases present are α-Ti, $TiCr_2$ intermetallic phase and two types of silicide phase (TiZrSi and Ti_3Si), at a ratio of 55%, 23% and 22% respectively.

Comparing this data with titanium-silicon and titanium-chromium phase diagrams indicates that the simulations are an accurate representation of the expectations.

4.5 Further Simulations and Analysis

Following the production of the previous samples, samples were tested for oxidation resistance and tensile strength. Following this it was clear that the originally suggested alloys, although showing some opportunity for a new alloy design, were not acceptable in terms of ductility for use in the intended application.

Based on this, the exploration of an alternative matrix was a tempting direction in which to overcome the poor ductility. Since the poor ductility is probably related to the high volume fraction of $TiCr_2$ intermetallic in high chromium content alloys, it seems appropriate to reduce the chromium content, and replace it with other advantageous elemental additions. Using the master alloys niobium-chromium and molybdenum-chromium, two new alloy matrices were explored. Using 80%Nb-20Cr% and 55%Cr-45%Mo the following alloy suggestions were proposed for thermodynamic simulation:

- Ti-8.8Cr-7.2Mo-4Zr-3.5Si, as shown in figure 4.5.1.
- Ti-12Nb-3Cr-4Zr-3.5Si, as shown in figure 4.5.2.

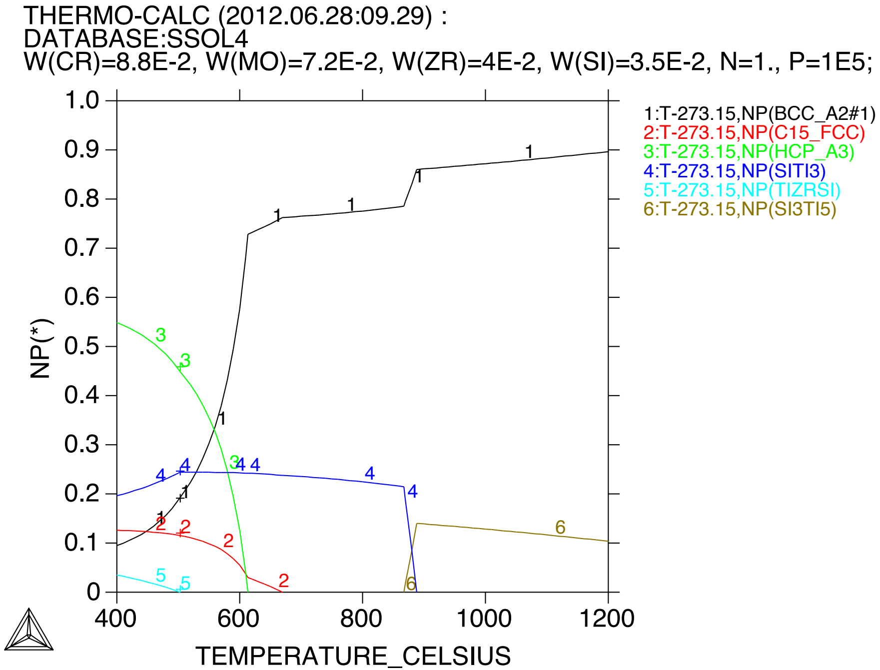

Figure 4.5.1 *ThermoCalc Step diagram for Ti-8.8Cr-7.2Mo-4Zr-3.5Si alloy.*

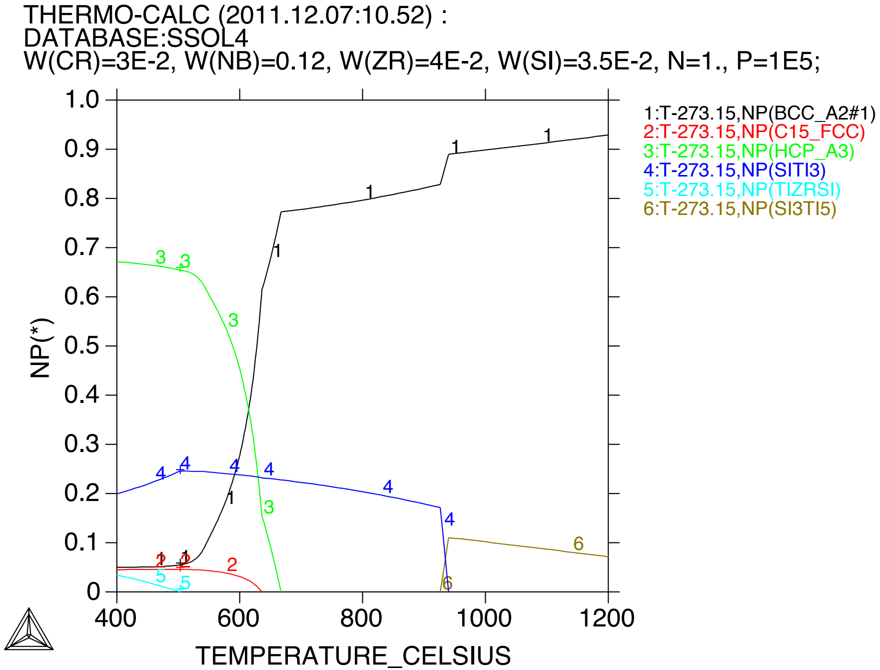

Figure 4.5.2 *ThermoCalc Step diagram for Ti-12Nb-3Cr-4Zr-3.5Si alloy.*

Similarly, literature around the topic has suggested that the addition of yttrium to nimonic alloys helps to produce a more compact and adherent scale. From this information, some yttrium addition was added to an alloy melt to determine its effect on titanium alloys. Figure

4.5.3 shows the ThermoCalc simulation for an alloy containing Ti-16Cr-4Zr-3.5Si-0.2Y (wt%).

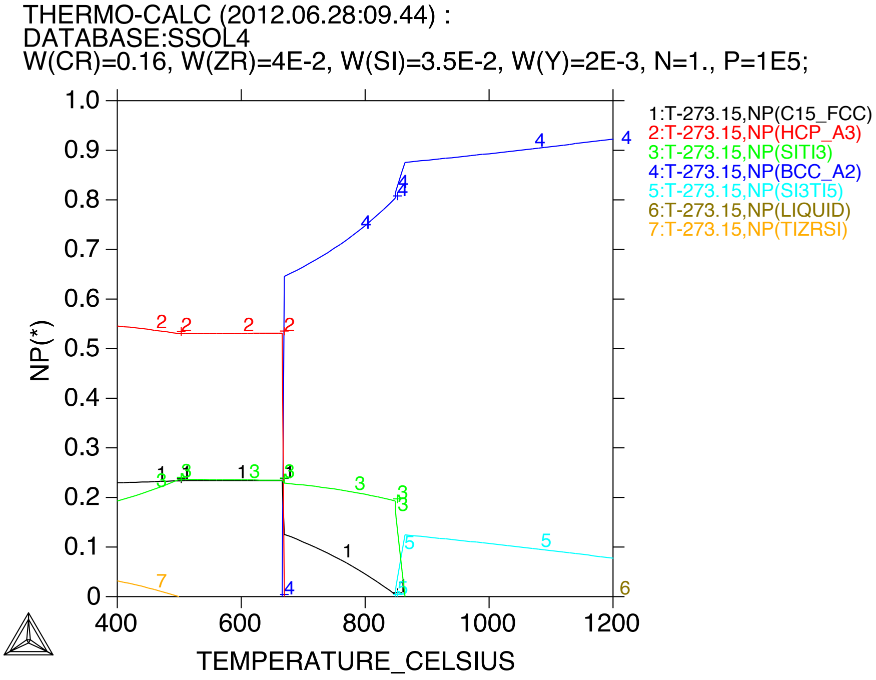

Figure 4.5.3 *ThermoCalc Step diagram for Ti-16Cr-4Zr-3.5Si-0.2Y alloy.*

In order to aid the analysis of the information provided by the diagrams, the data was again exported to Microsoft Excel. Pie charts showing the phases present at room temperature and at the proposed operating temperature (~700ºC) are shown in figures 4.5.4, 4.5.5 and 4.5.6 below.

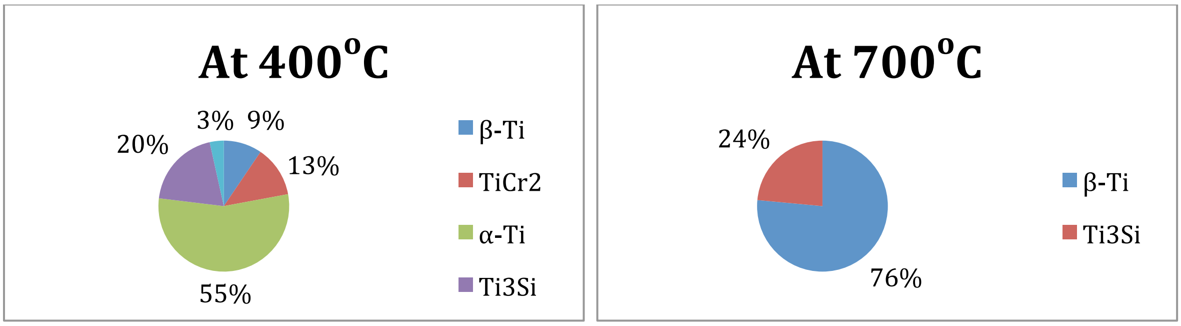

Figure 4.5.4 *Phases present at 400ºC (left) and 700ºC (right) for Ti-8.8Cr-7.2Mo-4Zr-3.5Si alloy.*

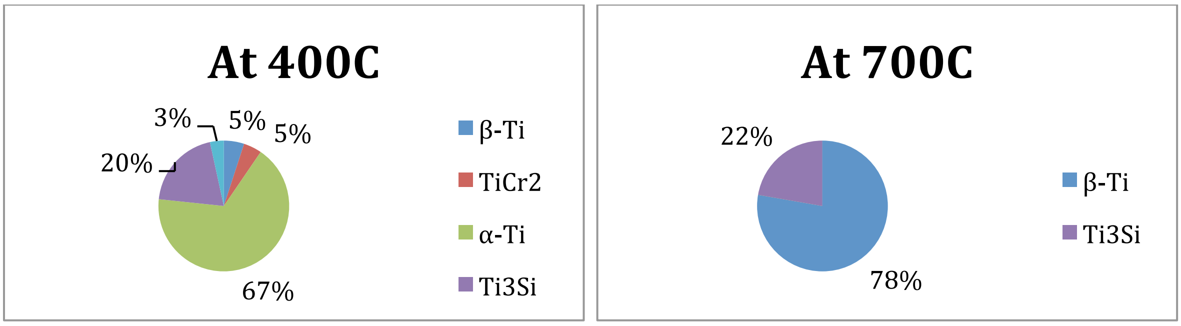

Figure 4.5.5 *Phases present at 400°C (left) and 700°C (right) for Ti-12Nb-3Cr-4Zr-3.5Si alloy.*

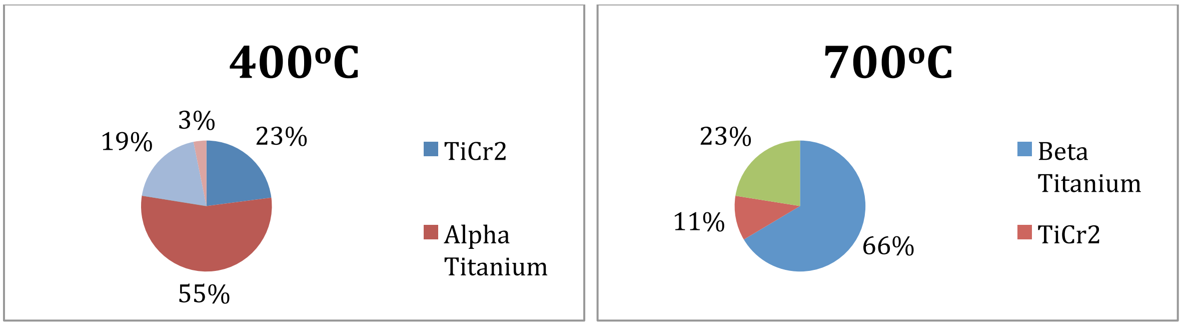

Figure 4.5.6 *Phases present at 400°C (left) and 700°C (right) for Ti-16Cr-4Zr-3.5Si-0.2Y alloy.*

This data indicates that for the alloy containing Ti-8.8Cr-7.2Mo-4Zr-3.5Si at 700˚C, the phases present are ß-Ti and Ti_3Si silicide phase, at a ratio of 76% and 24%. At room temperature (or 400˚C) the phases present are α-Ti, ß-Ti, $TiCr_2$ intermetallic phase as well as two types of silicide phase (TiZrSi and Ti_3Si), at a ratio of 55%, 9%, 13% and 23% respectively.

For the alloy containing Ti-12Nb-3Cr-4Zr-3.5Si at 700˚C, the phases present are again, ß-Ti and Ti_3Si silicide phase, at a ratio of 78% and 22%. At room temperature (or 400˚C) the phases present are α-Ti, ß-Ti, $TiCr_2$ intermetallic phase as well as two types of silicide phase (TiZrSi and Ti_3Si), at a ratio of 67%, 5%, 5% and 23% respectively.

In both these alloys between 5% and 9% ß-titanium is retained at room temperature and so these alloys were deemed the most assuring in terms of providing adequate ductility at room temperature.

Comparing this data with titanium-silicon and titanium-chromium phase diagrams indicates that the simulations are an accurate representation of the expectations.

Simulations completed for Ti-16Cr-4Zr-3.5Si-0.2Y alloy indicate that that the addition of yttrium provides little difference to the phases present wether at room temperature or at 700˚C. This may well be down to limitations in the software database for this elemental addition.

4.6 Table of Developed Alloys

From the justifications identified both within this chapter and chapter 3, table 4.6.1 below indicates the alloys that were developed as part of this work, along with a brief justification of the decision.

Table 4.6.1 *Table of developed alloys*

Developed Alloy	**Justification by Alloying Element**
Ti-16Cr-4Zr-0.35Si	Cr = ß-Eutectoid composition Zr = Good balance of alloy stability and ductility Si = Maintain silicon in solution
Ti-25Cr-4Zr-0.35Si	Cr = Greater oxidation resistance above 20 wt.%
Ti-40Cr-4Zr-0.35Si	Cr = Reduce risk of segregation
Ti-16Cr-4Zr-3.5Si	Si = Addition is typical of the volume fraction of γ' in nimonic alloys.
Ti-16Cr-4Zr-3.5Si-0.2Y	Y = Help to produce a more adherent scale during oxidation
Ti-8.8Cr-7.2Mo-4Zr-3.5Si	Cr /Mo = Use of available master alloy (55%Cr - 45%Mo).
Ti-3Cr-12Nb-4Zr-3.5Si	Cr/Nb = Use of available master alloy (80%Nb - 20Cr%).

4.7 Summary

This chapter has documented the data provided by thermodynamic simulations of the proposed alloy systems. The data has indicated that in alloys containing only 0.35 wt.% silicon very little silicide phase is precipitated within the matrix at either 700˚C or at room temperature. As is to be expected, increasing the silicon addition to 3.5 wt. % sufficiently increases the precipitation of silicides within the matrix to a level that, according to literature, may be beneficial in terms of alloy properties.

According to the simulations, alloys containing only chromium, are not expected to retain any ß-titanium phase at room temperature. Instead all of the titanium is transformed to the alpha (α) phase. In alloys containing molybdenum or niobium as well as chromium not all of the beta (ß) titanium is transformed and so between 5% and 9% is retained to room temperature. This indicates that the molybdenum or niobium added to these alloys stabilises the beta phase sufficient to allow this retainment of ß-titanium to room temperature. It is predicted that these alloys will provide a more beneficial ductility at room temperature than alloys where no ß-Ti is retained.

Chapter 5 looks at the metallographic examinations of the as-received materials simulated in this chapter and aims to collate the data from thermodynamic simulations with microscopic analysis to fully understand the as received microstructures.

5 Metallographic Analysis of As-Received Material

5.1 Introduction

Metallographic examination of the as received samples was carried out using scanning electron microscopy with backscatter detection. EDX analysis was also used as an aid to confirm the composition of the material received. This chapter will present the optical and electron micrographs of the alloy samples received.

5.2 SEM Micrographs

Initially the as-received material was examined using SEM with backscatter detection using the procedure outlined in Chapter 3.

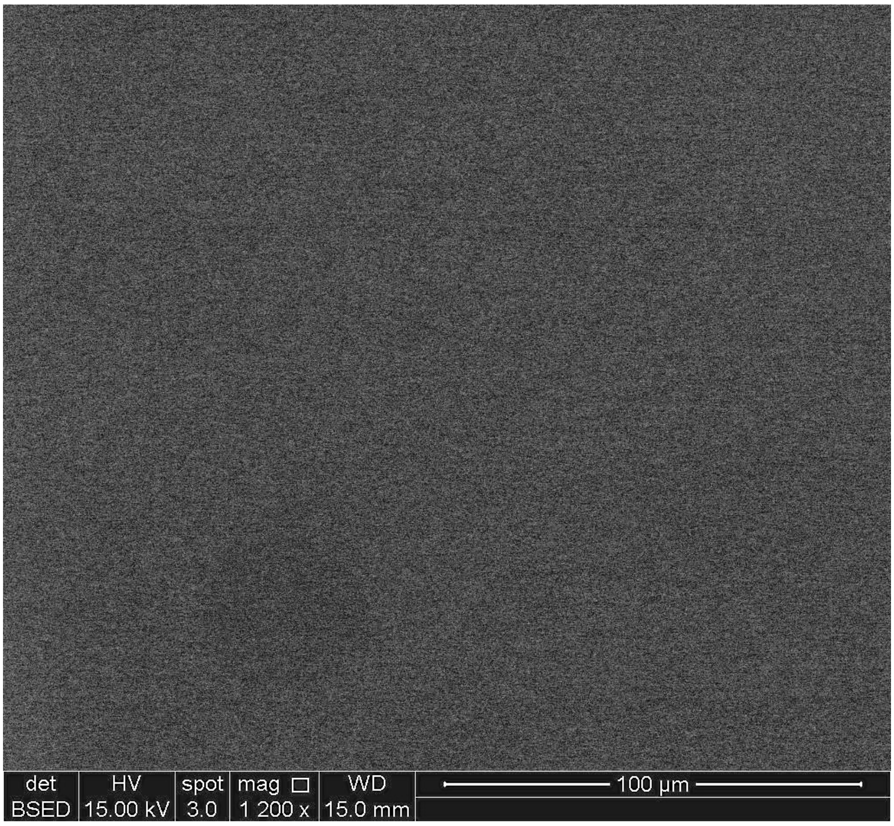

Figure 5.2.1 *Backscatter SEM image of as received Ti-16Cr-4Zr-0.35Si (Mag 1200X)*

Figure 5.2.1 above shows a backscatter SEM image of sample alloy Ti-16Cr-4Zr-0.35Si. The micrograph appears to be quite poor with no features visible. This could be the result of poor sample preparation, poor microscope configuration or simply due to features and/or precipitates are too small to examine under the microscope conditions set. Based on evidence from literature as well as thermodynamic simulations, one would expect that the small additions of silicon to this alloy would result in silicon remaining in solution at room temperature. This, combined with the high working distance used to image this sample could provide a reason for the lack of visible features.

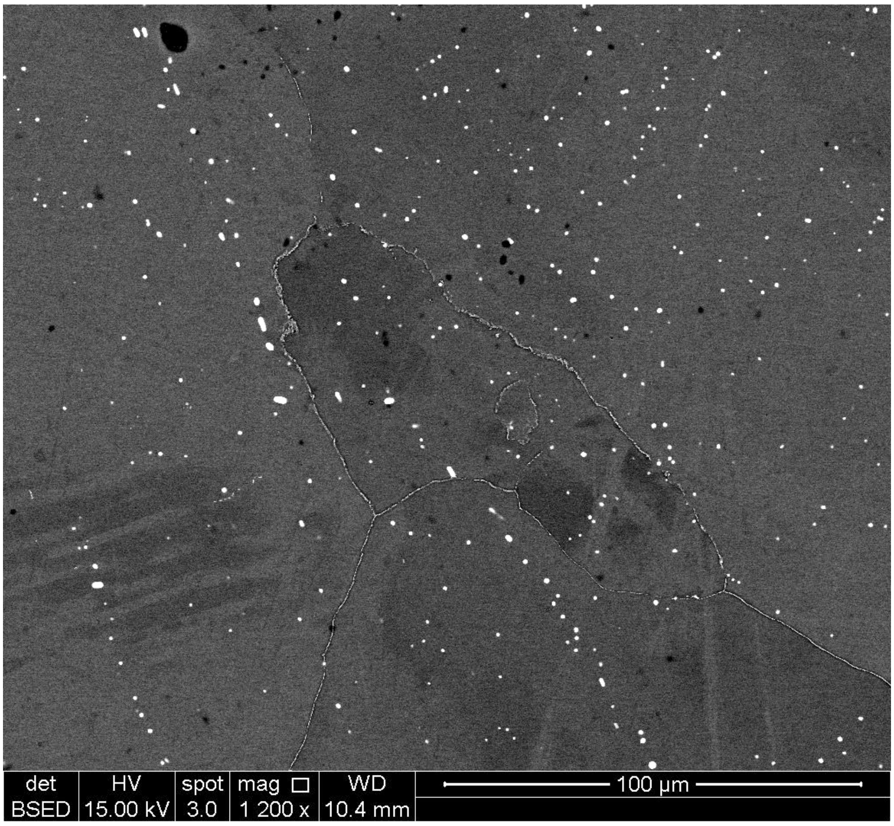

Figure 5.2.2 *Backscatter SEM image of as received Ti-25Cr-4Zr-0.35Si (Mag 1200X)*

Figure 5.2.2 above shows a backscatter SEM image of sample alloy Ti-25Cr-4Zr-0.35Si. Due to the phase contrast effect of backscatter electrons (see section 5.4), this image shows a bright phase, which seems to be situated on grain boundaries. This phase is probably rich in chromium or zirconium, as these elements possess a high atomic number. If correct, this alloy would be expected to behave well under oxidation testing due to the protection provided by chromium at the surface, however these precipitates could also detrimentally affect the room temperature ductility of this alloy. This image is in agreement with the predictions made in chapter 4, in that segregation of chromium to the grain boundaries is observed.

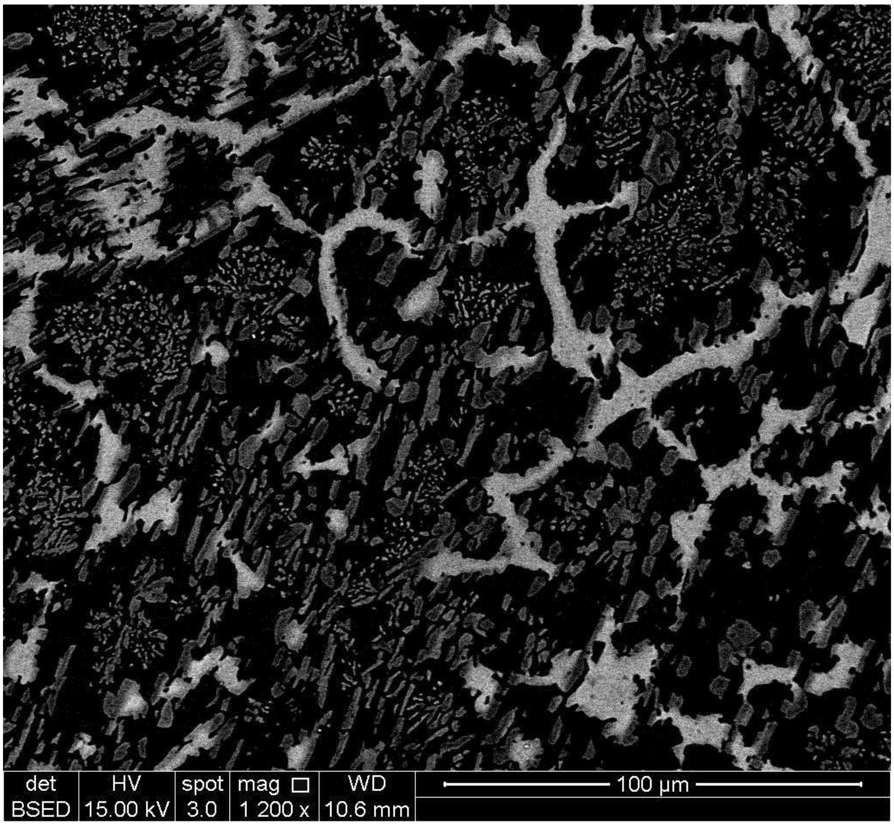

Figure 5.2.3 *Backscatter SEM image of as received Ti-40Cr-4Zr-0.35Si (Mag 1200X)*

Figure 5.2.3 above shows a backscatter SEM image of sample alloy Ti-40Cr-4Zr-0.35Si. This image shows a number of contrasting phases present within the microstructure. The brightest phase is probably the same chromium phase seen in the previous image however the level of segregation is reduced (as expected due to the high chromium content). This image helps to identify the phase as chromium rather than zirconium (as hypothesised based on the previous image) due to the larger volume fraction of the phase observed here. The less bright phase could again be a chromium based precipitate but with a reduced chromium content (in place of titanium or zirconium). This alloy would be expected to possess excellent oxidation resistance combined with extremely poor ductility due to the large volume fraction of precipitates present within the matrix.

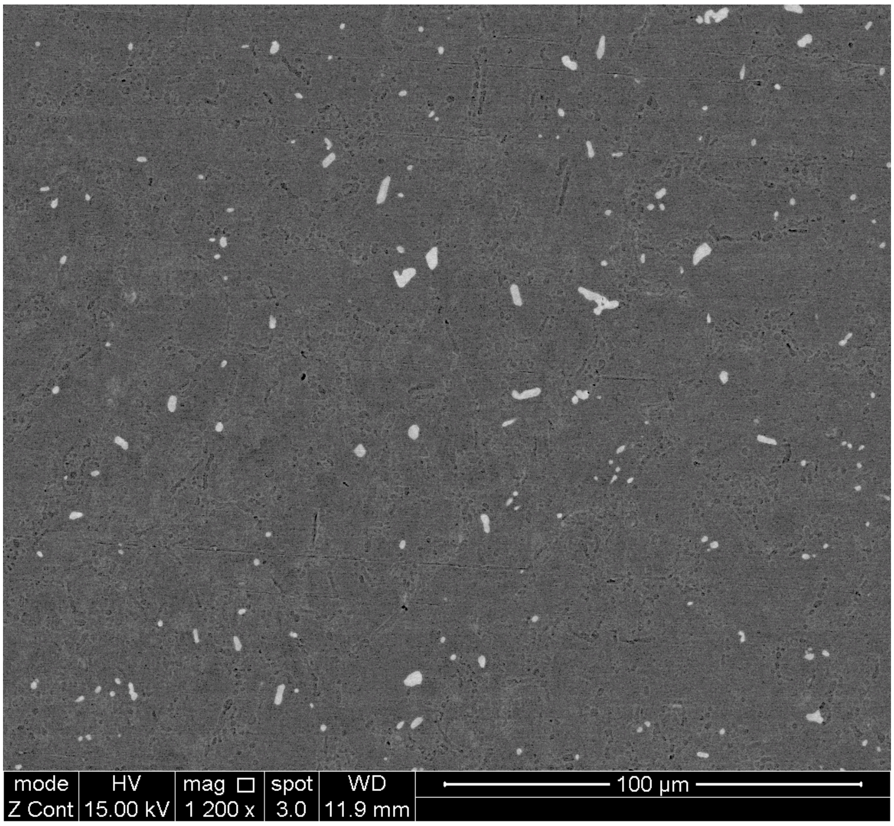

Figure 5.2.4 *Backscatter SEM image of as received Ti-16Cr-4Zr-3.5Si (Mag 1200X)*

Figure 5.2.4 above shows a backscatter SEM image of sample alloy Ti-16Cr-4Zr-3.5Si. From the phase contrast effect expected with backscatter detection, one would expect the increased addition of silicon to be visible as extremely dark (almost black) phases due to the low atomic number of silicon compared to the titanium rich matrix. Due to the tendency for silicon-containing precipitates to include zirconium (e.g.Ti,Zr_5Si_3), observed in literature as well as thermodynamic simulations, it is suggested that the bright phase is probably a zirconium-containing titanium silicide. By altering the brightness and contrast settings of the image, darker precipitates are also visible on grain boundaries see figure 5.2.5. These probably contain chromium as seen in the alloys containing lower silicon content.

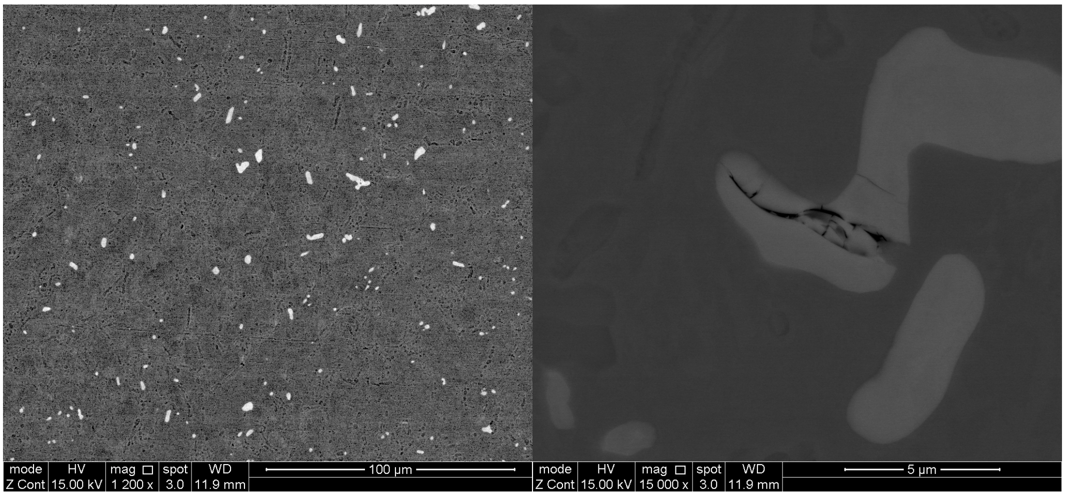

Figure 5.2.5 *Ti-16Cr-4Zr-3.5Si. Left, figure 5.2.4 with improved contrast. Right bright phase at high magnification (X15000)*

At high magnification, cracks are observed running through the suspected silicide phase. This damage was probably caused during sample preparation and is indicative of a phase that is brittle at room temperature.

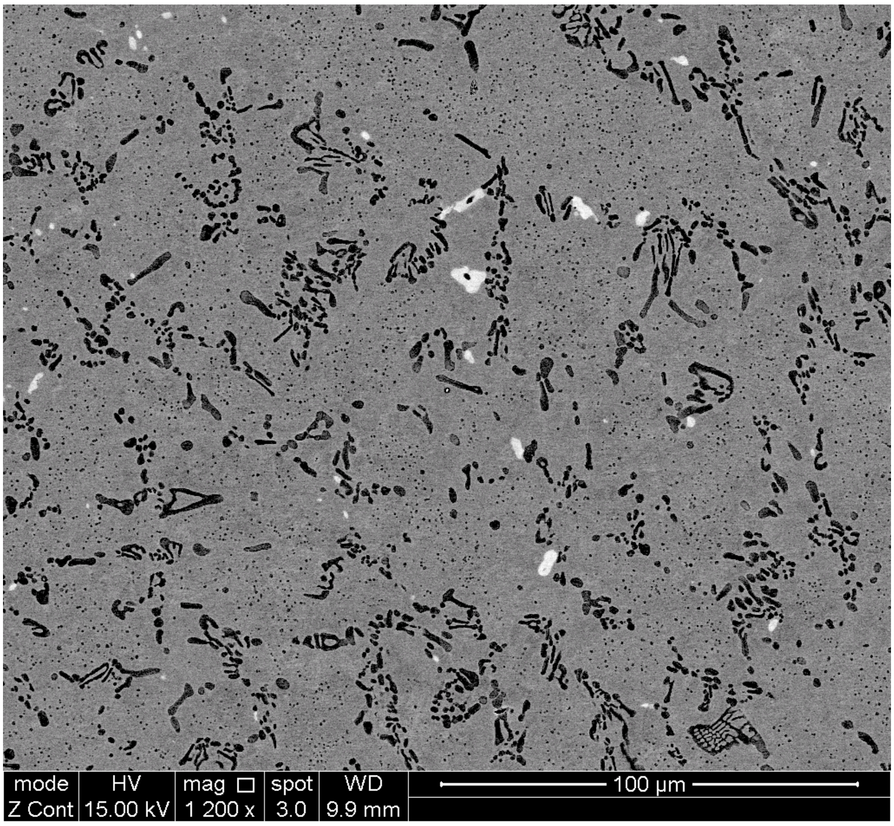

Figure 5.2.6 *Backscatter SEM image of as received Ti-8.8Cr-7.2Mo-4Zr-3.5Si (Mag 1200X)*

Figure 5.2.6 above shows a backscatter SEM image of sample alloy Ti-8.8Cr-7.2Mo-4Zr-3.5Si. This image appears to indicate chromium-containing precipitates located on grain boundaries (dark phase). The more dispersed, spherical dark phase is probably primary alpha titanium (seen more clearly in figure 5.2.7). A silicon zirconium precipitate is observed as bright phases, as in the previous images. Molybdenum and chromium in solution is suspected to be present in the beta titanium matrix.

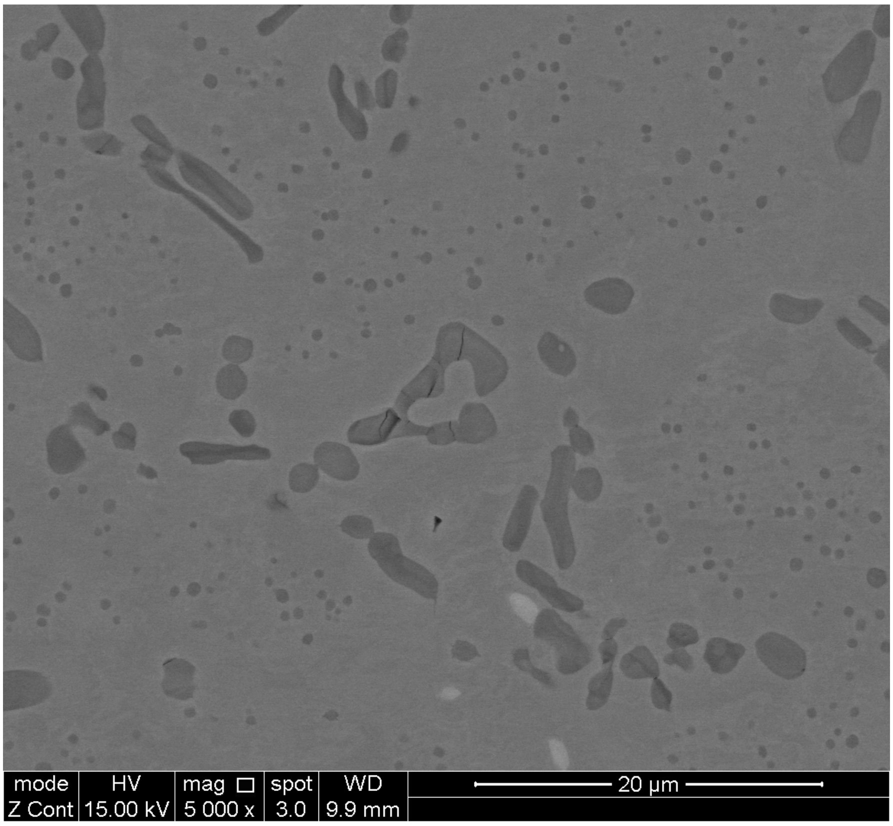

Figure 5.2.7 *Backscatter SEM image of as received Ti-8.8Cr-7.2Mo-4Zr-3.5Si (Mag 5000X)*

At high magnification, cracks are observed in the chromium-containing phase. This damage was probably caused during sample preparation and is indicative of a phase that is brittle at room temperature.

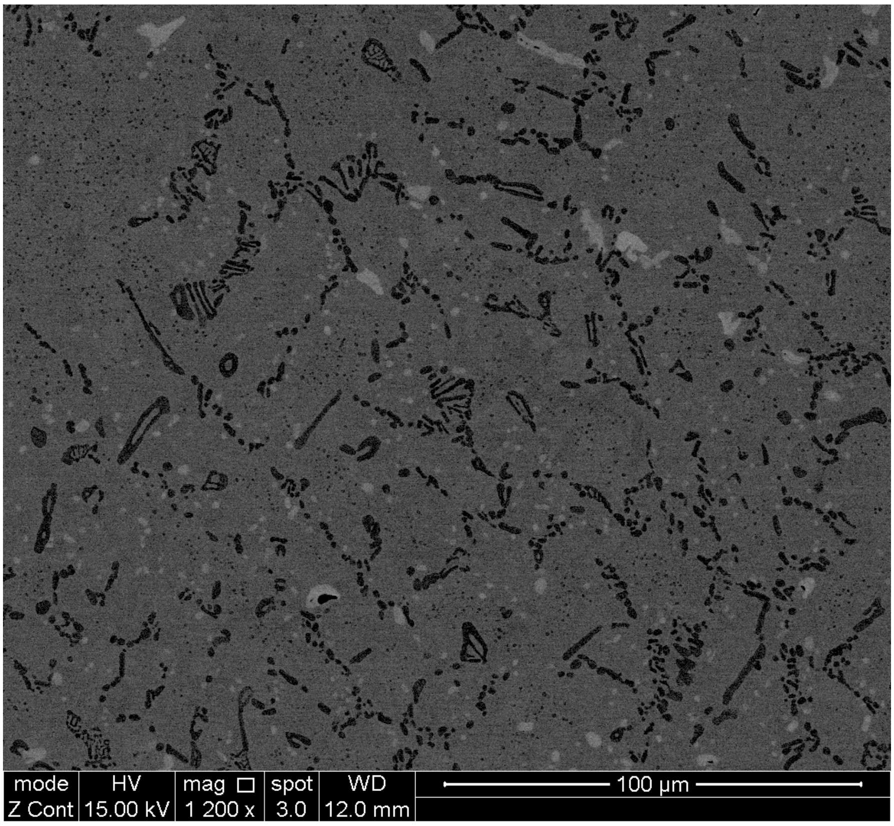

Figure 5.2.8 *Backscatter SEM image of as received Ti-12Nb-3Cr-4Zr-3.5Si (Mag 1200X)*

Figure 5.2.8 above shows a backscatter SEM image of sample alloy Ti-12Nb-3Cr-4Zr-3.5Si. This image indicates that the niobium chromium system is very similar to the molybdenum chromium system in producing chromium-containing precipitates at grain boundaries. The matrix for this alloy probably contains niobium and chromium in solution within the beta titanium matrix.

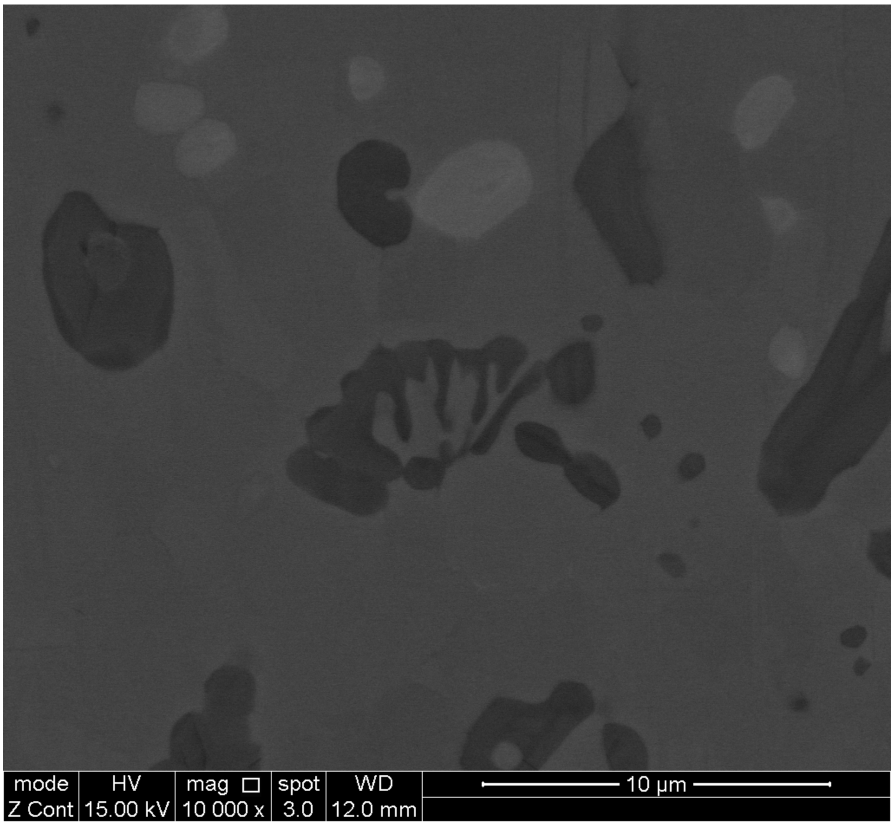

Figure 5.2.9 *Backscatter SEM image of as received Ti-12Nb-3Cr-4Zr-3.5Si (Mag 10000X)*

At high magnification, some phase contrast within the dark phase is observed (shown in figure 5.2.9). This is probably a pro-eutectoid phase containing chromium.

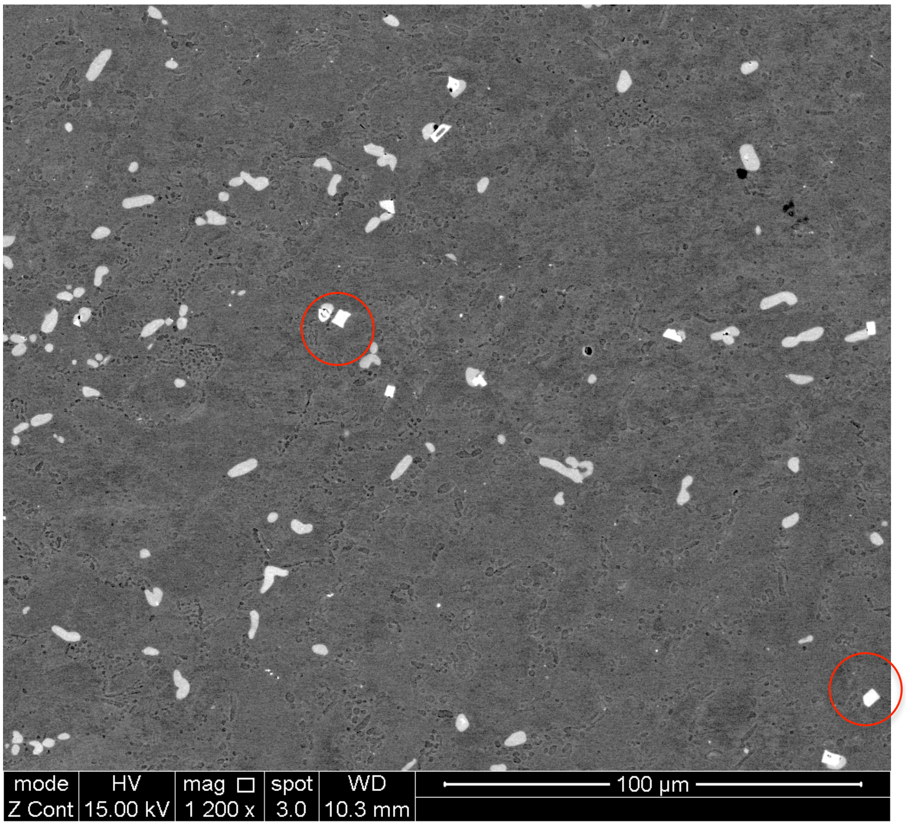

***Figure 5.2.10** Backscatter SEM image of as received Ti-16Cr-4Zr-3.5Si-0.2Y (Mag 1200X)*

The addition of yttrium to the alloy shown in figure 5.2.4 is now visible in figure 5.2.10 as a bright square shaped phase highlighted in this image.

5.3 EDX Spectrum

In order to provide some confidence that the supplied material was of the composition stated, EDX analysis was performed on the samples, again using the procedure outlined in Chapter 3.

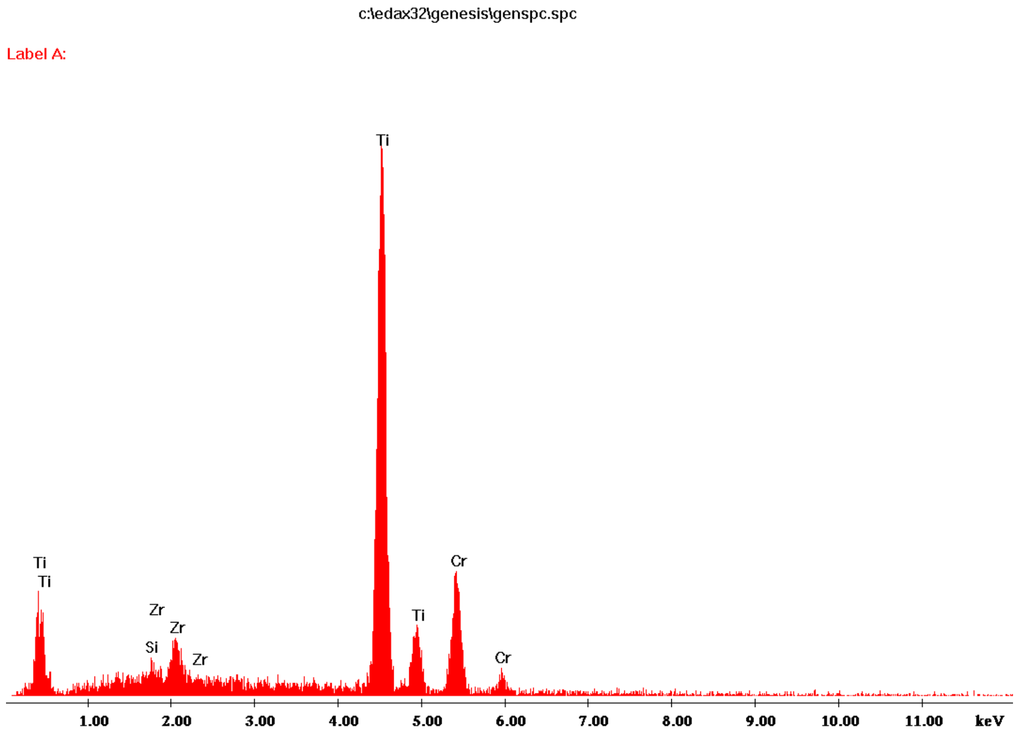

Figure 5.3.1 *EDX Spectrum showing elements present in as received Ti-25Cr-4Zr-0.35Si, and is typical of the spectrums observed in the samples containing 0.35 wt. % silicon.*

Figure 5.3.1 shows the EDX spectrum analysis for sample alloy Ti-25Cr-4Zr-0.35Si. It is worth noting that although this method of EDX provides an idea of the elements present in the material, the data is not quantitative, meaning that the height of the spectrum peaks are not representative of the quantities of each element detected. For the other samples measured, the elemental spectrum was also what was to be expected.

5.4 Microstructure Analysis

Due to the nature of how a backscatter image is produced, a level of compositional analysis can be determined by comparing the contrast of the phases present. The interaction of an accelerated electron beam with the surface of a polished sample (target) creates an assortment of elastic and inelastic collisions amongst electrons and atoms within the target material.

Elastic scattering alters the trajectory of the inward beam of electrons when they interact with a target sample, without affecting their kinetic energy significantly. In simple terms, the elastic scattering can be defined as small particles (electrons) colliding with larger particles (atoms). These larger atoms have a greater atomic number (Z) have a greater probability of interacting with the electrons and causing an elastic collision due to their larger cross sectional area. Therefore, the number of backscattered electrons (BSE) reaching the detector is relative to the average atomic number of the sample. For this reason, a ‘bright’ backscatter electron intensity means that the electrons have interacted with a phase that has a greater average atomic number in the sample. Disparately ‘dark’ areas have lower average atomic number. Using this information, it is possible to quickly distinguish and observe different phases present based on the atomic number of the elemental additions.

Table 5.4.1 below shows the atomic number of the elements contained with the alloy samples investigated during this work.

Table 5.4.1 *Atomic numbers of elements used in sample alloys.*

Element	Atomic Number (Z)
Titanium	22
Chromium	24
Zirconium	40
Silicon	14
Niobium	41
Molybdenum	42

Based on this information, it can be concluded that phases containing zirconium, molybdenum and niobium will appear brightest under backscatter detection. Phases containing titanium and chromium will appear darker with the darkest phases being those that contain silicon.

Combined with backscatter SEM images and EDX analysis some simple schematic diagrams have been created to depict the phases present in the alloy samples. EDX techniques adopted for this work include point analysis as well as window analysis to aid microstructural characterisation.

The alloys containing 0.35 wt.% silicon have been difficult to analyse due to the low composition of silicon. Therefore analysis has been focused on the other samples, which exhibit more potential for the intended application of this work, as described in chapter 4.

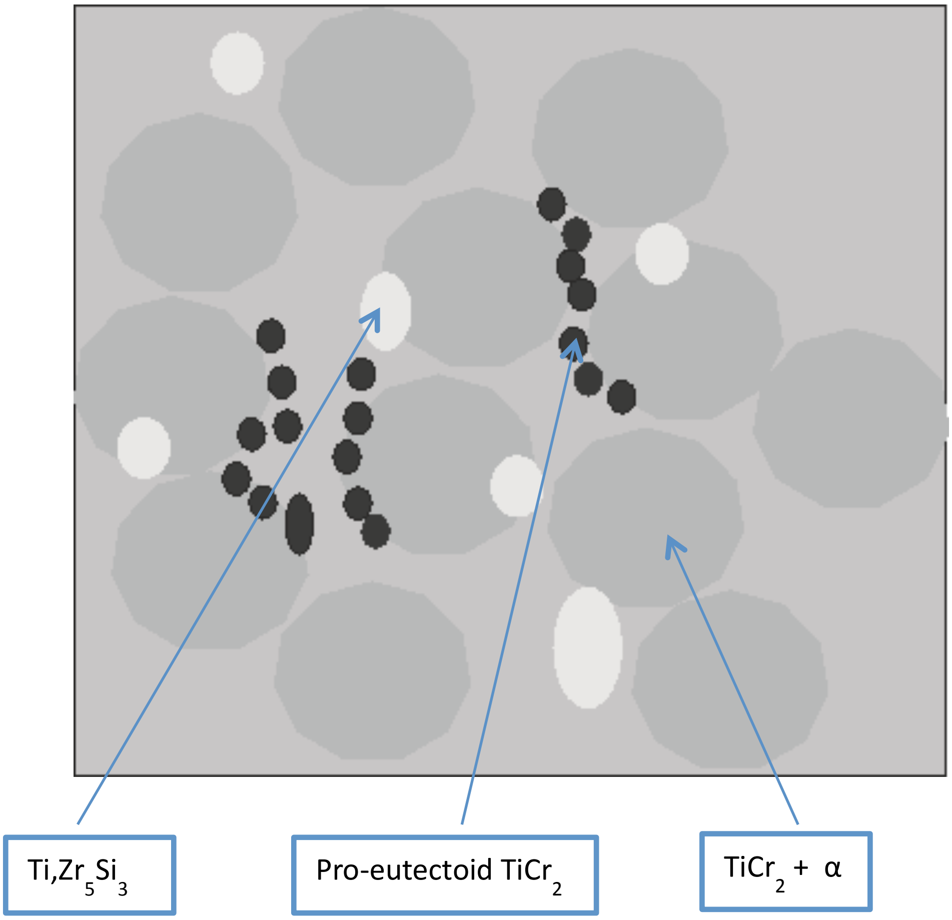

***Figure 5.4.2** Schematic diagram showing phases present in as received Ti-16Cr-4Zr-3.5Si, based on SEM backscatter image.*

Figure 5.4.2 shows the precipitates of Ti,Zr_5Si_3, observed as the bright phase. The reason this phase is shown so brightly is due to the presence of zirconium within the phase. Zirconium is often observed in titanium-containing phases due to the tendency of zirconium to occupy spaces in the titanium lattice sites.

Figures 5.4.3 and 5.4.4 show schematic diagrams for sample alloys Ti-12Nb-3Cr-4Zr-3.5Si and Ti8.8Cr-7.2Mo-4Zr-3.5Si respectively.

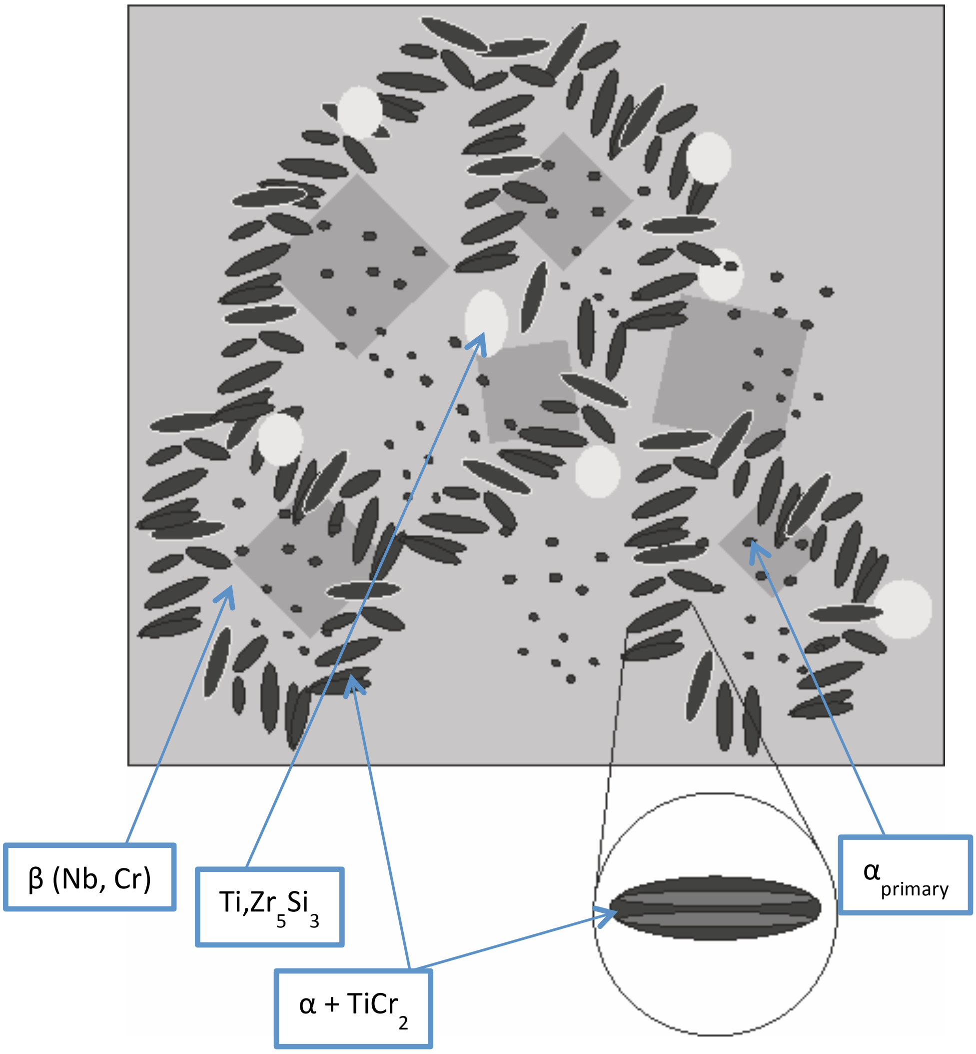

Figure 5.4.3 *Schematic diagram showing phases present in as received Ti-12Nb-3Cr-4Zr-3.5Si, based on SEM backscatter image.*

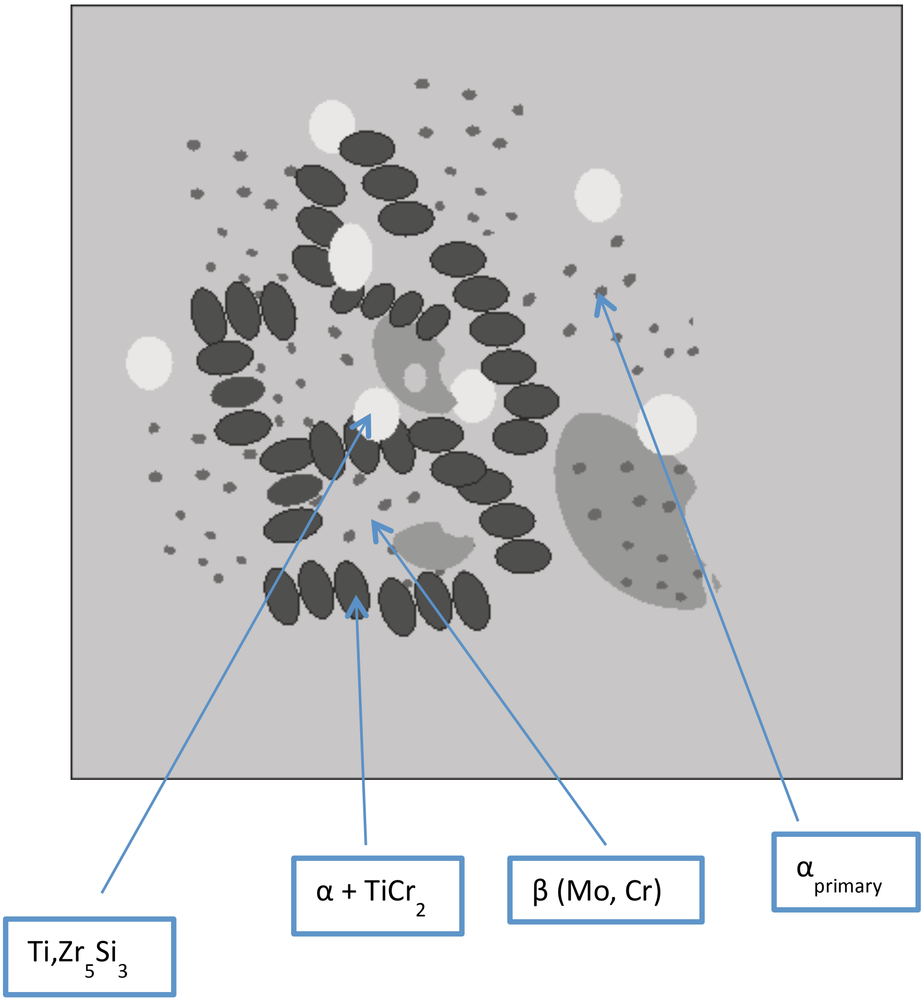

Figure 5.4.4 *Schematic diagram showing phases present in as received Ti-8.8Cr-7.2Mo-4Zr-3.5Si, based on SEM backscatter image.*

5.5 Summary

This chapter has illustrated the level of microstructural analysis carried out on as received material. The results have enabled a fuller understanding of the microstructures observed in such alloys. These observations will be carried forward and used to compare the microstructural changes as a result of time at temperature and mechanical deformation.

In the following chapter (Chapter 6), the resistance to oxidation will be examined on all of the alloys investigated as part of this work. Similarly, the effect time at temperature has on the microstructure of these alloys will be observed in order to understand the phase transformations that take place.

6 Oxidation Analysis

6.1 Introduction

In Chapter 5 the microstructure of the as received alloy samples was investigated. This chapter presents the results obtained from both furnace oxidation testing as well as thermo-gravimetric analysis of sample materials. This chapter will also investigate the resultant microstructure of the alloys subjected to high temperatures, which will provide further microstructural understanding of the sample alloys.

In order for the sample alloys to be successful within the intended application, it is important that materials are able withstand oxidation effects at high temperatures. As the intended operating temperature for this application is approximately 750˚C, then this temperature was chosen as a testing temperature for both thermo-gravimetric analysis as well as furnace heat treatment testing. As well as 750˚C, furnace testing was also carried out at 650˚C and 850˚C to try and get a better understanding of the oxidation effects at high temperatures.

6.2 Furnace Oxidation Analysis

Furnace oxidation test results, carried out on each of the developed alloys and as per the procedure outlined in chapter 3 are presented as percentage weight gain vs. temperature in figure 6.2.1 below. Also included for information purposes is the result for the benchmark alloy, TIMETAL 834.

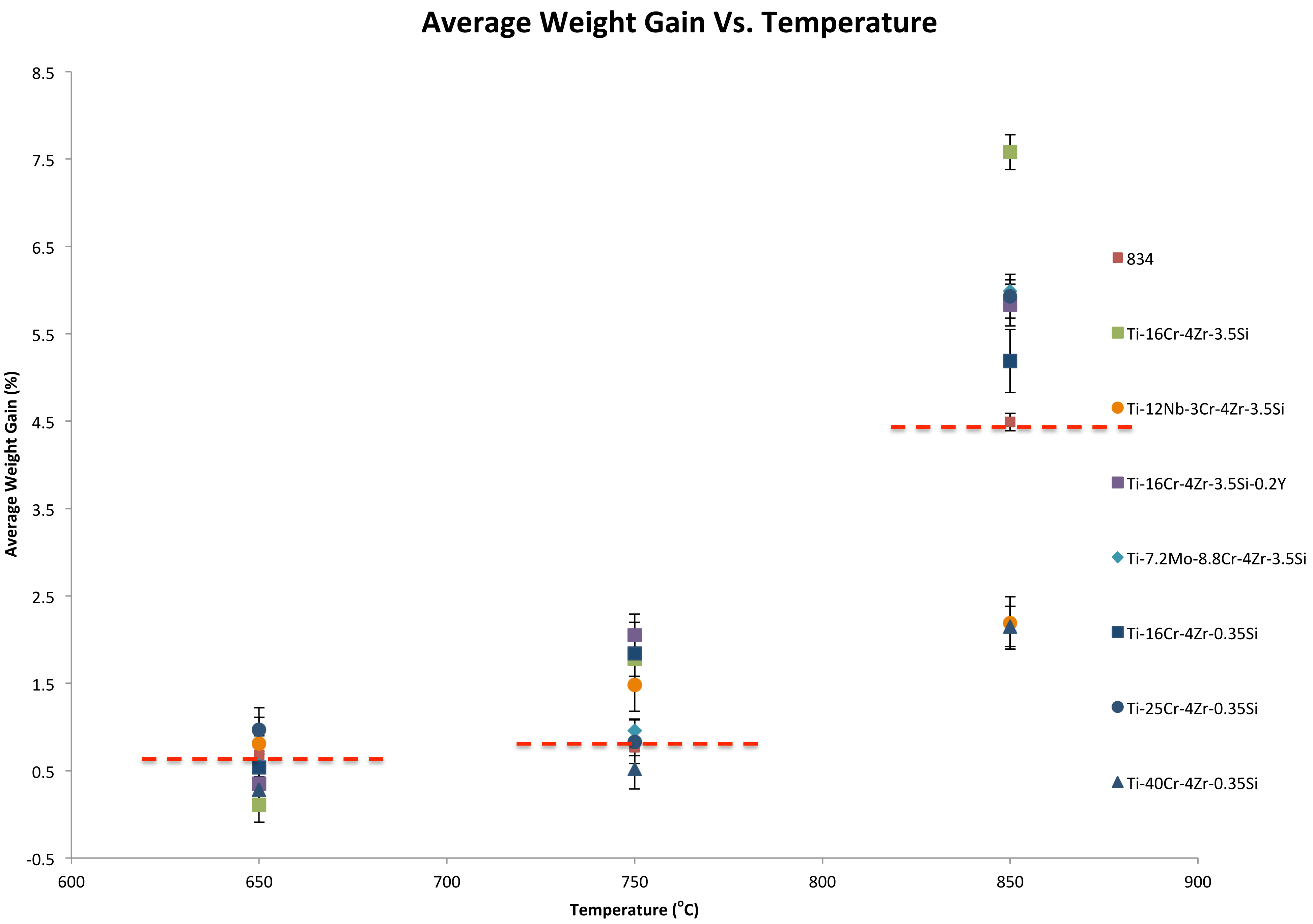

Figure 6.2.1. *Graph indicating average weight gain vs. Temperature after 150 hours for each of the suggested alloys as well as a benchmark alloy, Ti834.*

In terms of a reference point for oxidation resistance, TIMETAL 834 has been used and displayed along with the results. It is expected that if any of the suggested alloys are to be useful for the intended application, the oxidation resistance should exceed that of the TIMETAL 834, i.e. the plotted % weight gain should be below the orange dashed line. Using this data, Ti834 exhibits a 0.7 % weight gain at 650˚C. This increases slightly to approximately 0.9% at 750˚C, however above this temperature is where the limitations for Ti834 lie as the benchmark material exhibits a weight gain of 4.5% at 850˚C. This is a prime example of the reasons for this work. Timetal 834 is not an effective material for temperatures above 750˚C.

Comparing this with the results for the sample alloys, it has been observed that all alloys tested performed similarly to Ti834 at temperatures of 650˚C. Increasing the temperature to 750˚C, rules out all of the alloy samples containing 16 wt.% chromium. This implies that additions of above 16 wt.% chromium are required in these alloys in order to achieve comparable oxidation resistance to our benchmark material. At 850˚C, only the alloy containing 40 wt.% chromium and the niobium-containing alloy achieved better oxidation resistance than Ti834. This suggests that above 750˚C, the only the only alloy samples that can be suggested at this stage to be useful are:

- Ti-40Cr-4Zr-3.5Si;
- Ti-12Nb-3Cr-4Zr-3.5Si

It is suggested therefore that the presence of niobium within the alloy provides a more effective barrier to further oxidation than other alloys developed as part of this work.

As well as the error bars shown, it is believed that there are additional errors present in these results. The oxide scales on some of the samples appeared to suffer from spallation on cooling of the sample after the heat treatment. This would result in some of the oxide scale being ‘missing’ from the sample when it was weighed after the heat treatment, and so weight gain values would be showed as lower than the real value.

SEM micrographs showing the oxide scale after 150 hours at 750˚C are compared with the as cast microstructures as figure 6.2.2 (a to h) below:

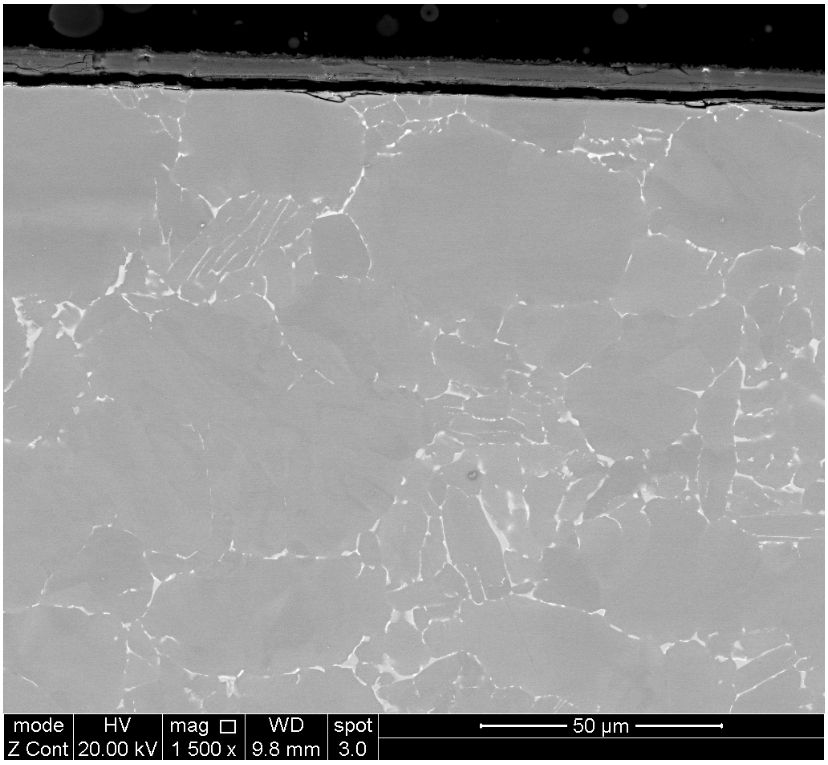

Figure 6.2.2a. *Back scattered electron SEM image showing surface microstructure of Timetal 834 alloy after heat treatment at 750˚C for 150 hours.*

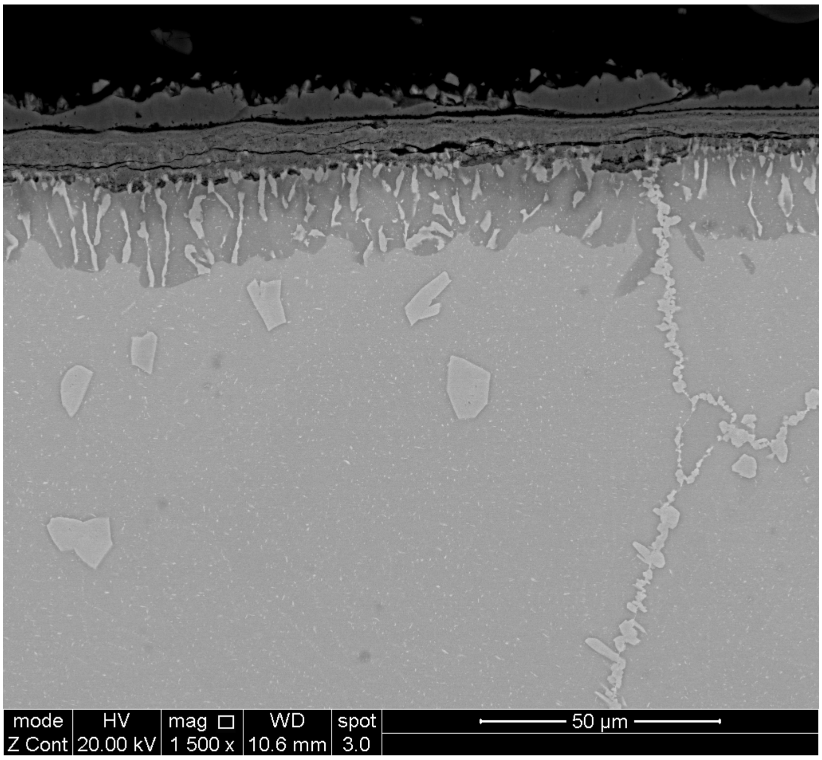

Figure 6.2.2b. *Back scattered electron SEM image showing surface microstructure of Ti-16Cr-4Zr-0.35Si alloy after heat treatment at 750˚C for 150 hours.*

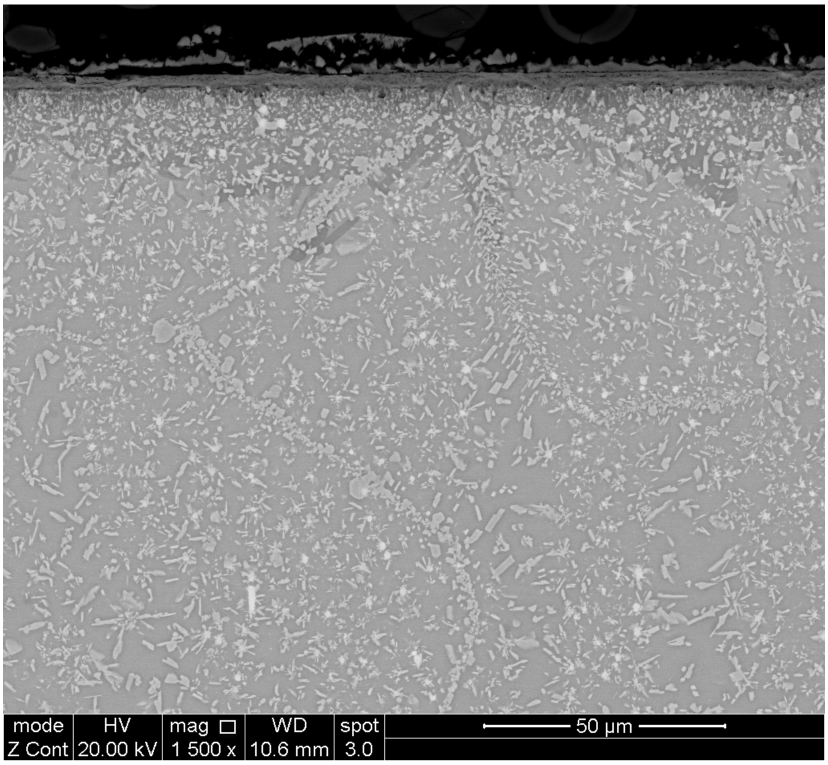

Figure 6.2.2c. *Back scattered electron SEM image showing surface microstructure of Ti-25Cr-4Zr-0.35Si alloy after heat treatment at 750˚C for 150 hours.*

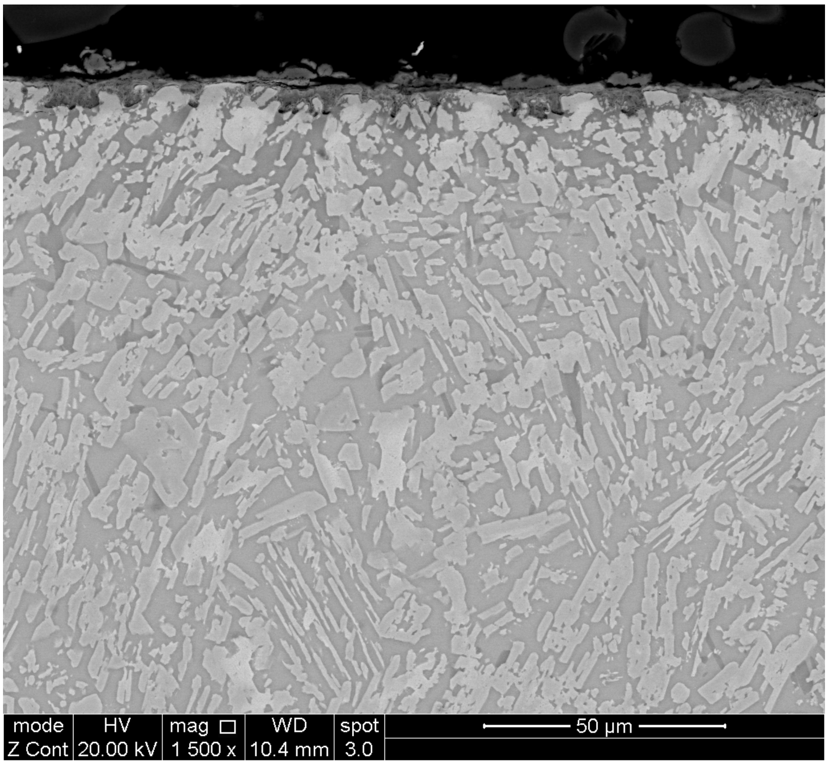

Figure 6.2.2d. *Back scattered electron SEM image showing surface microstructure of Ti-40Cr-4Zr-0.35Si alloy after heat treatment at 750˚C for 150 hours.*

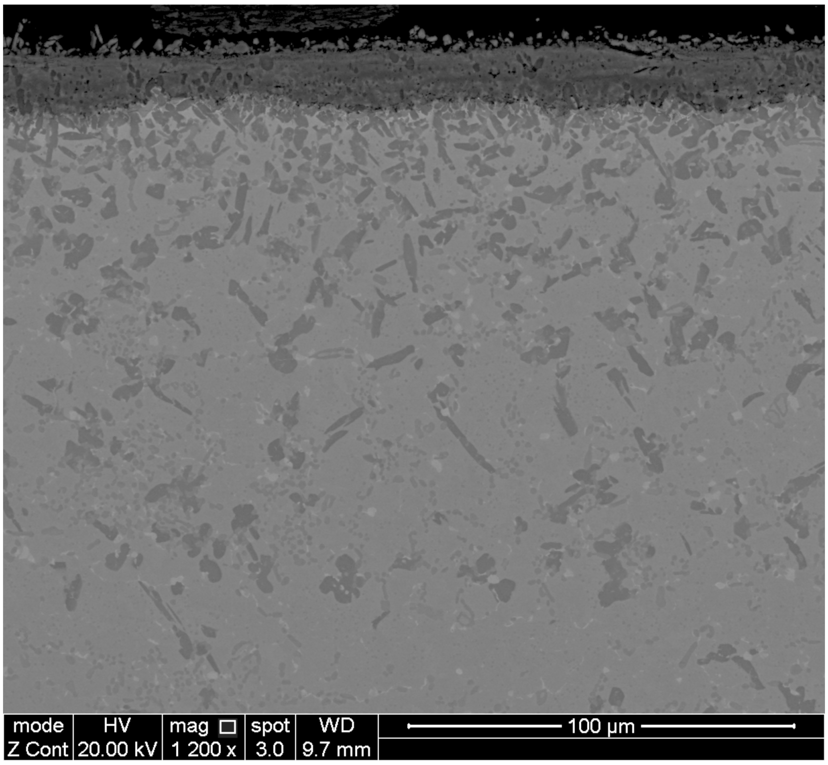

Figure 6.2.2e. *Back scattered electron SEM image showing surface microstructure of Ti-16Cr-4Zr-3.5Si alloy after heat treatment at 750˚C for 150 hours.*

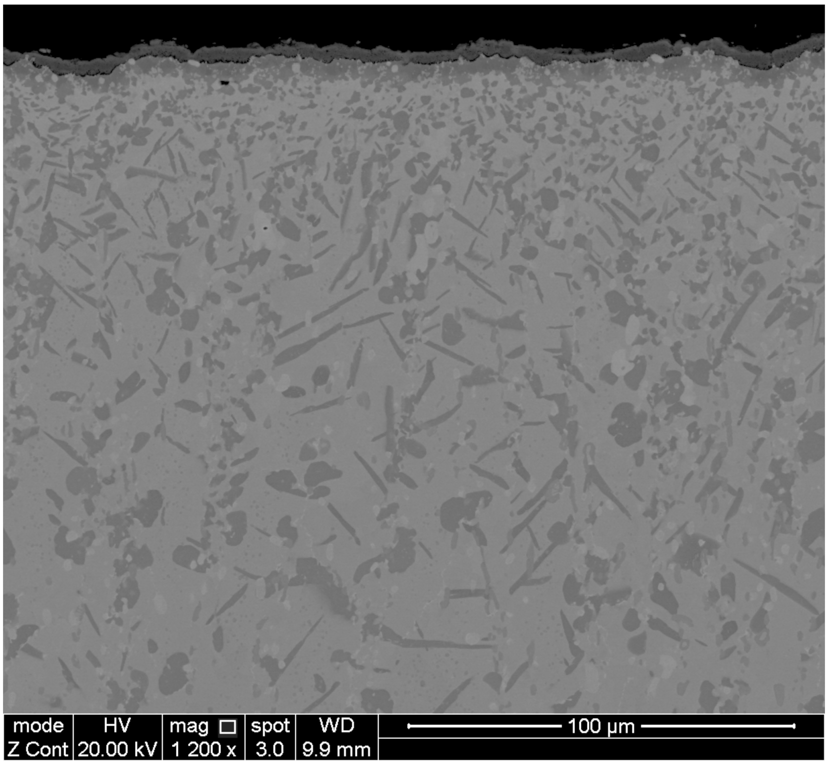

Figure 6.2.2f. *Back scattered electron SEM image showing surface microstructure of Ti-16Cr-4Zr-3.5Si-0.2Y alloy after heat treatment at 750˚C for 150 hours.*

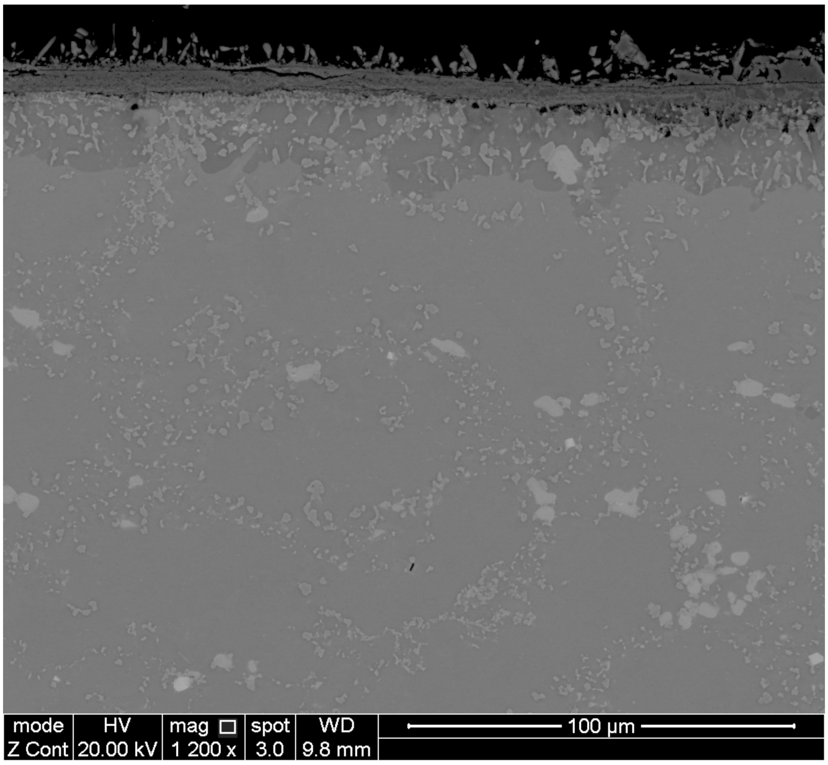

Figure 6.2.2g. *Back scattered electron SEM image showing surface microstructure of Ti-12Nb-3Cr-4Zr-3.5Si alloy after heat treatment at 750˚C for 150 hours.*

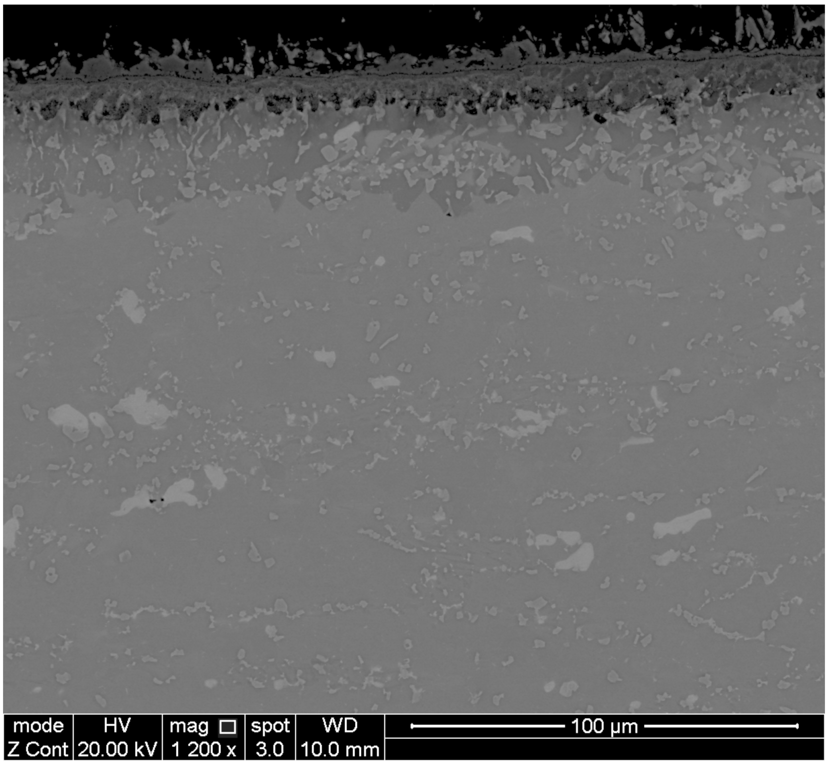

Figure 6.2.2h. *Back scattered electron SEM image showing surface microstructure of Ti-7.2Mo-8.8Cr-4Zr-3.5Si alloy after heat treatment at 750˚C for 150 hours*

Comparing the oxide scale thickness of these alloys, it is observed that benchmark alloy Ti834 exhibits a scale thickness of ~15µm, with little significant cracking. Once oxidised. the dense, adherent scale is thought to provide a barrier to further oxidation hence providing the excellent oxidation resistive properties exhibited by Ti834 up to 750˚C. Alloy containing 16Cr-4Zr-0.35Si exhibits a scale which is ~20µm thick with some further 20µm sub surface effect. There also appears to be some cracking in the scale. Alloy containing 25Cr-4Zr-0.35Si exhibits a scale, which is approximately 10µm thick, again with some sub surface effect. However in the alloy containing Ti-40Cr-4Zr-0.35Si, very little scale is observed but we still have a small sub surface effect. Alloy containing 16Cr-4Zr-3.5Si exhibits a scale which is ~20µm thick. Alloy containing 16Cr-4Zr-3.5Si-0.2Y exhibits a scale which is ~10µm thick with some further 10µm sub surface effect. In the alloy containing niobium, a scale thickness of ~15µm is observed along with a sub surface effect of ~20µm thickness. Finally, in the alloy containing molybdenum, a scale thickness of ~20µm is observed along with a sub surface effect of ~25µm thickness.

It is believed that the sub surface discolouration observed is the result of the surface layer of the alloy becoming depleted in titanium and hence rich in chromium, making the sub surface layer a titanium rich region *[24; 26]*. An interesting fact to note is that it appears as though the $TiCr_2$ precipitates oxidise less rapidly than the alloy matrix, as the oxide scale penetrates deeper into the metal at locations not occupied by a precipitate.

The information obtained here tells us that firstly, the increase in silicon content from 0.35 wt.% to 3.5 wt.% improves the adherence of the scale to the base material and provides a scale which contains fewer horizontal cracks. The increase in silicon also appears to increase the volume fraction of precipitates within the microstructure.

Similarly, the increase in chromium content from 16 wt.% to 25 wt.% and then to 40 wt.% provides a significant improvement in oxidation resistance. Looking at the microstructure, it is suggested that this improvement in oxidation resistance could be related to the increased volume fraction of chromium-containing precipitates that is present as the chromium content is increased. The volume fraction of chromium containing precipitates also relates to the thickness of the chromium rich region at the surface as there is less chromium remaining in solution to migrate to the surface during oxidation.

Based on the information shown here, the 0.2 wt.% addition of yttrium to the developed alloy does not appear to have a lasting effect on the oxidation resistance despite its apparent facilitation in the production of a more compact scale.

The addition of niobium in place of 16 wt.% chromium provides better oxidation resistance at temperatures above 650˚C. Examining the microstructure at 750˚C, the reason for this improved resistance to oxidation seems to be related to the presence of a bright precipitate phase at the surface of the alloy, combined with the more compact oxide scale offered by additions of niobium. Examining the bright phase using energy dispersive x-ray on a SEM indicates that the phase is rich in titanium, zirconium and silicon probably in the form Ti,Zr_5Si_3. This suggests that the reduced chromium content promotes the formation of this silicide phase, which provides improved resistance to oxidation.

While replacing 16 wt.% chromium with additions using a molybdenum chromium master alloy also promotes the formation of the silicide phase described above, the scale observed on the Ti-7.2Mo-8.8Cr-4Zr-3.5Si alloy is less compact and contains significant cracking. There appears to be a lower volume fraction of the apparent silicide phase in this microstructure, suggesting that the level of chromium within the alloy is a restrictor to the growth of the silicides. Therefore it is suggested that the presence of molybdenum in the alloy is not as effective in providing resistance to oxidation as that of alloys containing niobium in the levels investigated in this work.

Although the Ti-40Cr-4Zr-0.35Si alloy appears to be an alloy with oxidation resistance sufficient to cope with the intended application, there is an issue with ductility, as shown in figure 6.2.3. This poor ductility is probably caused by the high volume fraction of intermetallic phases present within the microstructure. This along with the unstable phase transformations at in service temperatures will mean that this alloy does not seem suitable for this application.

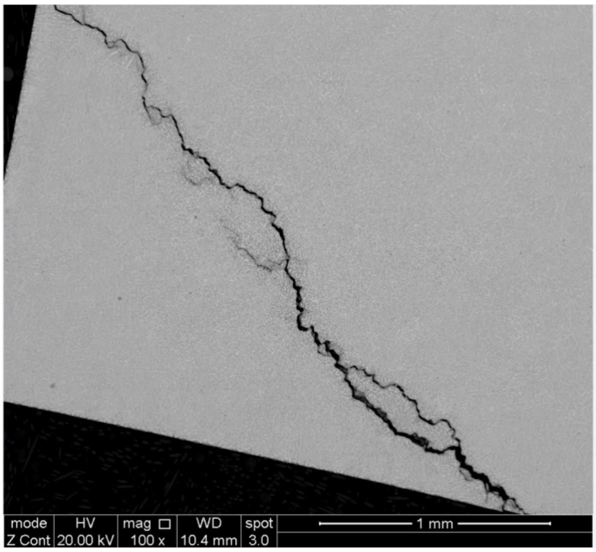

Figure 6.2.3. *SEM micrograph showing suggested alloy: Ti-40Cr-4Zr-0.35Si. Cracks running through the sample indicate its poor ductility characteristics.*

6.3 Thermo-gravimetric Analysis

As described in chapter 4, alloy samples were investigated for oxidation resistance using thermo-gravimetric analysis (TGA). For the purposes of this investigation the following experimental conditions were used on alloy samples containing 3.5 wt.%:

- Isothermal temperature: 750˚C (1382˚F);
- Test Time: 50 hrs;
- Air purge (25mL/min) was used as the controlled atmosphere.

Oxidation plots in percentage weight gain and weight gain per unit area (mg/cm) are shown in Figures 6.3.1 and 6.3.2, respectively. Total weight change (gain) of the samples is provided in Figures 6.3.3 and 6.3.4.

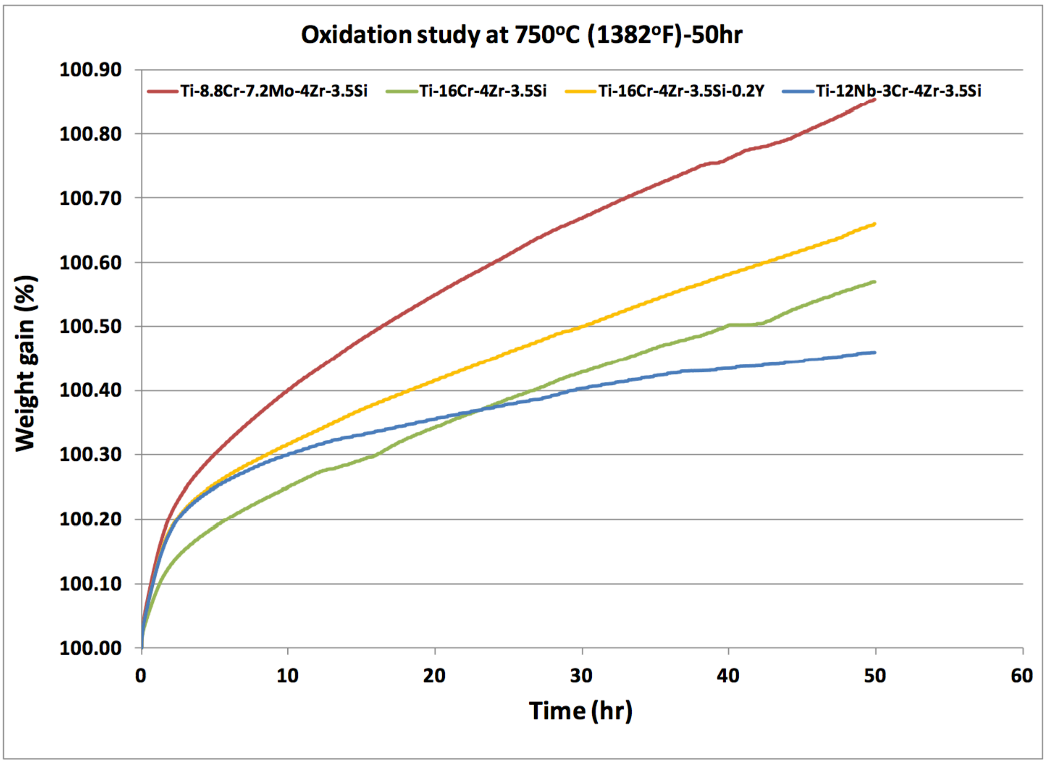

Figure 6.3.1. *Weight gain (%) vs. time plot for the oxidation of the alloys at 750˚C (1382˚F) tested for 50 hours.*

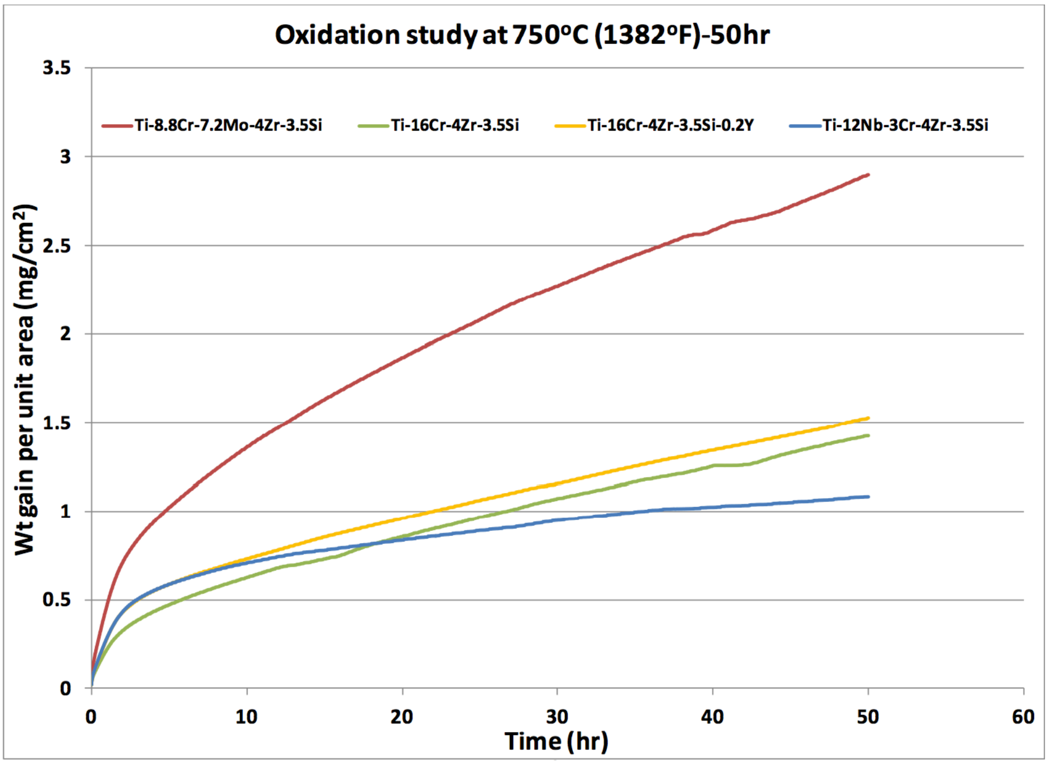

Figure 6.3.2. *Weight gain per unit surface area (mg/cm^2) vs. time plot for the oxidation of the alloys at 750˚C (1382˚F) tested for 50 hours.*

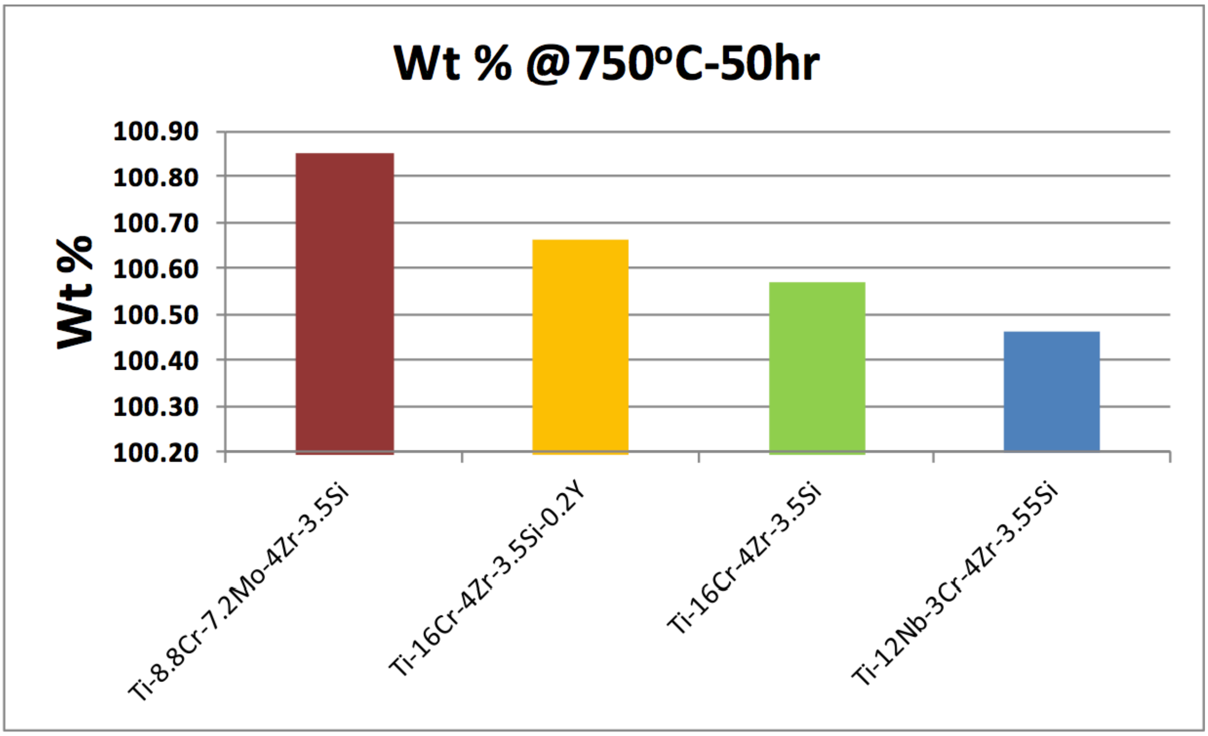

Figure 6.3.3. *Total weight gain in wt% of the alloys at750˚C (1382˚F)-50hr test.*

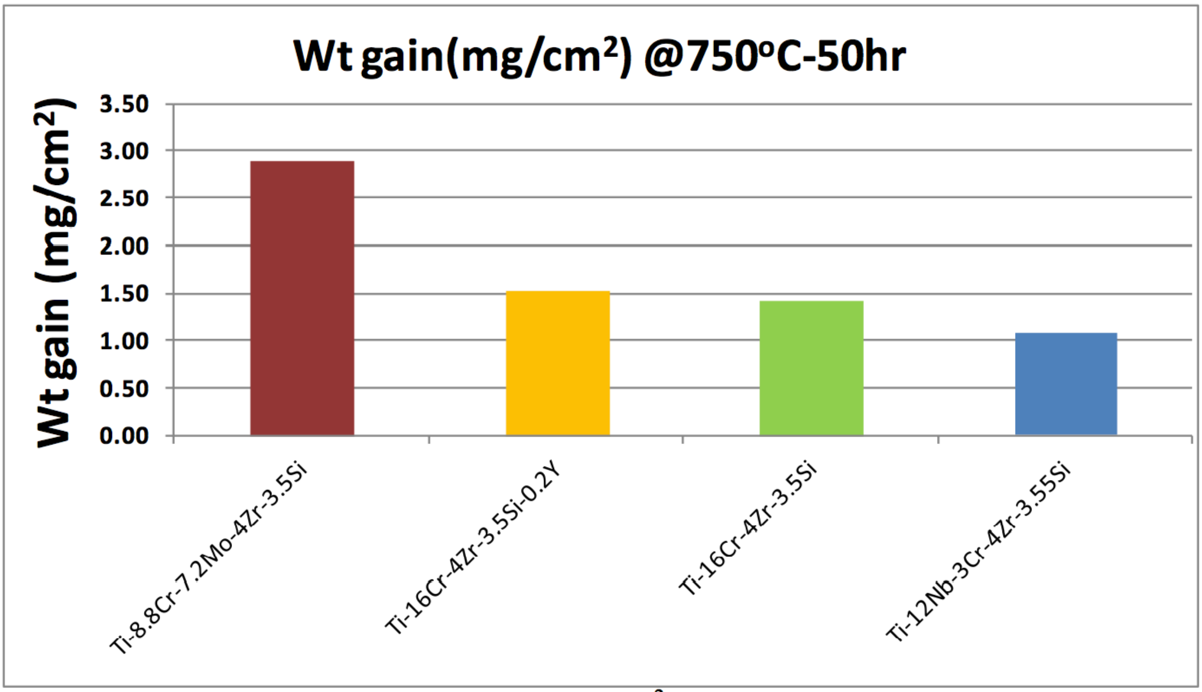

Figure 6.3.4. *Weight gain per unit surface area (mg/cm2) of the alloys at750˚C (1382˚F)-50hr test.*

Photomicrographs of the samples after the test are given below. All the photomicrographs are at the same magnification, 500X.

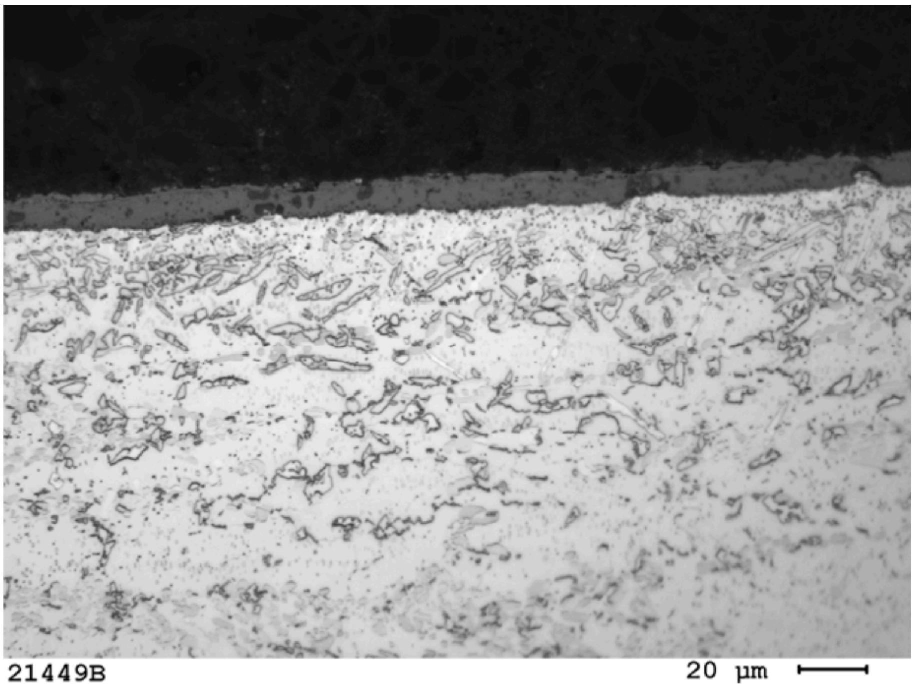

Figure 6.3.5. *Alloy Ti-8.8Cr-7.2Mo-4Zr-3.5Si*

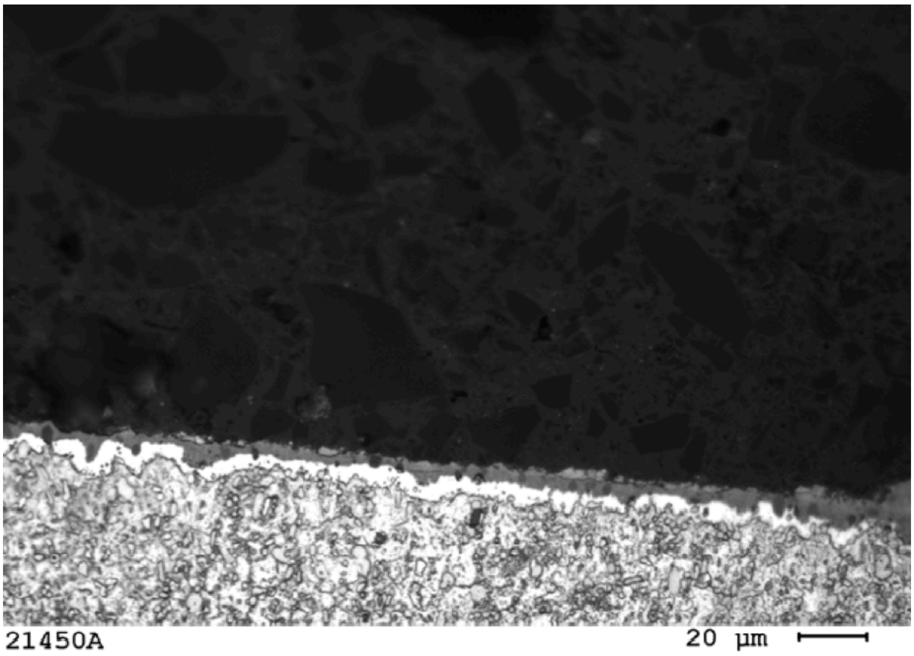

Figure 6.3.6. *Alloy Ti-16Cr-4Zr-3.5Si*

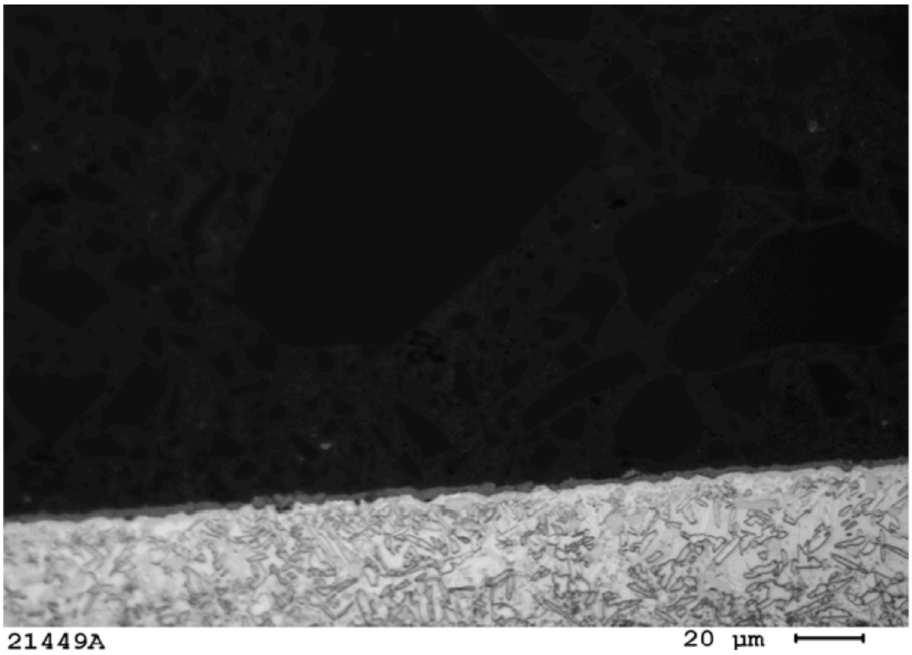

Figure 6.3.7. Alloy Ti-16Cr-4Zr-3.5Si-0.2Y

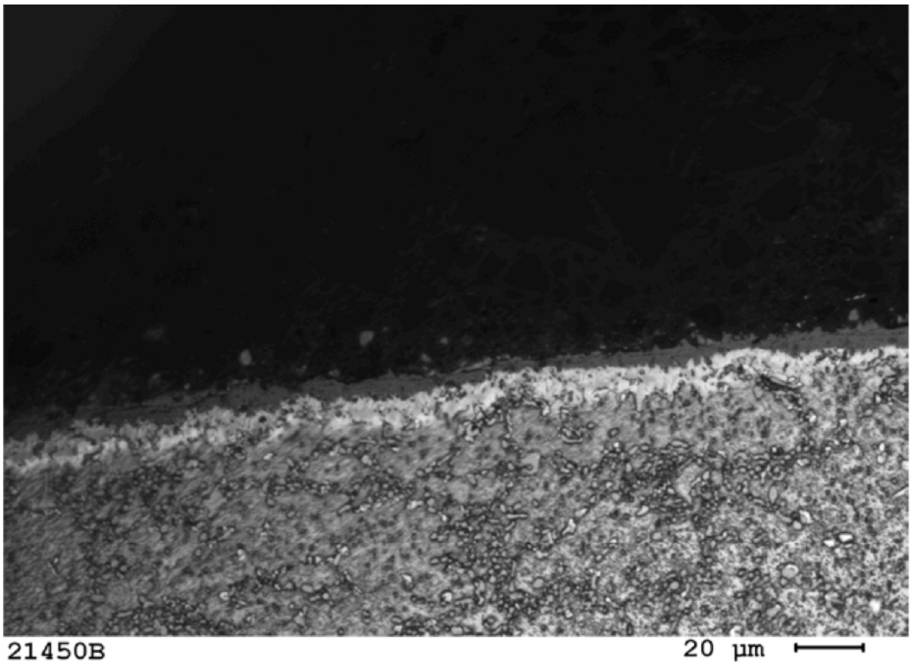

Figure 6.3.8. Alloy Ti-12Nb-3Cr-4Zr-3.5Si

The results obtained from the TG analysis are in agreement with that from the furnace oxidation testing. It can be observed that samples containing niobium showed very good oxidation resistance which is evident from the very thin oxide layer seen in Figure 6.3.8. An increase in chromium content in the alloy is beneficial in improving oxidation resistance. It can be observed that the oxide layer formed on the alloy Ti-16Cr-4Zr-3.5Si (Figure 6.3.6) is thinner than the oxide layer formed on alloy Ti-8.8Cr-7.2Mo-4Zr-3.5Si (Figure 6.3.5).

Small addition of yttrium to the alloy decreased the oxidation resistance of the alloy. Since the yttrium content is so low (0.2wt.%), no significant increase in oxide layer thickness is observed in the microstructure (Figure 6.3.7).

From the results obtained from TGA, the following observations can be concluded:

1. Increase in Cr seems beneficial in providing better oxidation resistance.
2. Alloys with Nb showed very good oxidation resistance.
3. Yttrium decreases the oxidation resistance, even with very low alloying content.

These results are concurrent with the results of the furnace oxidation analysis for the same alloys.

6.4 Effect of Heat Treatment on Alloy Microstructure

The suspicions arising from the thermodynamic simulations regarding phase transformations at higher temperatures appear to be proven by comparing micrographs with those of the as cast samples. The following images (figures 6.4.1, 6.4.2 and 6.4.3) compare the effect of heat treatments on the alloy microstructures. By comparing samples that were quenched after heat treatment with those that were slow cooled, an understanding of the microstructural changes during cooling can be observed.

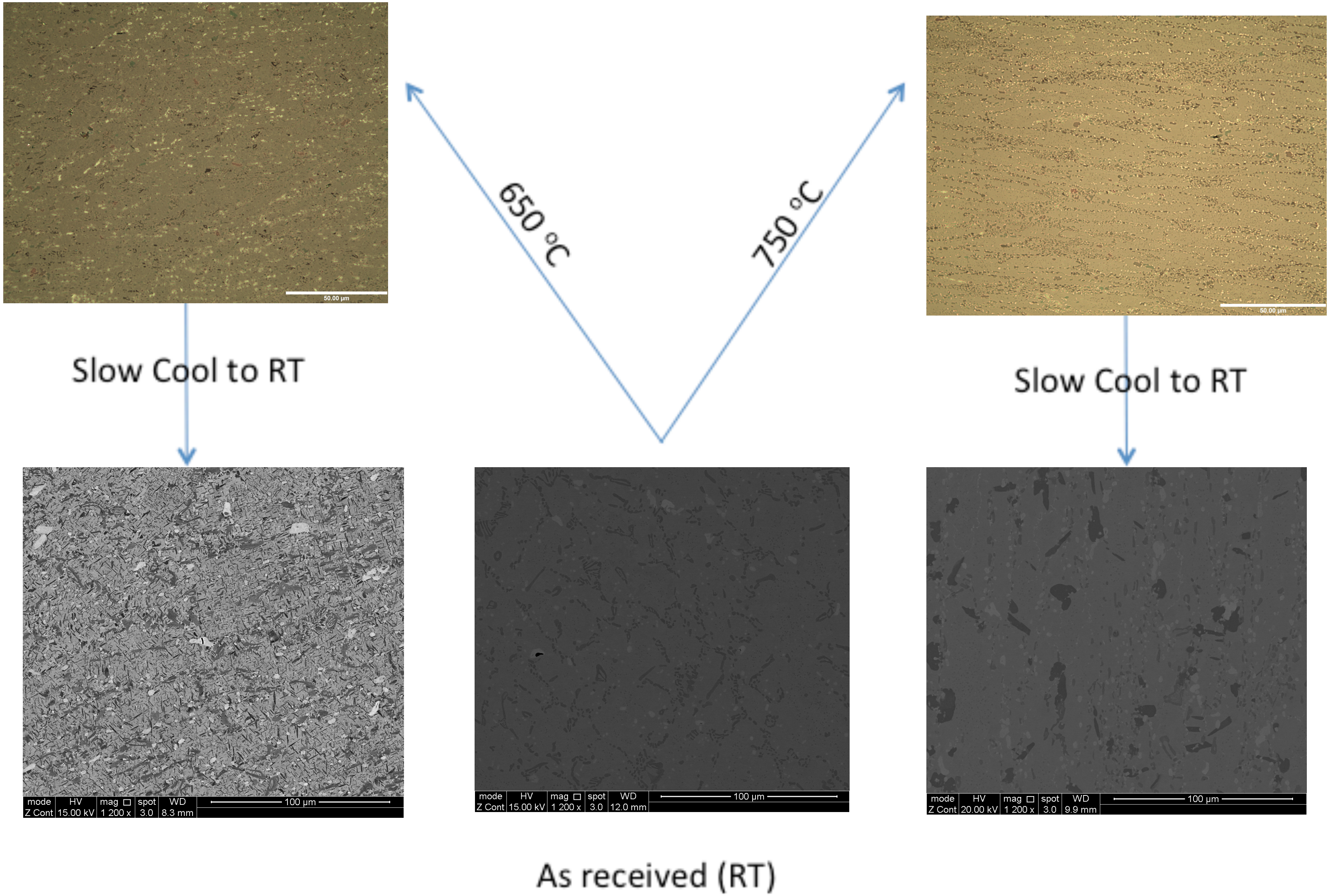

Figure 6.4.1. *Diagram indicating microstructural changes as a result of heat treatment for alloy sample Ti-12Nb-3Cr-4Zr-3.5Si*

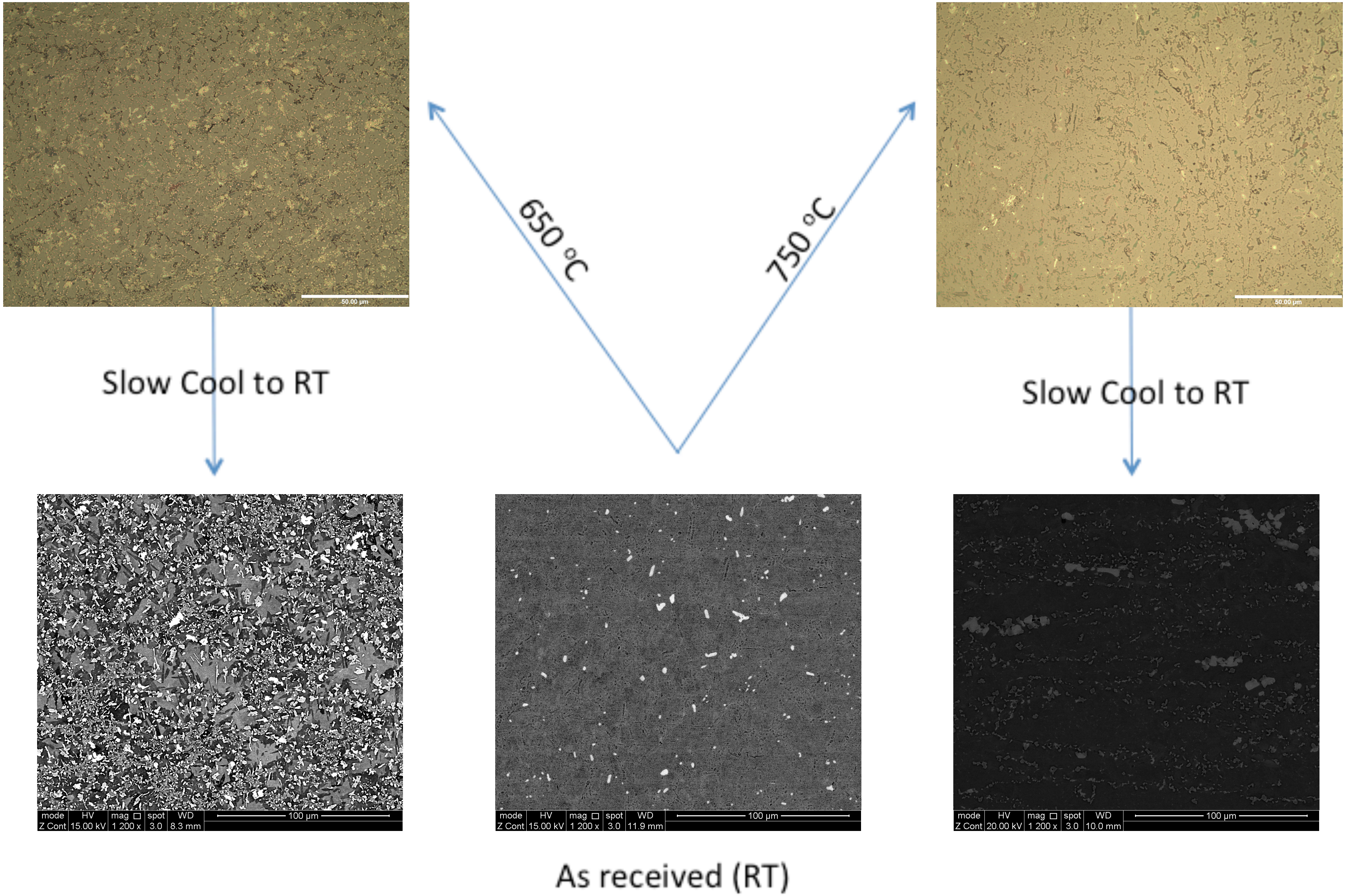

Figure 6.4.2. *Diagram indicating microstructural changes as a result of heat treatment for alloy sample Ti-16Cr-4Zr-3.5Si*

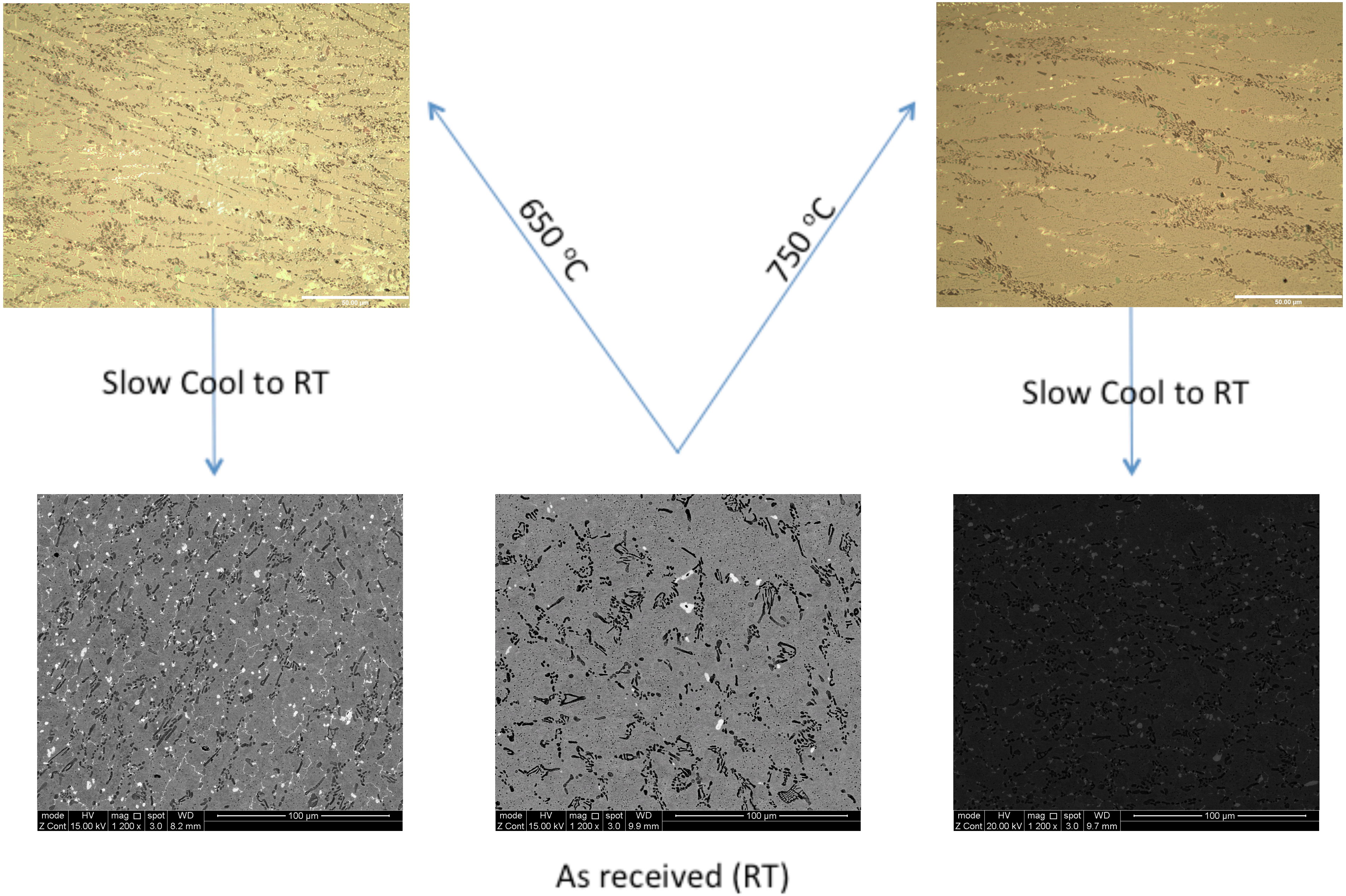

Figure 6.4.3. *Diagram indicating microstructural changes as a result of heat treatment for alloy sample Ti-7.2Mo-8.8Cr-4Zr-3.5Si*

In order to gain a better understanding of these microstructural changes, some schematics were prepared with the help of EDX spot analysis. Those for alloy Ti-16Cr-4Zr-3.5Si are shown below in figures 6.4.4, 6.4.5 and 6.4.6 as an example:

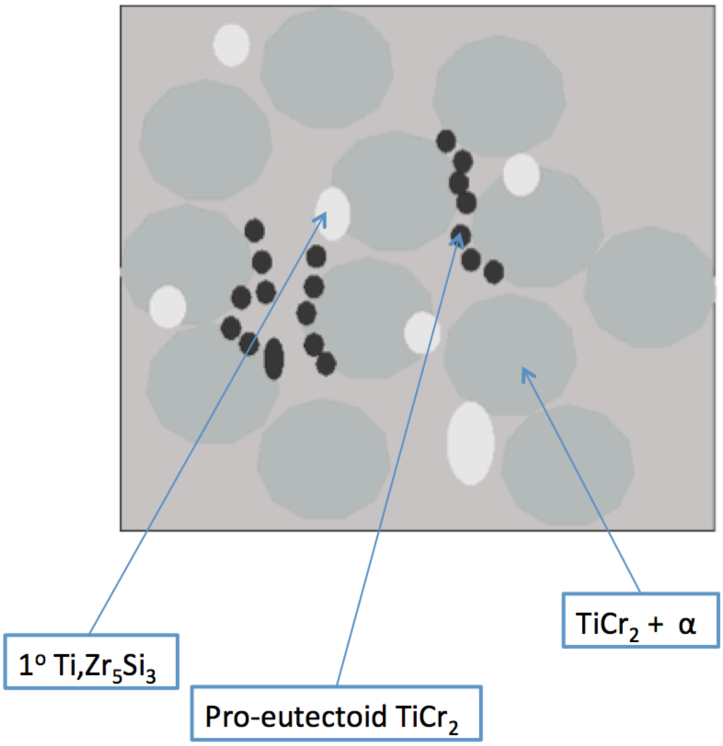

Figure 6.4.4. *Schematic diagram indicating the phases present in* ***as received*** *Ti-16Cr-4Zr-3.5Si.*

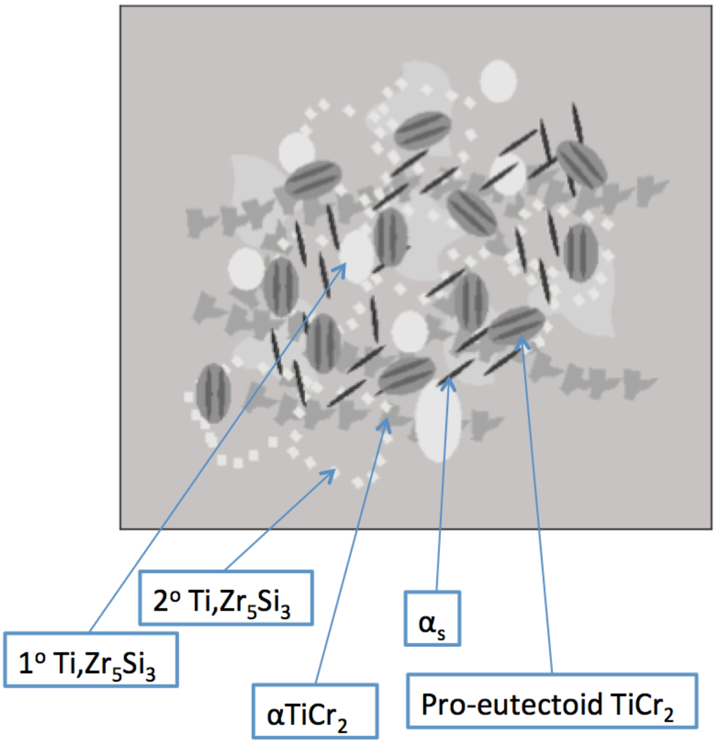

Figure 6.4.5. *Schematic diagram indicating the phases present as a result of slow cooling from* ***650°C*** *for alloy Ti-16Cr-4Zr-3.5Si.*

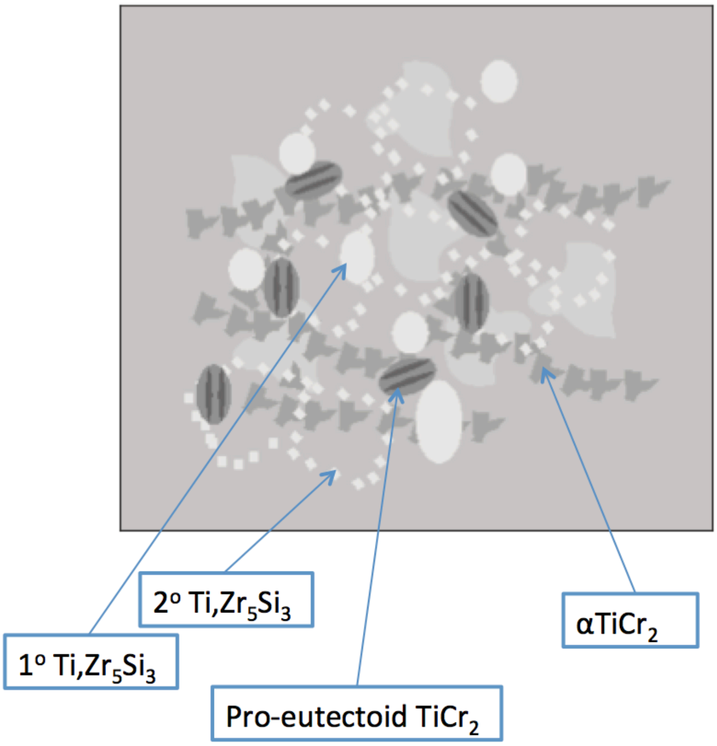

Figure 6.4.6. *Schematic diagram indicating the phases present as a result of slow cooling from* ***750°C*** *for alloy Ti-16Cr-4Zr-3.5Si.*

From these images it is reassuring to note that the phases present are in agreement with those predicted during thermodynamic simulations. This was observed in all cases of alloys examined, which further proves the benefits, and accuracy/effectiveness of thermodynamic simulations. Also unsurprisingly, the slow cooling of all of the developed alloys has the effect of an increase in the volume fraction of precipitates or pro-eutectoid phases within the microstructure. This growth of the phases appears to have an effect in improving the oxidation resistance particularly for chromium containing precipitates located at the alloy surfaces.

6.5 Summary

In this chapter, the effect of oxidation in each of the alloy samples has been examined using a variety of methods. A number of conclusions, some of no surprise have been identified. The amount of chromium added to sample alloys improves its oxidation resistance while detrimentally affecting its ductility. The oxidation resistance of alloy samples is improved by increasing the silicon content from 0.35 wt% to 3.5 wt.%. The addition of niobium to alloys investigated as part of this work greatly improves oxidation resistance. The alloy Ti-12Nb-3Cr-4Zr-3.5Si appears to be the most beneficial in terms of oxidation resistance as it exhibits comparable or better resistance than Timetal 834, which was used as the benchmark material.

Chapter 7 will compare the mechanical properties of sample alloys. The information gained here will enable a detailed conclusion and comparison between all the samples examined as part of this work and their suitability to the intended application.

7 Analysis of Mechanical Properties

7.1 Introduction

Chapter 7 will focus on the testing of the mechanical properties associated with the sample alloys. Room temperature tensile tests as well as alloy densities and hardness will be examined. Microstructural analysis of the failed tensile specimens will be examined to try and link the microstructure with the tensile strength.

7.2 Alloy Density

The densities of the sample alloys were calculated by combining the densities of all the elemental additions at the respective ratios in which they occur within each alloy. The calculations were then compared with existing alloys to determine the appropriateness of the suggested alloys within the application for which they are being designed. The inclusion of Inconel 718 and Timetal 834 has been included as the nimonic and titanium alloy benchmarks respectively. The density of the alloy samples has been calculated and reported in figure 7.2.1 below:

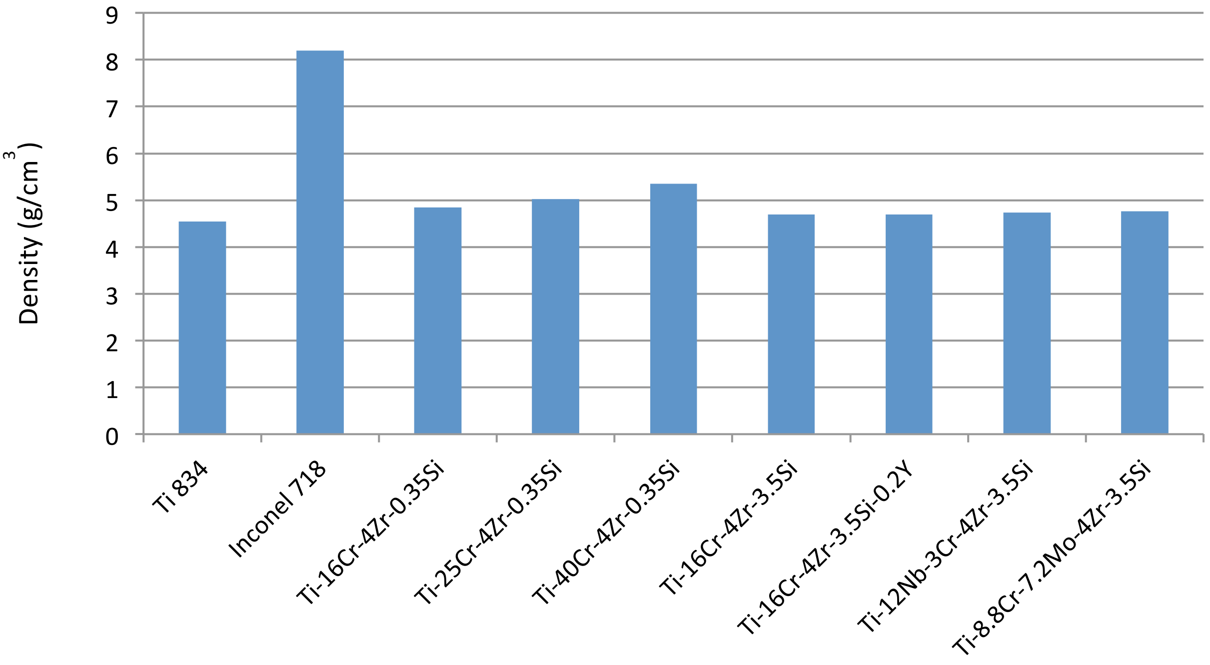

Figure 7.2.1. *Chart comparing calculated densities of as received sample alloys in g/cm^3.*

The density of the alloys increases with added chromium content, which is to be expected. Similarly, the niobium containing alloy also has a (slightly) higher density than Timetal 834.

Density, of course, is an important factor in material selection for the aerospace industry in that any unnecessary increase in density is an unnecessary increase in cost for airlines. Although the density of all the sample alloys is higher than that of Ti834, a comparable nimonic alloy (which is currently used in this application) INCONEL 718 has a density of 8.19g/cm^3, considerably higher than any of the suggested alloys. It can therefore be assumed that the densities of these alloys should not be a cause for concern.

7.3 Alloy Hardness

The hardness of the as received sample alloys has been measured using a Vickers hardness testing machine. A comparison of the hardness for each of the alloys is shown in figure 7.3.1 below. The hardness values are given in **'Vickers Pyramid Number'(Hv).** The parameters used for the test were 10kg force with a 10 second dwell.

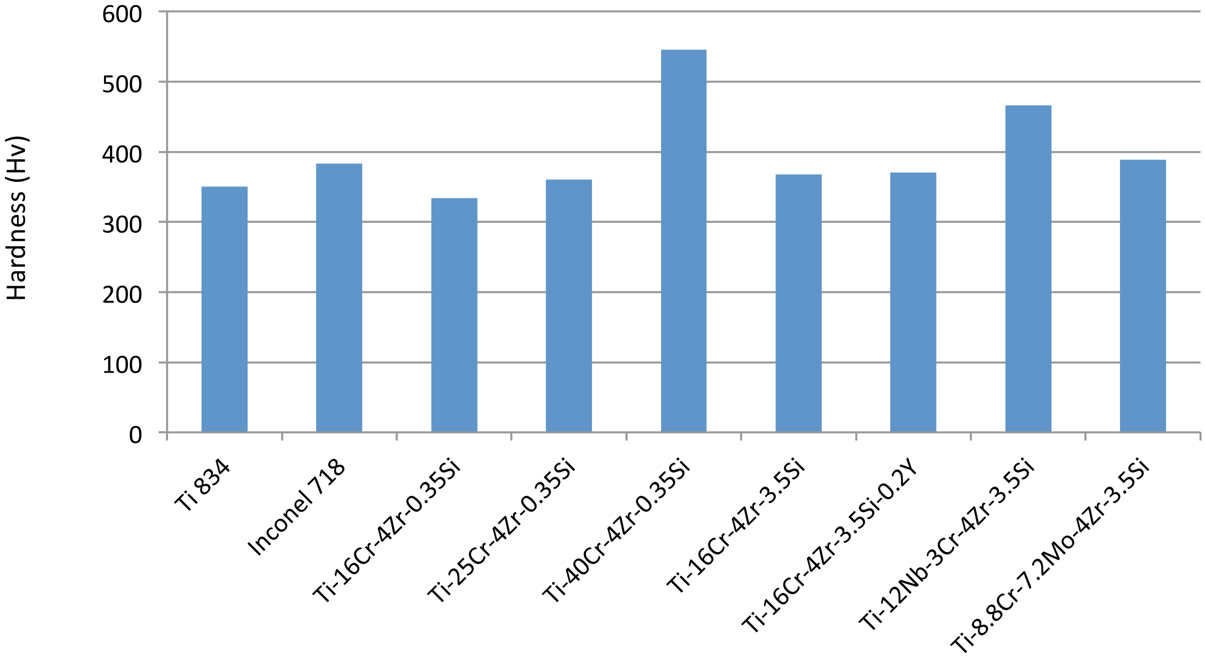

Figure 7.3.1. *Comparison of as-received hardness values.*

Comparing the hardness values of the sample alloys with current in service alloys, all samples tested are relatively similar in terms of hardness. The alloys Ti-40Cr-4Zr-0.35Si and Ti-12Nb-3Cr-4Zr-3.5Si exhibit considerably higher hardness values than Timetal 834. Of course, it is known from the oxidation analysis section in Chapter 6 that the alloy containing 40 wt.% chromium is poor in terms of ductility.

7.4 Tensile Testing

Room temperature tensile tests carried out as per the methods section of this thesis were attempted for each of the sample alloys. However, it was not possible to machine a specimen from the alloy containing 40 wt.% Cr due to its brittleness so no results were obtained for that composition.

7.4.1 Room Temperature Tensile Test (RTT)

The stress-strain curves for alloys Ti-16Cr-4Zr-0.35Si Ti-25Cr-4Zr-0.35Si are shown in figure 7.4.1.

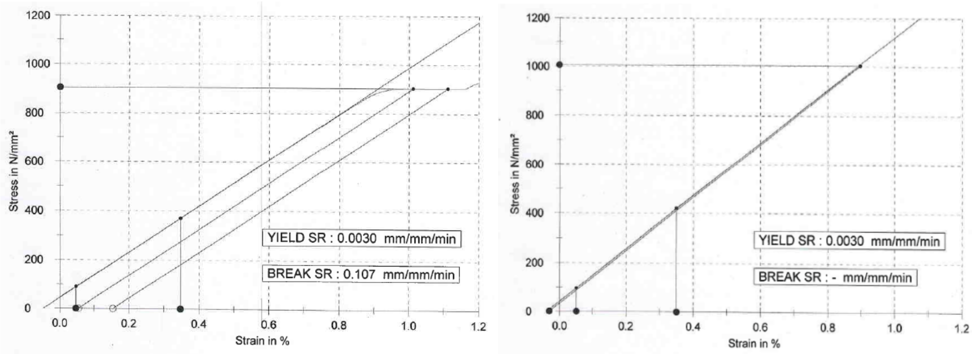

Figure 7.4.1. *Stress-Strain curves for Ti-16Cr-4Zr-0.35Si (left) and Ti-25Cr-4Zr-0.35Si (right).*

From investigating the data in the stress strain curves resulting from the tensile tests it is clear that ductility is a huge problem for these alloys. Poor ductility is almost definitely the result of the high volume fraction if $TiCr^2$ precipitates observed within the alloy, particularly at grain boundaries. The alloy containing 40 wt.% Cr was too brittle to withstand the stresses of machining proving its poor suitability for this application and while the alloy containing 25 wt.% Cr was machined, no values were obtainable for %elongation or %reduction in area, also rendering this alloy unsuitable due to its brittle fracture before reaching proof stress. However, the 25 wt.% Cr alloy did exhibit an ultimate tensile stress of 1004MPa, which is only slightly below that of Timetal 834, the benchmark material which exhibits a UTS of 1050MPa.

The alloy containing 16 wt.% Cr completed the test with a UTS of 967MPa and a 0.2% proof stress of 903MPa. The Young's modulus for the alloy was calculated to be 94.3GPa, which is comparable to Timetal 834, which possesses a Young's modulus of 120GPa. The ductility of this alloy is again a concern, with an elongation value of only 1.5%. Comparing that to

Timetal 834, which has an elongation of 11% under the same conditions; it appears that this alloy is unsuitable in terms of ductility for the application proposed.

Comparing the UTS for all of the sample alloys, it is clear that the addition of chromium is having a strengthening effect on the alloys with the more chromium added the higher UTS observed. It is expected that if the alloy containing 40 wt.% Cr had been tested, a higher UTS than that of the alloy containing 25 wt.% Cr would have been observed.

The stress-strain curves for alloys Ti-16Cr-4Zr-3.5Si, Ti-12Nb-3Cr-4Zr-0.35Si and Ti-7.2Mo-8.8Cr-4Zr-3.5Si are shown in figure 7.4.2, 7.4.3 and 7.4.4 respectively.

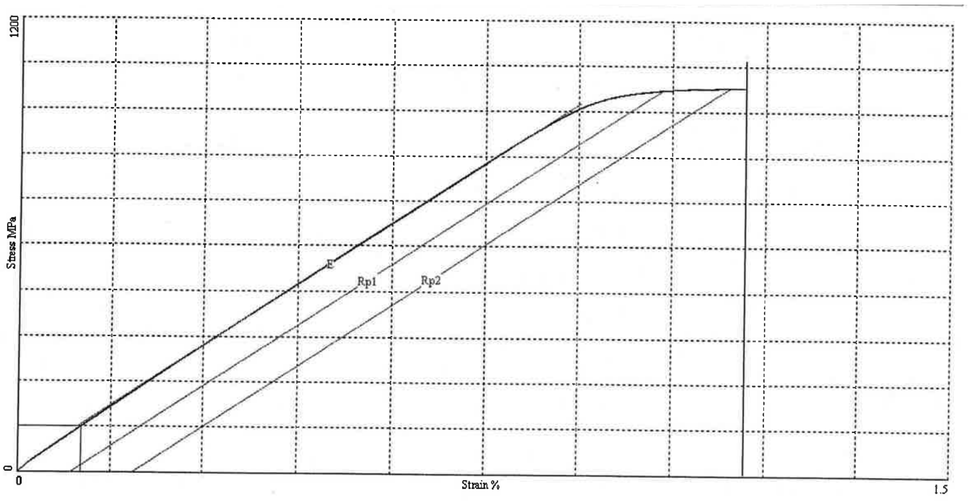

Figure 7.4.2. *Stress-Strain curves for Ti-16Cr-4Zr-3.5Si*

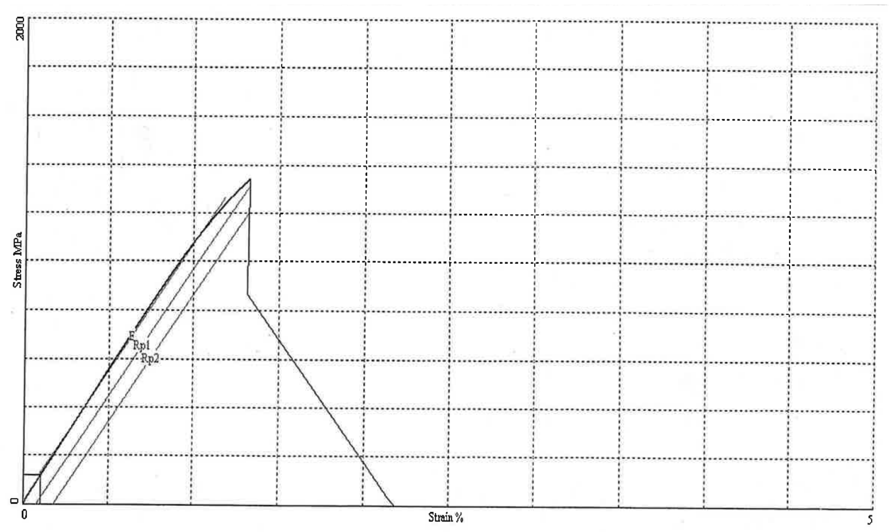

Figure 7.4.3. *Stress-Strain curves for Ti-12Nb-3Cr-4Zr-3.5Si*

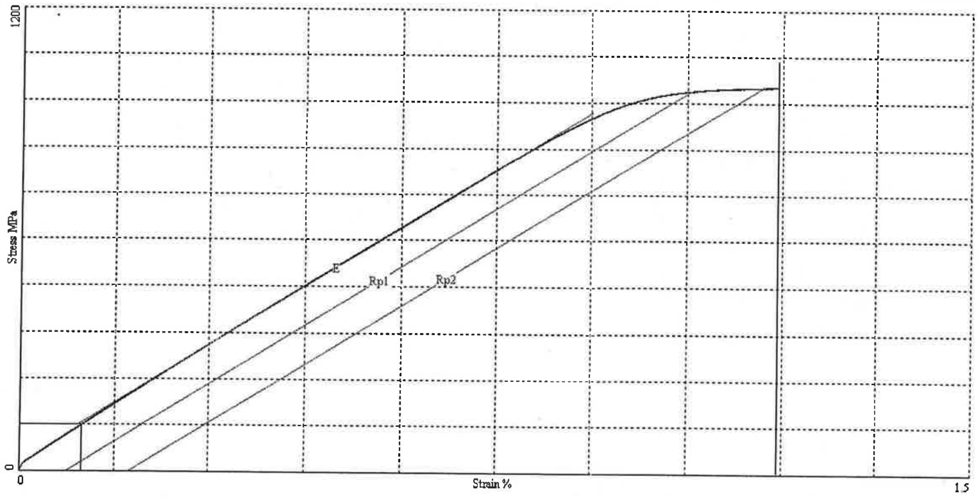

Figure 7.4.4. *Stress-Strain curves for Ti-8.8Cr-7.2Mo-4Zr-3.5Si*

Information taken from the tensile data for all alloy samples tested is collated in the chart below. The chart in figure 7.4.5 below compares the Young's modulus, ultimate tensile strength and 0.2% proof stress of the materials tested. Also shown are those figures for the benchmark alloy, Timetal 834.

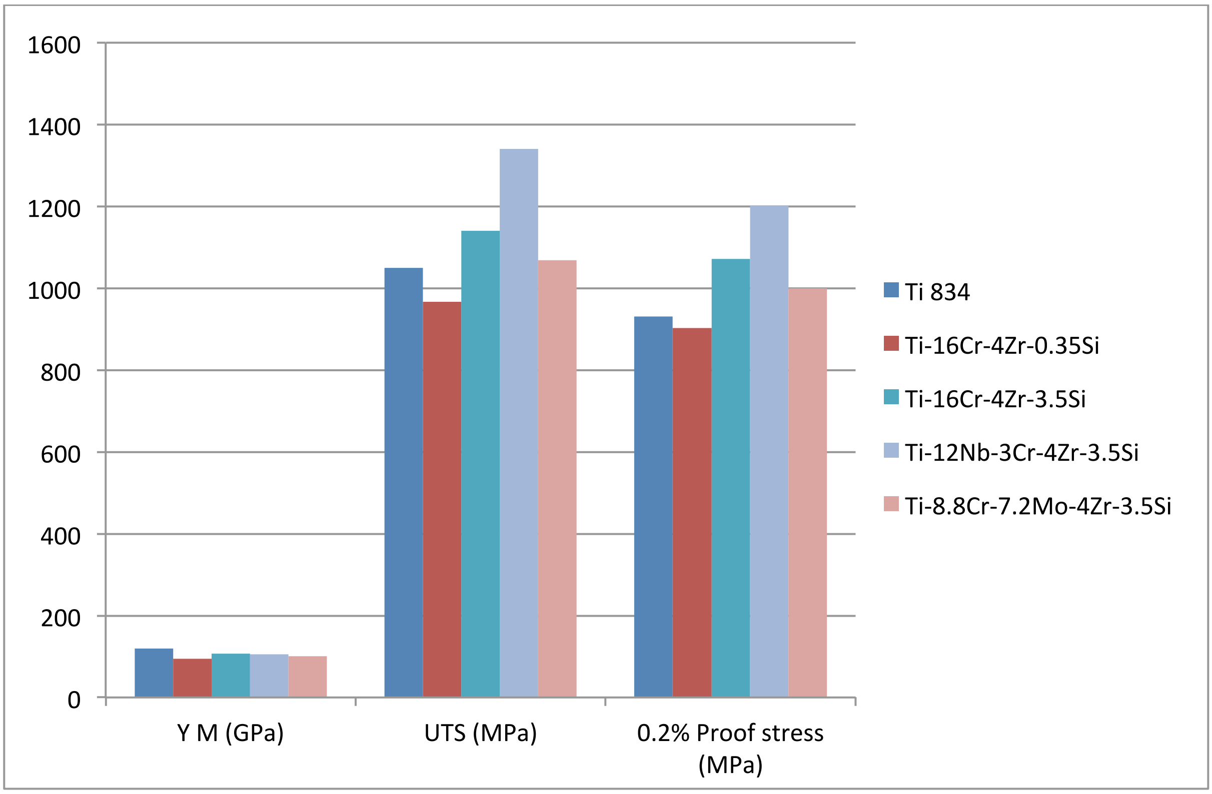

Figure 7.4.5 *Comparison of tensile properties obtained for all alloy samples tested including Timetal 834, used as a benchmark alloy.*

The data in figure 8.4.5 shows that for Young's modulus, Ti834 exhibits a modulus of 120GPa. All of the alloys tested are comparable with this figure with Ti-16Cr-4Zr-3.5Si being the closest to the benchmark with a modulus of 107GPa. Both Ti-12Nb-3Cr-4Zr-3.5Si and Ti-8.8Cr-7.2Mo-4Zr-3.5Si exhibit moduli above 100GPa.

Comparing ultimate tensile strength, the benchmark provided by the value for Timetal 834 is 1050MPa. The only alloy to exhibit UTS below this value is Ti-16Cr-4Zr-0.35Si. All other alloys (which contain 3.5Si) exceed the benchmark value with Ti-12Nb-3-Cr-4Zr-3.5Si exhibiting the highest UTS with a value of 1340MPa.

The 0.2% proof stress (or yield point) obtained by the alloys tested is compared with the benchmark value of 930MPa for Timetal 834. This indicates that Timetal 834 is able to withstand 930MPa of force before permanent plastic deformation occurs. All deformation before this point is elastic. Again, the only alloy not to exceed this value is Ti-16Cr-4Zr-0.35Si. All other alloys exceeded the benchmark value with Ti-12Nb-3Cr-4Zr-3.5Si exhibiting the highest yield point with a value of 1200MPa.

In order to determine the ductility of the alloys examined, the chart in figure 7.4.6 reports the % elongation (strain to failure) of those alloys.

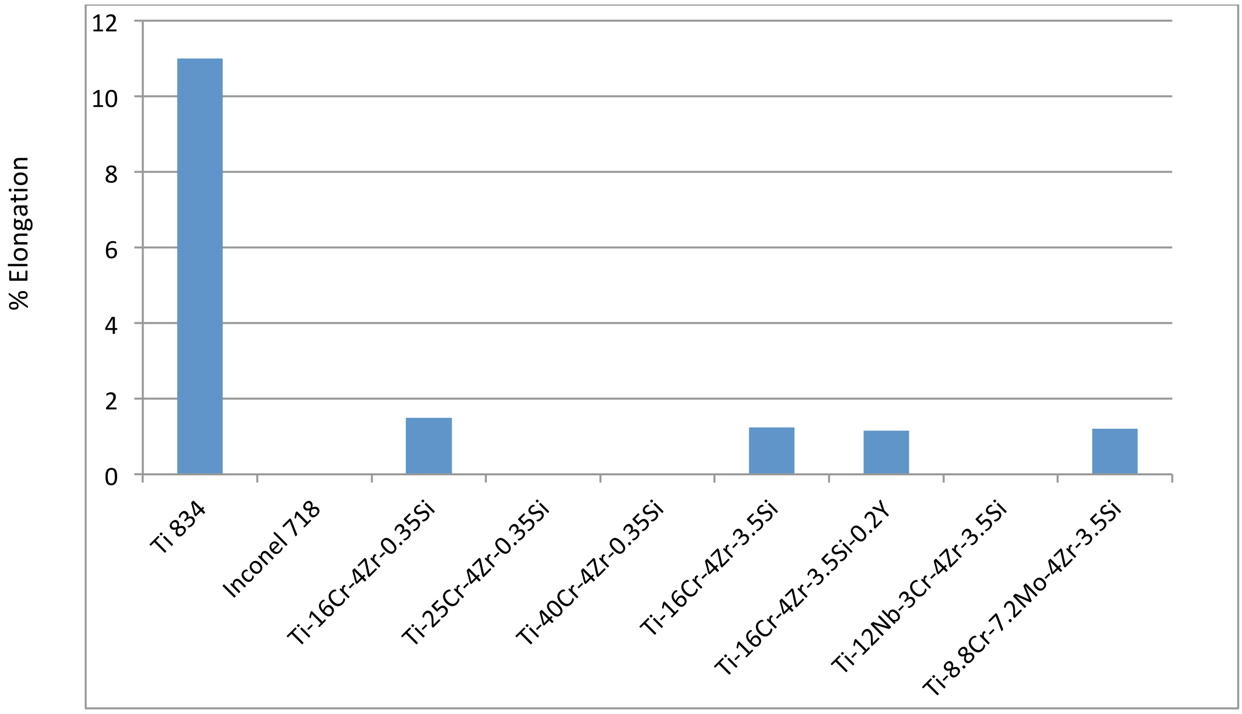

***Figure 7.4.6** Comparison of % Elongation obtained for all alloy samples tested including Timetal 834, used as a benchmark alloy.*

Timetal 834 achieves 11% elongation during this test. None of the tested alloys were able to compete with Timetal 834 for ductility. Based on the data, the alloy Ti-16Cr-4Zr-0.35Si appears to be the most ductile material tested with an elongation recorded at 1.5%. When the silicon content is increased to 3.5 wt.%, the % elongation is reduced to 1.24% indicating that the ductility is reduced by addition of silicon, which is what was expected from the literature. Alloy Ti-12Nb-3Cr-4Zr-3.5Si did not plastically deform, hence the 0% elongation value recorded, indicating that the high level of niobium in the material reduces ductility.

The data obtained in this area of work indicates that all alloys containing 3.5 wt.% silicon exceed the performance of existing alloy Timetal 834 in terms of strength and Young's modulus, however ductility is dramatically reduced by the increased silicon content. The results support what was expected from the literature. The presence of silicon tends to increase the strength of an alloy while reducing the ductility. In order to understand this in more detail, the fractured samples were examined microscopically.

7.4.2 Microscopic Analysis of Fractured Samples

Figure 7.4.7 a to c below shows the tensile specimen after fracture for alloys containing 3.5 wt.% silicon as seen using backscatter electron SEM.

A)

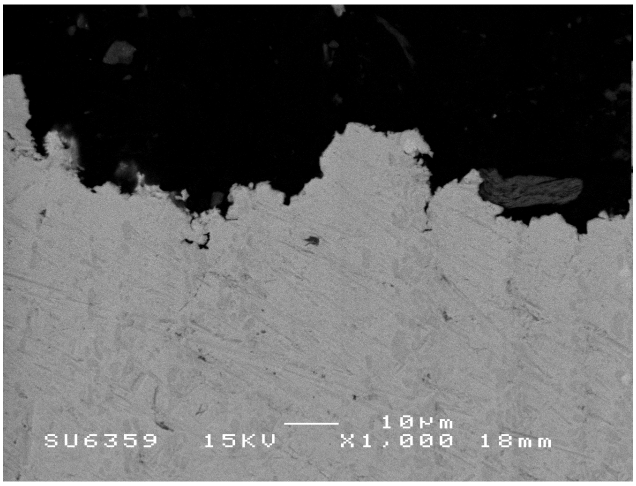

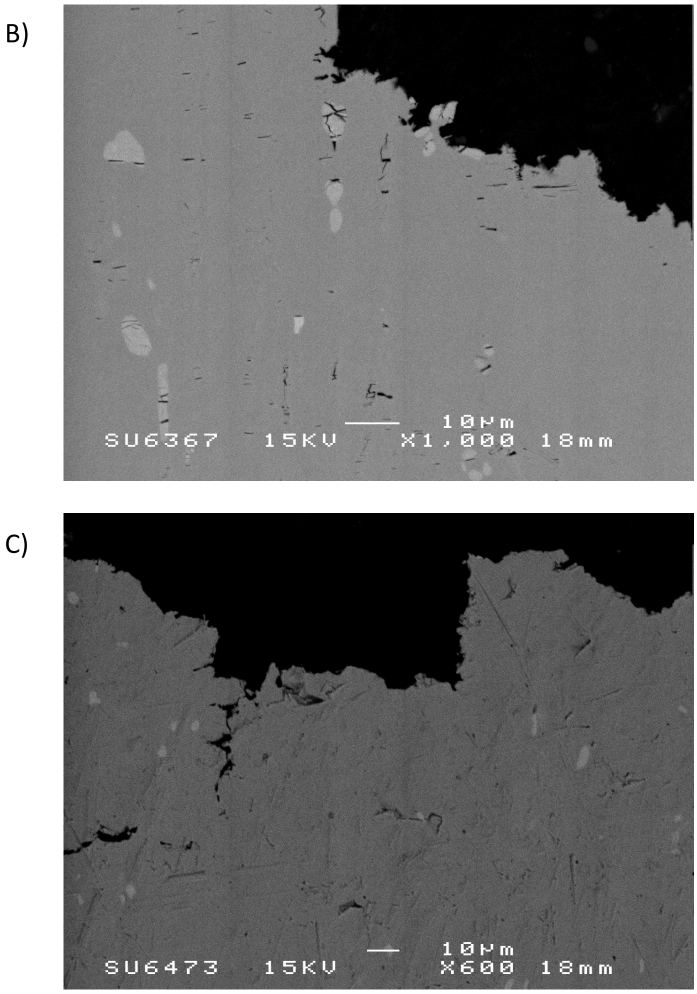

Figure 7.4.7 *Backscatter SEM images showing fractured tensile specimens for a)Ti-16Cr-4Zr-3.5Si, b)Ti-12Nb-3Cr-4Zr-3.5Si and c) Ti-8.8Cr-7.2Mo-4Zr-3.5Si.*

It is clear from the images that cracking has occurred through the sample. However, In alloy Ti-12Nb-3Cr-4Zr-3.5Si there appears to be cracking which initiates in intermetallic phases. Figure 7.4.8 below is a higher magnification image of this alloy using backscatter SEM.

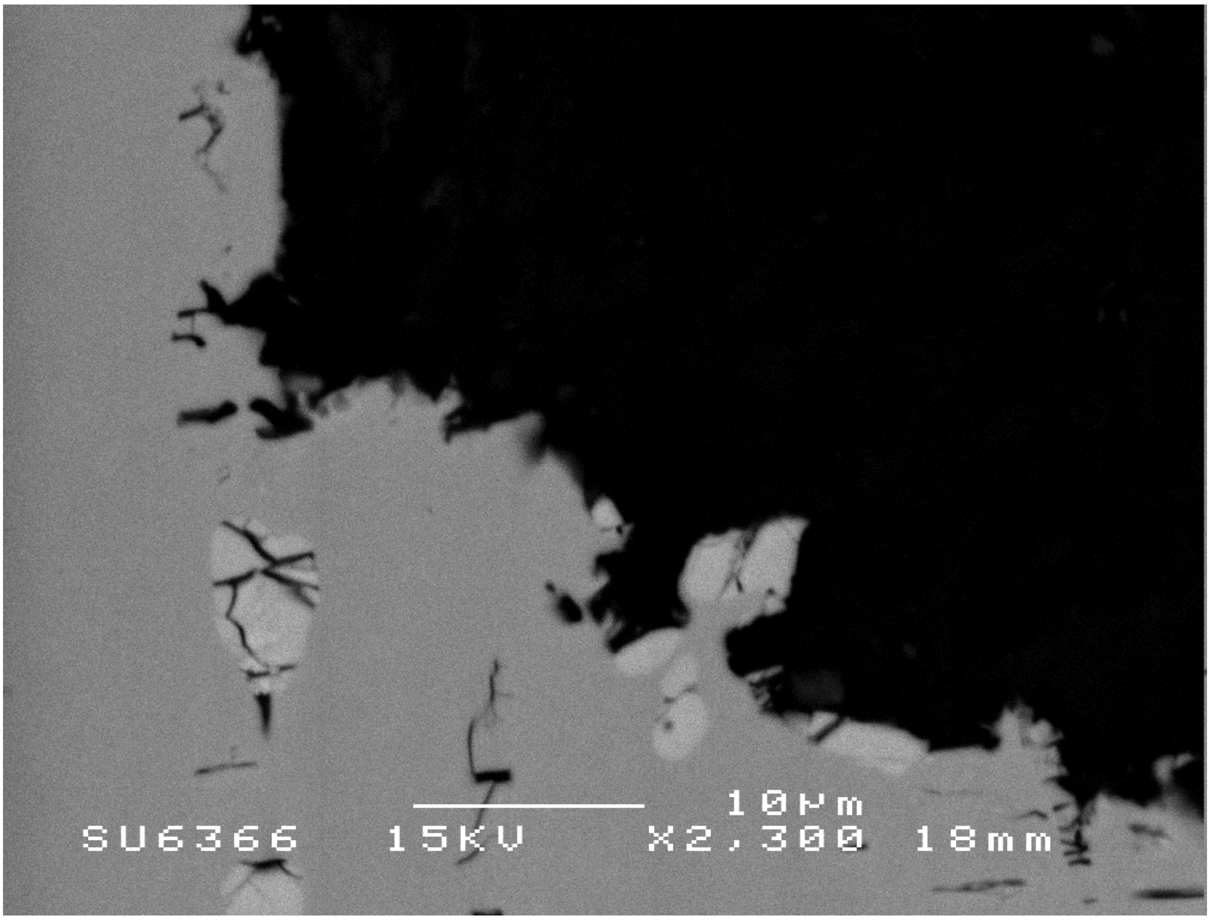

Figure 7.4.8 *Backscatter SEM images showing fractured tensile specimens for Ti-12Nb-3Cr-4Zr-3.5Si at X2300 magnification.*

In order to understand the composition of the intermetallics where crack initiation observed, EDX analysis was performed on the alloy Ti-12Nb-3Cr-4Zr-3.5Si with elemental mapping. Results are shown in figure 7.4.9 below.

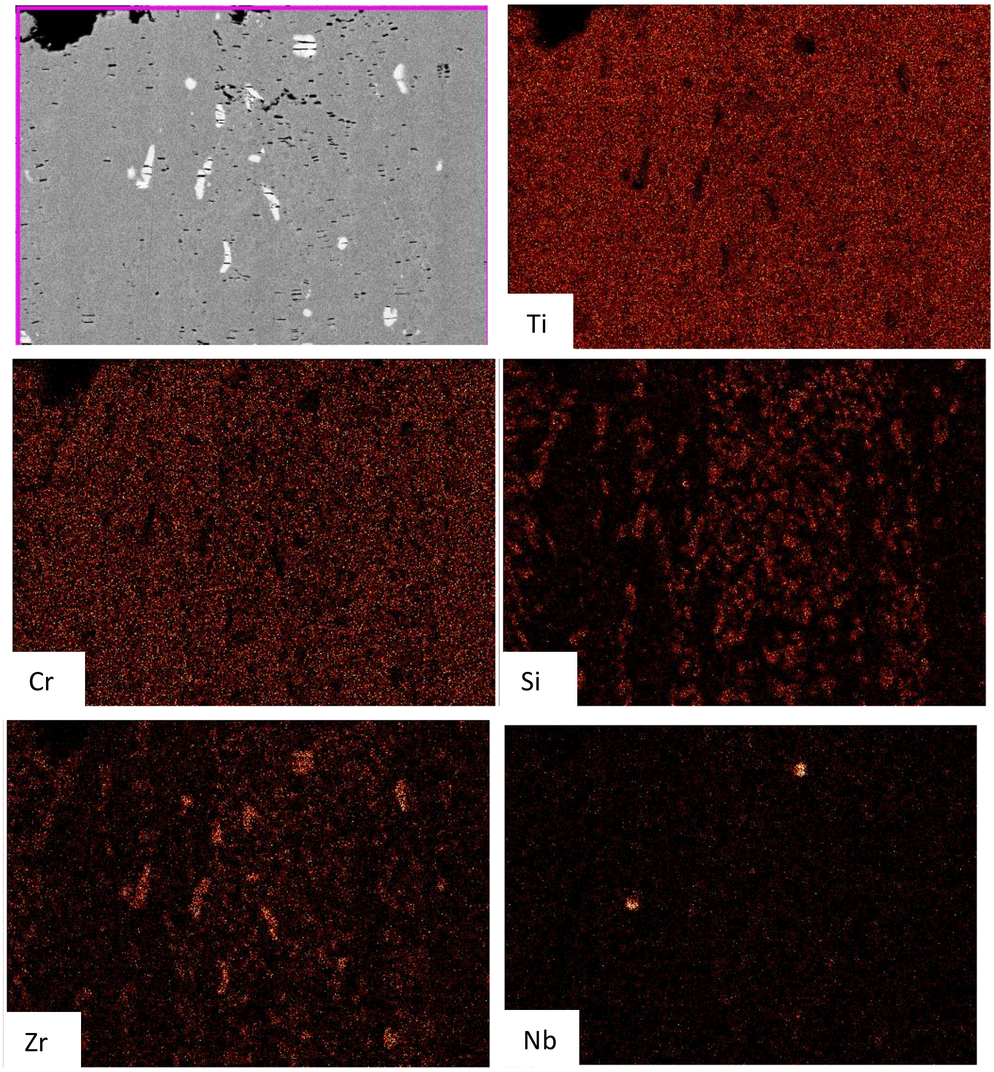

***Figure** 7.4.9 EDX elemental map showing fractured tensile specimen for Ti-12Nb-3Cr-4Zr-3.5Si.*

The chemical map above indicates that the intermetallic phase where cracking has initiated, a concentrated level of silicon, zirconium and niobium is present. This is consistent with literature in terms of Ti_5Si_3 ($(Ti,Nb,Zr)_5Si_3$ in this case) precipitates contributing to high strength but low ductility in alloys and as such can be held accountable for the brittle phase within the alloy, owing to the alloy's low ductility.

7.5 Summary

This chapter has investigated the mechanical properties of sample alloys investigated as part of this work. During the analysis high strength is achieved with the sample alloys but due to the relatively high levels of silicon added as well as that of other elements like niobium and chromium, ductility has been compromised. Hardness and densities of all alloys has been shown to be comparative if not better than Timetal 834, which is used as the benchmark material.

Chapter 8 will provide a more detailed discussion into the results documented in this chapter, as well as chapters 4, 5 and 6.

8 Discussion

8.1 Introduction

This chapter will discuss the data obtained from the works completed, with the aim being to provide links to the results observed in chapters 4, 5, 6 and 7.

Based on the observations obtained as part of this work, table 8.1 below has been constructed to provide a comparison of the performance of the developed alloys with that of Timetal 834, the benchmark alloy.

***Table 8.1.1** Comparison between the performances of the developed alloys against that of Timetal 834.*

Developed Alloy	Performance as compared with Timetal 834.						
	Oxidation Resistance (above 750°C)	Density	Hardness	Young's Modulus	UTS	0.2% Proof Stress	Ductility
Ti-16Cr-4Zr-0.35Si	✖	✖	✓	~	✖	✖	✖
Ti-25Cr-4Zr-0.35Si	✖	✖	~	✖	✖	✖	✖
Ti-40Cr-4Zr-0.35Si	✓	✖	✖	✖	✖	✖	✖
Ti-16Cr-4Zr-3.5Si	✖	~	~	~	✓	✓	✖
Ti-16Cr-4Zr-3.5Si-0.2Y	✖	~	~	~	✓	✓	✖
Ti-12Nb-3Cr-4Zr-3.5Si	✓	~	✖	~	✓	✓	✖
Ti-8.8Cr-7.2Mo-4Zr-3.5Si	✖	~	✖	~	~	✓	✖

Key: *✓ = Superior, ✖ = Inferior, ~ = Comparable*

Table 8.1.1 indicates that compared to Timetal 834, the developed alloy Ti-12Nb-3Cr-4Zr-3.5Si appears to be comparable or improved on all of the properties investigated with the exception of hardness and ductility. The developed alloy Ti-12Nb-3Cr-4Zr-3.5Si exhibits improved oxidation resistance as well as room temperature tensile properties, while maintaining similar density and Young's modulus to that of Timetal 834. Therefore, it is not unreasonable to say that this alloy could be a suitable alternative to Timetal 834, providing the ductility of the alloy can improved through the development of an alternative processing route (thermal cycles etc).

8.2 Discussion of Relationships

Using table 8.1.1 it is possible to draw on the relationships between the properties, thermodynamic simulations and the microstructures for each developed alloy, observed in the preceding chapters.

8.2.1 Ti-16Cr-4Zr-0.35Si

Alloy Ti-16Cr-4Zr-0.35Si exhibited the highest ductility of the test alloys, although the ductility is significantly inferior to that of Timetal 834. Similarly, alloy Ti-16Cr-4Zr-0.35Si is inferior in terms of oxidation resistance and mechanical properties than Timetal 834. Comparing figure 4.4.2 and 5.2.1 (shown again below) the lower volume fraction of the intermetallic phase $TiCr_2$ observed in figure 4.4.2 probably owes to the ductility observed. The reduced number of these precipitates at grain boundaries, indicated in figure 5.2.1, will improve ductility at the same time as reducing tensile properties (UTS and 0.2% proof stress). Precipitates hinder dislocation motion and so fewer precipitates at the grain boundaries allow enhanced dislocation motion providing ductility while reducing strength.

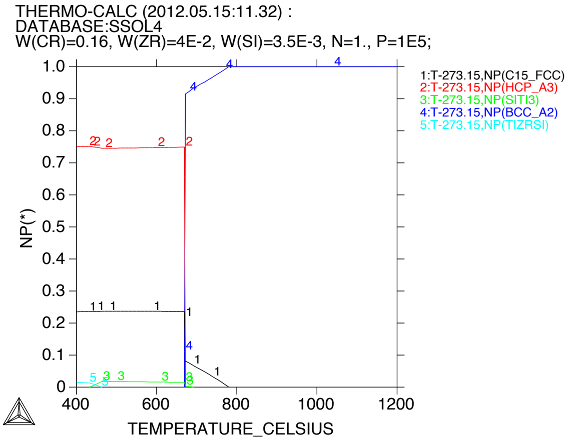

Figure 4.4.2 (left) *ThermoCalc Step diagram for Ti-16Cr-4Zr-0.35Si alloy.*

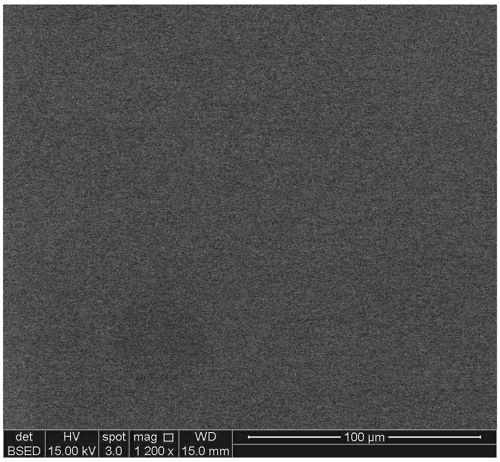

Figure 5.2.1 (right) *SEM image of as received Ti-16Cr-4Zr-0.35Si (Mag 1200X)*

In terms of oxidation resistance above 750˚C, the presence of horizontal cracks within the scale on the surface of the developed alloy (figure 6.2.2b) allows spallation and further oxidation of the alloy. This spallation prevents the formation of a protective oxide scale, reducing the oxidation resistance. In comparison, the scale on Timetal 834 is much more compact and adherent to the base material owing to its improved resistance to oxidation through the protection offered by the oxide scale.

8.2.2 Ti-25Cr-4Zr-0.35Si

Similar to the previously discussed alloy, the developed alloy containing 25 wt% chromium is inferior to the benchmark alloy in all categories including ductility. Figure 4.4.3 indicates an increased volume fraction of $TiCr_2$ precipitates compared to that of the alloy containing 16 wt% chromium. The presence of these precipitates at grain boundaries has improved the alloy strength through impeding dislocation motion, however the improvement is not sufficient enough to exceed the alloy strength exhibited by Timetal 834. Through the same precipitation hardening phenomenon, the alloy ductility has been worsened by the presence of grain boundary precipitates as indicated in figure 5.2.2 (shown again below).

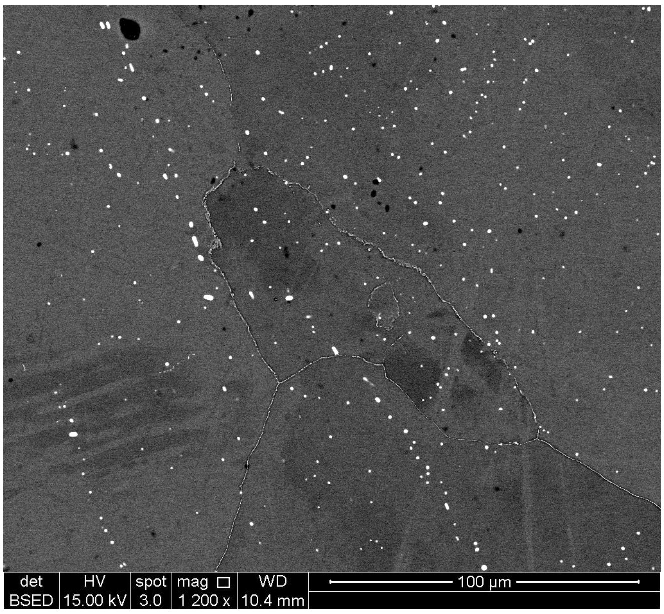

Figure 5.2.2 *SEM image of as received Ti-25Cr-4Zr-0.35Si (Mag 1200X)*

Again, the increase in chromium content in this alloy has improved oxidation resistance through the promotion of a more adherent oxide scale (as seen in figure 6.2.2c), however the improvement is not sufficient to provide superior oxidation resistance to that of Timetal 834.

8.2.3 Ti-40Cr-4Zr-0.35Si

The developed alloy containing 40 wt% chromium was too brittle to exhibit any improvement in tensile properties, owing to the precipitation hardening of the larger volume fraction of $TiCr_2$ phase. However, the increased volume fraction of chromium at the surface of the alloy has contributed to a thin, dense protective scale which is adherent with the chromium rich surface of the base material allowing improved resistance to oxidation compared to Timetal 834.

8.2.4 Ti-16Cr-4Zr-3.5Si (-0.2Y)

The increase in silicon content compared to the developed alloy described in section 8.2.1 has contributed to an increase in tensile properties, albeit with the accompanying decrease in ductility. The oxidation resistance is only marginally improved through the increase in silicon content, but not to the extent required to make the developed alloy superior to that of Timetal 834. Figure 4.4.5 shown again below indicates that the increase in silicon content supports the formation of silicides within the alloy (silicide type disputed previously in this thesis).

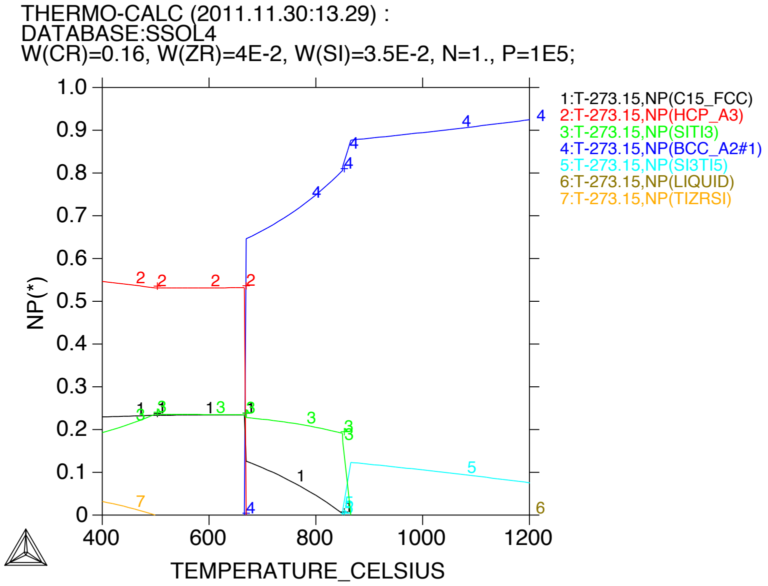

Figure 4.4.5 *ThermoCalc Step diagram for Ti-16Cr-4Zr-3.5Si alloy.*

The increase in silicon means a larger volume fraction of precipitates are present within the alloy, owing to the improvement in strength and reduced ductility observed for this alloy, again due to the precipitation strengthening effect.

The small increase in oxidation resistance is probably due to the scale being denser with little horizontal cracking as observed in figure 6.2.2e. This figure also shows that there is a larger volume fraction of chromium precipitates at the surface of the alloy, which can be explained by comparing figures 4.4.2 and 4.4.5. These two figures show that at 750˚C, the volume fraction of $TiCr_2$ precipitates increases from 6% to 11% through the increased silicon additions to the developed alloy.

The addition of yttrium has had little effect on the properties investigated as part of this works.

8.2.5 Ti-12Nb-3Cr-4Zr-3.5Si

As noted earlier, this alloy is the most beneficial in terms of superiority over Timetal 834 for the properties investigated, with the exception of ductility. These improvements can again be explained through the theory of precipitation strengthening. This alloy exhibits 28% volume fraction of precipitate phases present in a beta titanium matrix according to figure 4.5.2 shown again below.

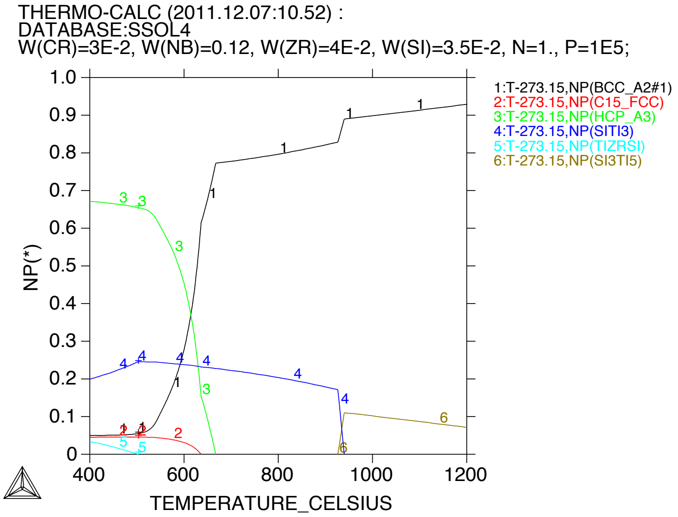

Figure 4.5.2 *ThermoCalc Step diagram for Ti-12Nb-3Cr-4Zr-3.5Si alloy.*

Comparing this to Timetal 834 in figure 4.3.2 shown below which exhibits approximately 2% volume fraction of precipitates within the alloy matrix.

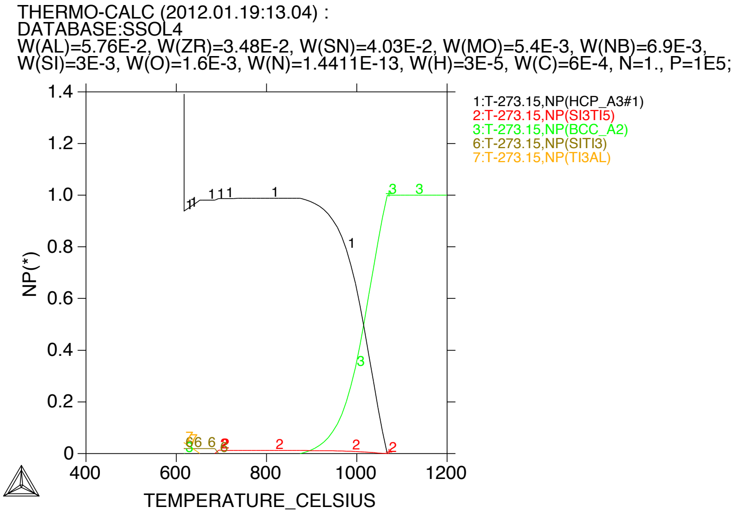

Figure 4.3.2 *ThermoCalc Step Diagram for Timetal 834*

The poor ductility in this alloy is explained by the initiation of cracks within the precipitate phases as shown in figure 7.4.8.

Oxidation resistance is dramatically improved for the developed alloy Ti-12Nb-3Cr-4Zr-3.5Si compared with Timetal 834. This is thought to be due to the presence of Ti,Zr_5Si_3 precipitates at the surface of the base material after oxidation as shown again in figure 6.2.2g. The reduced chromium content in this alloy (compared to other developed alloys) seems to promote the formation of this silicide phase, which in turn provides effective resistance to oxidation.

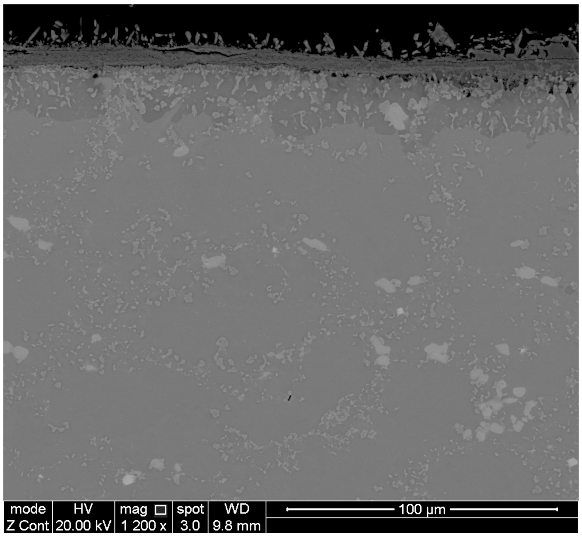

Figure 6.2.2g. *Back scattered electron SEM image showing surface microstructure of Ti-12Nb-3Cr-4Zr-3.5Si alloy after heat treatment at 750˚C for 150 hours.*

The presence of niobium in solution within the alloy matrix also appears to contribute to the formation of a protective oxide and hence improving the oxidation resistance.

8.2.5 Ti-8.8Cr-7.2Mo-4Zr-3.5Si

Unsurprisingly, precipitation strengthening is again involved in the slight improvements to strength (over Timetal 834) observed in this alloy as well as for the inferior ductility, with this alloy containing 36% volume fraction of precipitate phases at room temperature (as seen in figure 4.5.1). However the level of chromium added to this alloy appears to be a restrictor in the growth of silicides at the surface, and so the alloy Ti-8.8Cr-7.2Mo-4Zr-3.5Si does not provide the improved oxidation resistance observed in the niobium-containing alloy. The scale observed on the molybdenum-containing alloy (figure 6.2.2h) is also less dense and contains horizontal cracking, helping to explain the inferior resistance to oxidation.

8.3 Summary

The effect of precipitation strengthening contributes largely to the comparison of the tensile properties between the developed alloys and Timetal 834. Based on the results described in table 8.1.1, and in chapter 4 of this thesis, a relationship can be formed between the volume fractions of precipitates present within the developed alloys at room temperature. None of the developed alloys displayed improved ductility over Timetal 834. It appears that, for the alloying system explored in this work, the volume fraction of precipitate phase is too great to improve the room temperature properties to a level that is superior to Timetal 834. However it is worth noting that the brittle nature of some of the precipitates observed, particular those within the niobium containing alloy, could be another contributing factor to ductility.

The resistance to oxidation appears to be controlled by the ability to promote the growth of a protective oxide scale which is dense and free from significant cracking. This is best achieved through the presence of a chromium rich sub surface layer, which is prevalent in alloys containing high chromium additions by wt%. Adversely, the formation of Ti,Zr_5Si_3 silicides at the alloy surface during oxidation is also beneficial to improving oxidation resistance, the formation of which relies on a reduced chromium content.

9 Conclusions

During this work new alloying systems for application in low to medium pressure compressor stages of jet turbine aircraft engines has been investigated. In order to successfully displace nickel with titanium in these conditions, the requirements for a new alloying system include:

- Resistance to oxidation / alpha case growth in service (up to 750°C);
- Room temperature ductility;
- Strength/Creep resistance at service temperature.

Using analogies with nimonic alloys to include intermetallic phases within alloy matrices a number of suggested alloys were input into thermodynamic simulation software. On the basis of this, sample alloy buttons were requested from TIMET. The alloy samples investigated were:

- Ti-16Cr-4Zr-0.35Si;
- Ti-25Cr-4Zr-0.35Si;
- Ti-40Cr-4Zr-0.35Si;
- Ti-16Cr-4Zr-3.5Si;
- Ti-16Cr-4Zr-3.5Si-0.3Y;
- Ti-12Nb-3Cr-4Zr-3.5Si;
- Ti-8.8Cr-7.2Cr-4Zr-3.5Si.

These samples were analysed in the as received state, and then oxidation and mechanical testing was performed.

Conclusions drawn from this work can be sub categorized into two main categories; resistance to oxidation and mechanical properties. The section below collates conclusions summarised in Chapters 7 and 8.

9.1 Oxidation behaviour

- Above 750°C, the addition of chromium, niobium, and silicon to titanium improves the oxidation resistance to the point where Ti-12Nb-3Cr-4Zr-3.5Si exhibits better oxidation resistance than Timetal 834 during furnace oxidation testing;

- Scale thickness observed on sample alloys decreases as chromium/niobium/silicon addition is increased. Ti-12Nb-3Cr-4Zr appears to produce an oxide scale comparable with that of Timetal 834.
- The addition of silicon to titanium produces Ti_5Si_3 silicides, which precipitate at increased temperatures and appear to provide better oxidation resistance than the alloy matrix.
- Alloy samples with more than 16 wt.% chromium appear to be too brittle for the intended application. This has been concluded from the presence of cracking observed during oxidation analysis by microscopy.

9.2 Mechanical Properties

- The densities of all sample alloys investigated as part of this work are, although slightly higher than Timetal 834, are considerably lower than any nickel alloy counterpart and so can be deemed acceptable for the intended application.
- The hardness values obtained from as received sample alloys are all comparable with benchmark alloy, Timetal 834.
- Alloys containing more than 16 wt.% chromium are not fit for the proposed application due to extremely poor ductility. Poor ductility in these samples is related to large volume fraction of $TiCr_2$ intermetallic phases present in the material.
- The ultimate tensile strength of the materials investigated exceed that of benchmark material Timetal 834 in alloys which contain 3.5 wt% silicon. This is due to the presence of Ti_5Si_3 precipitates observed in these alloys which contribute to increased strength as described by precipitation strengthening theory.
- Ductility measured by % elongation is poor in the sample alloy which contain 12 wt.% niobium. This is believed to be caused by cracks which initiate in the intermetallic phase $(Ti,Nb,Zr)_5Si_3$ as seen by SEM and EDX chemical mapping. Ductility is also reduced in alloys which contain 3.5wt.% silicon compared to those which contain only 0.35 wt.% silicon. This is thought to be the result of the formation of Ti_5Si_3 precipitates and the increased volume fraction of this phase associated with the increased addition of silicon and again can be described by precipitation strengthening.

9.3 Overall Conclusions

Comparing oxidation data with mechanical properties, of the samples investigated as part of this work the alloy which appears to be the most beneficial within the intended application are:

- Ti12Nb-3Cr-4Zr-3.5Si.

The above alloy exhibits comparable and better oxidation resistance to Timetal 834 as well as improved tensile strength. However ductility is still an issue for the alloy. Chapter 10 will consider further study that could be completed to progress this work.

10 Further Work

This chapter will suggest further work based on the conclusions and overall findings of this work.

As outlined in chapter 9, the alloy samples investigated have produced some promising results in terms of oxidation resistance and tensile strength. However, there appears to be an issue with ductility which is poorer than existing, benchmark, alloy Timetal 834. In order to improve the output, it would be beneficial to investigate the effect of the processing route, and therefore the starting microstructure of such alloys. It is proposed that a schedule of tests be completed, in which the heat treatment and reduction in area achieved from each pass during the rolling process is altered. The aim of these investigations being to reduce the volume fraction and size of intermetallic phases precipitated during alloy processing.

This series of testing will indicate the influence of the starting microstructure and help to determine whether ductility can be improved in these alloys while maintaining strength and oxidation resistance at high temperature.

Another proposed study for further work would be the inclusion of elevated temperature tensile testing on sample alloys. The aim of this would be to determine the effect of in service temperatures on mechanical properties of such alloys. The investigation could be completed using a tensile testing machine which has a small furnace chamber fitted around where a sample is placed. The sample is brought up to temperature before the tensile test is performed. Suggested temperatures for this work are 650°C, 750°C and 850°C.

11 References

[1] C. Leyens and M. Peters, *Titanium and titanium alloys : fundamentals and applications*. Weinheim, Chichester: Wiley, 2003.

[2] G. Lütjering. (2007). *Titanium (2nd ed.)* Available: http://www.myilibrary.com?id=104528

[3] I. J. Polmear, *Light alloys: metallurgy of the light metals*, 3rd ed. London: Butterworth Heinemann, 1995.

[4] S. Naka. “Advanced titanium based alloys,” *Current Opinion in Solid State & Materials Science (USA) Vol 1*, pp 333-339. 1996.

[5] W. Betteridge and J. Heslop, *The Nimonic Alloys*, Second Edition ed. London: Edward Arnold (Publishers) Ltd., 1959.

[6] I. Weiss and S. L. Semiatin, "Thermomechanical processing of alpha titanium alloys - an overview," *Materials Science and Engineering A,* vol. 263, pp. 243-256, 1999.

[7] M. J. Donachie, *Titanium : a technical guide*. Metals Park, OH: ASM International, 1988.

[8] P. Blenkinsop, and D. Neal. “High temperature titanium alloys: the metallurgical understanding, development, and achievements of conventional alloys”. *Conference Metallurgy and Technology of Practical Titanium Alloy*s, Chiba, Japan, 7-10 Dec. 1993. Minerals, Metals and Materials Society/AIME, Warrendale, PA 15086, USA. Published 1994.

[9] J. Williams, "Structure and High Temperature Properties of Ti_5Si_3 with Interstitial Additions," PhD, Ames Laboratory, Iowa State University, Iowa, 1999.

[10] N. Poryadchenko, M. Kuz’menko, I. Oryshych, N. Khmelyuk, L. Kulak, and L. Kalashnikova, "High Temperature Strength of Titanium Alloys Alloyed with Silicon, Aluminium and Zirconium in Air," *Materials Science,* vol. 41, pp. 230 - 236, 2005.

[11] M. Thomas, "The Effect of Thermomechanical Process Parameters on the Microstructure and Crystallographic Texture Evolution of Near-α Aerospace Alloy Timetal®834," Doctor of Philosopy, Engineering Materials, University of Sheffield, Sheffield, 2007.

[12] E. Crist, P. Russo, H. Phelps, and L. Clark, "Influences of Chemistry and Processing on Microstructure and Mechanical Properties for Ti-6Al-2Sn-2Zr-2Cr-2Mo-0.15Si," *Ti-2003: Science and Technology,* vol. III, pp. 1631-1638, 2003.

[13] R. Thomas, "Project Proposal – Blue Sky Alloy Development," ed. Birmingham: TIMET, UK, 2010.

[14] E. Ezugwu, J. Bonney, and Y. Yamane, "An Overview of the Machineability of Aeroengine Alloys," *Journal of Materials Processing Technology,* vol. 134, pp. 233 - 253, 2003.

[15] B. Tian, C. Lind, and O. Paris, "Influence of Cr23C6 carbides on dynamic recrystallization in hot deformed Nimonic 80a alloys," *Materials and Engineering A,* vol. 358, pp. 44 - 51, 2003.

[16] B. Tian, G. A. Zickler, C. Lind, and O. Paris, "Local microstructure and its influence on precipitation behavior in hot deformed Nimonic 80a," *Acta Materialia,* vol. 51, pp. 4149–4160, 2003.

[17] Y. Xua, Q. Jin, X. Xiao, X. Cao, G. Jia, Y. Zhu*, et al.*, "Strengthening mechanisms of carbon in modified nickel-based superalloy Nimonic 80A," *Materials Science and Engineering A,* vol. 528, pp. 4600–4607, 2011.

[18] Z. Jiang, X. Dai, and H. Middleton, "Effect of silicon on corrosion resistance of Ti-Si alloys," *Materials Science and Engineering: B,* vol. 176, pp 79 – 86, 2011.

[19] R. L. Saha, T. K. Nandy, R. D. K. Misra, and K. T. Jacob, "Microstructural changes induced by ternary additions in a hypo-eutectic titanium-silicon alloy," *Journal of Materials Science,* vol. 26, pp. 2637-2644, 1991.

[20] N. Paton and M. Mahoney, "Creep of titanium-silicon alloys," *Metallurgical and Materials Transactions A,* vol. 7, pp. 1685-1694, 1976.

[21] D. Vojtech, B. Bártová, and T. Kubatík, "High temperature oxidation of titanium-silicon alloys," *Materials Science and Engineering A,* vol. 361, pp. 50-57, 2003.

[22] D. Vojtech, H. Cízová, K. Jurek, and J. Maixner, "Influence of silicon on high-temperature cyclic oxidation behaviour of titanium," *Journal of Alloys and Compounds,* vol. 394, pp. 240-249, 2005.

[23] M. Kuz'menko, "Structure and Mechanical Properties of Cast Alloys of the Ti-Si System," *Materials Science,* vol. 44, pp. 49 - 53, 2008.

[24] N. P. Brodnikovskii, I. V. Oryshich, and N. E. Poryadchenko, "Resistance of Titanium-Chromium and Zirconium-Chromium Alloys to Air Oxidation," *Powder Metallurgy and Metal Ceramics,* vol. 49, pp. 7-8, 2010.

[25] A. M. Chaze and C. Coddett, "Influence of Chromium on the Oxidation of Titanium between 550C and 700C," *Oxidation of Metals,* vol. 21, 1984.

[26] I. V. Oryshich, N. E. Poryadchenko, and N. P. Brodnivoskii, "High Temperature Oxidation of Intermetallics formed by Group IV Transition Metals with Chromium," *Powder Metallurgy and Metal Ceramics,* vol. 43, pp. 9-10, 2004.

[27] M. Codell and G. Norwitz, "Colorimetric and gravimetric determination of silicon in titanium and titanium alloys," *Analytica Chimica Acta,* vol. 16, pp. 327-332, 1957.

[28] M. J. Bermingham, S. D. McDonald, M. S. Dargusch, and D. H. S. John, "The mechanism of grain refinement of titanium by silicon," *Scripta Materialia,* vol. 58, pp. 1050-1053, 2008.

[29] J. Murray, "Equilibrium phase diagram for a titanium-silicon alloying system," *Binary Alloy Phase Diagrams,* vol 10, p. 219, 1989

[30] J. Murray, "Ti-Cr Equilibrium Diagram," *Bulletin of alloy phase diagrams,* vol 2, p. 174, 1981

[31] A. K. Singh and C. Ramachandra, "Characterization of silicides in high-temperature titanium alloys," *Journal of Materials Science,* vol. 32, pp. 223 - 234, 1997.

[32] A. Kelly and G. Groves, *Crystallography and crystal defects*. Harlow: Longman, 1970.

[33] A. S. Ramos, C. A. Nunes, and G. C. Coelho, "On the peritectoid Ti_3Si formation in Ti-Si alloys," *Materials Characterization,* vol. 56, pp. 107-111, 2006.

[34] C. Hammond, *The basics of crystallography and diffraction*, 2nd ed. Oxford: International Union of Crystallography: Oxford University Press, 2001.

[35] K. Chen, S. Allen, and J. Livingston, "Microstructures of two phase Ti-Cr alloys containing the TiCr2 laves phase intermetallic," *Journal of Materials Research,* vol. 12, 1997.

[36] D. Bombač, M. Fazarinc, G. Kugler, and S. Spajić, "Microstructure development of Nimonic 80A superalloy during hot deformation," *RMZ – Materials and Geoenvironment,* vol. 55, pp. 319-328, 2008.

[37] W. Ho, T. Chiang, S. Wu, and H. Hsu, "Mechanical properties and deformation behavious of cast binary Ti-Cr alloys," *Journal of Alloys and Compounds,* vol. 468, pp. 533-538, 2009.

[38] M. Ashby and D. Jones, *Engineering materials 2: an introduction to microstructures, processing and design*, 2nd ed. Oxford: Butterworth-Heinemann, 1998.

[39] O. N. Senkov, M. Cavusoglu, and F. H. Froes, "Synthesis of a low-density Ti-Mg-Si alloy," *Journal of Alloys and Compounds,* vol. 297, pp. 246-252, 2000.

[40] P. Perez, G. Salmi, A. Munoz, and M. A. Monge, "Influence of yttria additions on the oxidation behaviour of titanium prepared by powder metallurgy," *Scripta Materialia,* vol. 60, pp. 1008-1011, 2009.

[41] S. Firstov, S. Tkachenko, and N. Kuz'menko, "Titanium 'Irons' and Titanium 'Steels'," *Metal Science and Heat Treatment,* vol. 51, pp. 12-18, 2009.

[42] U. Prasad, Q. Xu, and M. C. Chaturvedi, "The effect of silicon on the near-surface microstructural evolution during high temperature heat treatment of a TiAl based alloy," *Materials Science and Engineering: A,* vol. 297, pp. 1-9, 2001.

[43] W. D. Callister and D. G. Rethwisch, *Materials science and engineering : an introduction*, 7th ed. New York: John Wiley, 2007.

[44] W. Wang, and F. Wang, "Influence of cyclic frequency on oxidation behaviour of K38 superalloy with yttrium additions at 1273K," *Journal of Rare Earths,* vol. 29, 2011.